POLITECNICO

MILANO 1863

Analysis and Thermal Design of a Two-Level SiC Three-Phase Inverter

Tesi di Laurea Magistrale in
Electrical Engineering - Ingegneria Elettrica

Author: **Giulio Santapà**

Abstract

The Polimi Motorcycle Factory (PMF) racing team is the team that represents the Politecnico at the Moto Student International Competition. For some time, the team had and felt the need to have a home-made three-phase inverter. The goal was to have more design flexibility and be able to improve its performance. The thesis project involves the study and sizing of the power part of the three-phase inverter.

In the second chapter, attention will be drawn to the principles of the single-phase and three-phase inverter and to its main components: the MOSFETs and the characteristics of the materials they are made of, showing their peculiarities. The Voltage Source Inverter designed for the team uses SiC, Silicon Carbide MOSFETs, and is based on a two-level Pulse Width Modulation (PWM) control.

The third chapter will describe the study of the thermal analysis of the board with the inverters, done through software that uses the finite element method, F.E.M., such as Ansys Icepack. This program was used to size the aluminum heat exchanger. Subsequently, the temperatures detected were used to define the thermal parameters of the heatsink.

In the fourth chapter a thermo-electric model developed on Simulink by Mathwork will be presented, with which specific tests have been made to verify the junction temperatures of the MOSFETs. The different simulations allowed to carry out both static and dynamic functioning tests.

Finally, a purely electrical model of a two-level three-phase inverter was tested with Simulink to verify its powers and efficiency.

Keywords: Inverter, SiC, VSI, Thermo-Electric Model, F.E.M., PWM

Abstract in lingua italiana

Il Polimi Motorcycle Factory (PMF) racing team è il team che rappresenta il Politecnico al Moto Student International Competition. Da tempo, il team aveva e sentiva la necessità di avere un inverter trifase fatto in casa. L'obiettivo era quello di avere una maggiore flessibilità di progettazione ed essere in grado di migliorarne le prestazioni. Il progetto di tesi prevede lo studio e il dimensionamento della parte di potenza dell'inverter trifase.

Nel secondo capitolo si richiamerà l'attenzione sui principi dell'inverter monofase e trifase e su i suoi componenti principali: i MOSFETs e le caratteristiche dei materiali di cui sono fatti, mostrandone le peculiarità. Il Voltage Source Inverter progettato per il team utilizza MOSFET SiC, Silicon Carbide, e si basa su un controllo PWM, Pulse Width Modulation, basato su un due livelli.

Nel terzo capitolo verrà descritto lo studio dell'analisi termica dell'inverter, fatta attraverso un software che usa l'analisi degli elementi finiti, F.E.M., come Ansys Icepack. Questo programma è stato utilizzato per dimensionare lo scambiatore di calore in alluminio. Successivamente le temperature rilevate sono state usate per definire i parametri termici dello scambiatore.

Nel quarto capitolo verrà presentato un modello termo-elettrico sviluppato su Simulink di Mathwork, con il quale sono stati fatti dei test specifici per verificare le temperature di giunzione dei MOSFETs. Le diverse simulazioni hanno permesso di effettuare prove di funzionamento sia statico che dinamico.

Infine è stato testato con Simulink un modello puramente elettrico di un inverter trifase a due livelli per verificarne le potenze e il rendimento.

Parole chiave: Inverter, SiC, VSI, modello termo-elettrico, F.E.M., PWM

Contents

1 | Introduction

The Moto Student International Competition is a challenge promoted by Moto Engineering Foundation and Technopark Motorland and it is open to the with University Student teams among all over the world. The main goal of each student teams is to create a moto using the knowledge acquired during their university studies, applying all the skills taken and develop other types of skills that could not be develop studying and attending courses. There are two categories:

- MotoStudent Petrol (internal combustion engine)

- MotoStudent Electric (100% electric propulsion system)

The organizers assign an engine, electric for the electric categories, petrol for the others, the same for each team, in order to allow each competitor to race starting from the same potential.

The competition has two phases:

- Phase MS1: in this part of the challenge the prototype is judged from an industrial point of view, verifying the knowledge of the students, they are asked to explain in detail the characteristics of each section of the project.

- Phase MS2: is the safety and functionality test where the bike is tested. If the prototype is safe and suitable for the competition rules, the team can take part to the race. The race is composed by several tests. The main ones are:

  - Brake test: will be measured the distance taken to stop the motorbike from a speed at least of 80km/h

  - Gymkhana: complete a gymkhana in the shortest time possible

  - Acceleration: achieve the highest acceleration in a 150m-long straight

This part is real time, each team has its pilot that ride the motor in the three different race. In this phase there is the last proof where the performances of the prototype are under test.

The competition not only requires technical competences to create a motorcycle around the given engine, but also other logistical skills to achieve this goal. For example, each team can contact companies asking to sponsor them with their products, getting more sponsorships will reduce the amount of costs.

Figure 1.1: Nyx, the Polimi Motorcycle Factory 2021 Electric Prototype

In figure 1.1, Nyx, the prototype for the last competition, has been developed using the following components:

- Hybrid chassis with steel trellis aluminium plates. No standard steering headstock

- Battery pack custom-designed for the prototype, with a capacity of 8 kWh, managed by an in-house built BMS

- Carbon fibre front fork sheaths with measurement system connect by optical fibres

- Data acquisition system integrated in the dashboard, designed and programmed in-house

- Vehicle aerodynamics studied by developing the shape of the fairing with the aim of minimising the drag force

- The weight of the motorbike is 137 kg, the petrol version is forty kilos lighter, the

heaviest part is the battery pack that is bigger than a petrol tank of a motorbike. In addition, when the battery runs out, it does not lose weight...

The Polimi Motorcycle Factory is composed by several main divisions as following:

- Chassis & Dynamics

- Fairing & Aerodynamics

- Powertrain Petrol

- Powertrain Electric

- PR-Business & Communication

- Technical Director

The electric unit develop is the one interested in:

- Battery

- BMS, Battery Management System

- Electric Control Unit

- Inverter & its board

- Dashboard and sensors
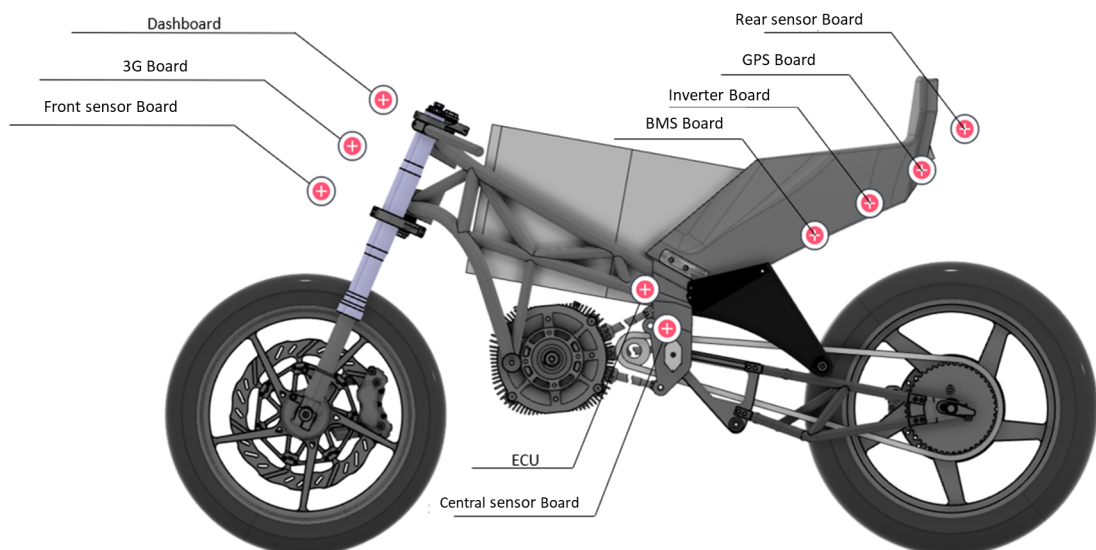
Figure 1.2: Motocycle development parts

The figure 1.2 shows the motorcycle with the sections developed by Polimi team.

The new motor granted from the organizers is a three phase permanent magnet synchronous motor. The motor data for nominal and maximal operating conditions is reported in tables 1.1 and 1.2 respectively.

Nominal Operation			
Torque	T_{nom}	50	Nm
Power	P_{nom}	22	kW
Speed	n_{nom}	5500	rpm
Phase rms-current	I_{nom}	250	A
Battery voltage (DC)	U_{nom}	100	V
Electric frequency	$f_{el,nom}$	TBA	Hz
Power factor	$\cos(\phi)$	TBA	

Table 1.1: Motor nominal operation condition

Maximal Values			
Torque	T_{max}	120	Nm (2min)
Power	P_{max}	48	kW (2min)
Speed	n_{max}	7500	rpm
Phase rms-current	I_{max}	600	A
Battery voltage (DC)	U_{max}	140	V
Electric frequency	$f_{el,max}$	TBA	Hz

Table 1.2: Motor maximal operation condition

In 2022, the team had and felt the need to have an home-made three-phase inverter by Polimi. The aim was to have more design flexibility and be able to improve performance.

This will be the principal argument developed in this elaborate.

2 | Inverter Technology

2.1. DC-AC Converter

The DC-AC converter is a widely used device for traction applications, motor control and for all those applications related to motors that require control.
The input voltage is DC, while the output voltage supplied to the load is AC; this is accomplished by controlled switches which are set to have an AC output.

This converter works with a DC to AC power flow most of the time, but it allows the flow to be reversed, i.e., going from AC to DC that is why it is called rectifier. Power reversal occurs in braking phases, a situation where the mechanical torque vector drags the rotor in this case the motor works as a generator. In the braking phase the motor provides active power to the DC source thanks to the Diode.

In order to reverse the power the converter should operate at least in two quadrants.

Another important use of the three-phase inverter is the interconnection of two AC sides connected with two converters. This type of connection is used when you want to connect two network points that have different frequencies.

The basic configuration of an inverter is shown in the figure 2.1, the single-phase and three-phase configurations derive from this circuit.
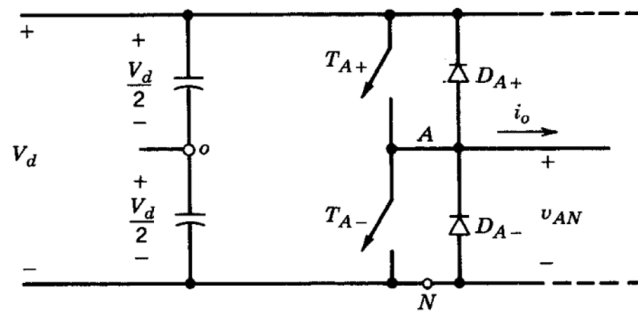
Figure 2.1: Single leg inverter

The input of the inverter is a constant DC voltage source; the most common configuration is the VSI, which stands for Voltage Source Inverter, the VSI can be further controlled with 3 different method modulation techniques that are:

- PWM - Pulse Width Modulation

- Square Wave

- Voltage Cancellation

For motor control applications, PWM and square wave are mainly used.

2.2.   PWM - Pulse Width Modulation

PWM control is the most widely used method to control the switches, it is used to create a sinusoidal output voltage by controlling the applied DC voltage. It is derived from a comparison of two signals: one is called control signal $\boldsymbol{v}_{control}$ and it is usually a sine wave. The other signal is a repetitive sequence, in this case, a triangular wave $\boldsymbol{v}_{tri}$ at a constant frequency higher than the $f_{control}$. The output of their comparison is:

- 1 if $\boldsymbol{v}_{control} > \boldsymbol{v}_{tri}$

- 0 if $\boldsymbol{v}_{control} < \boldsymbol{v}_{tri}$

The most important advantage of these control methods is that with them is possible to control the output voltage quantities. The voltage $\boldsymbol{v}_{control}$ manages variation of the output controlling its:

- Amplitude

- Phase

- Frequency

The main feature of $\boldsymbol{v}_{control}$ is that it is the reference voltage of the output signal, because changing the parameters of the control sine wave changes the output voltage of the first harmonic order. For these reasons this type of inverter is named Voltage Source Inverter, VSI is the short version, and this is because the controlled signal is voltage.

Instead $\boldsymbol{v}_{tri}$ is a triangular waveform, which defines the switching frequency of the inverter, indicated with $\boldsymbol{f}_s$, which is also called carrier frequency. The voltage and frequency of the carrier are kept constant and are defined at the design stage.

To evaluate the output quantities, it is important to define two parameters: $\boldsymbol{m}_a$ and $\boldsymbol{m}_f$. The first one is called modulation ratio, it is defined as:

$$m_a = \frac{v_{control}}{v_{tri}}, \tag{2.1}$$

Instead $\boldsymbol{m}_f$ is the frequency modulation ratio:

$$m_f = \frac{\boldsymbol{f}_{tri}}{\boldsymbol{f}_{control}}, \tag{2.2}$$

These two signals, control and carrier, are important because from their comparison a third signal is obtained (see fig: 2.2). The signal that comes out of the comparison is characterized by the duty cycle, which can be constant or variable, this depends on the type of control signal that is given.

PWM has a non-constant duty cycle because the $v_{control}$ signal is a sinewave, up to the square wave technique the duty cycle is variable, in square wave it is constant.
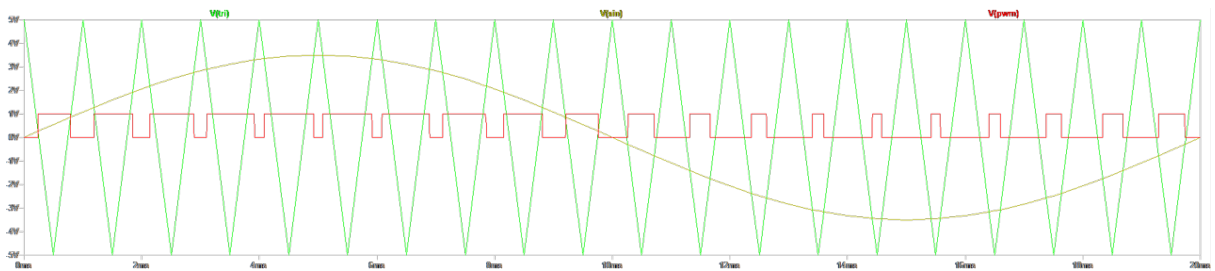
Figure 2.2: PWM signals

The output of the comparator indicates the state of the switch; if the value is one, the switch is closed and current is drawn, while if the value is zero, the switch is open and the current cannot pass.

A leg is defined as the connection of two switches, one for the high side and one for the low side, the source of the high side switch is connected to the drain of the low side switch. In figure 2.3, the connection to the load is taken between the two switches.
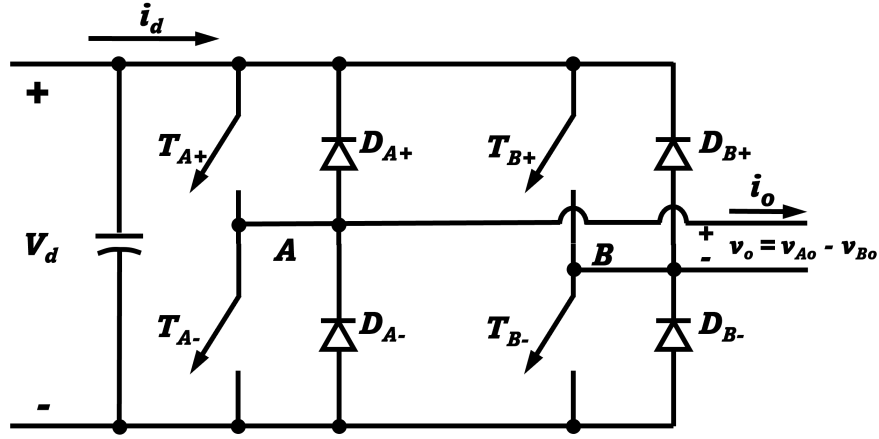
Figure 2.3: Single Phase Inverter

The aforementioned logic is used to control the valves T_{A+} and T_{a-}:

- $\boldsymbol{v}_{control} > \boldsymbol{v}_{tri}$, T_{A+} is closed, T_{A-} is open

- $\boldsymbol{v}_{control} < \boldsymbol{v}_{tri}$, T_{A-} is closed, T_{A+} is open

It is important to point out that switches that are in the same leg are never closed at the same time because then the DC source would be shorted.

The output voltage $\hat{V}_{AO_1}$, related to the phase voltage of the first harmonic has a maximum value equal to $m_a \dfrac{V_d}{2}$, it depends by the modulation ratio m_a, and it is equal to:

$$\boldsymbol{V}_{ao} = \frac{\boldsymbol{v}_{control}}{\hat{\boldsymbol{V}}_{tri}} \frac{\boldsymbol{V}_d}{2}, \qquad v_{control} \leq \hat{V}_{tri} \tag{2.3}$$

A sinusoidal $v_{control}$ is chosen, with a frequency equal to $f_1 = \omega/2\pi$, that is equal to the frequency of the desired output:

$$\boldsymbol{v}_{control} = \hat{V}_{control} \sin \omega_1 t \quad \text{where} \quad \hat{V}_{control} \leq \hat{V}_{tri} \tag{2.4}$$

In this way it is possible to say that the first harmonic of the output voltage varies sinusoidally and in phase with $v_{control}$. Thus, the first harmonic is:

$$\boldsymbol{V}_{Ao1} = \frac{\hat{V}_{control}}{\hat{\boldsymbol{V}}_{tri}} \sin \omega_1 t \frac{\boldsymbol{V}_d}{2} \tag{2.5}$$

$$= m_a \sin \omega_1 t \frac{V_d}{2} \quad m_a \leq 1.0, \tag{2.6}$$

The last result shows that the voltage output varies linearly with m_a, if and only if m_a is less or equal to 1. The assumption that m_a should be less or equal to 1 is called linear zone. If m_a has value over 1, the control is in over modulation.

In figure 2.4 are reported the carrier and control voltages, as well as v_{ao}.
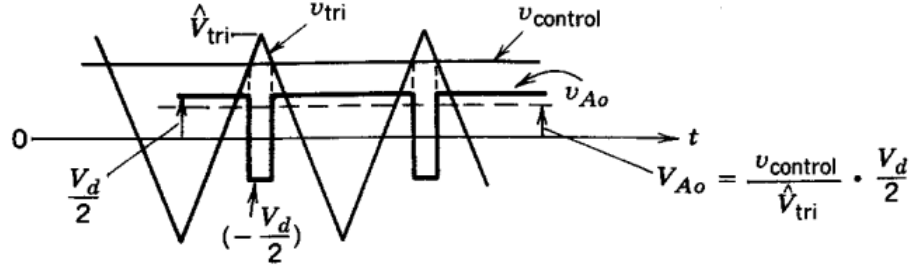
Figure 2.4: PWM signals [5]

2.3. Harmonic Content

Harmonics of the output voltage are present at each multiple of the switching frequency as sidebands, and they are located around integer multiples of m_f.

$$f_h = (j \cdot m_f \pm k)f_1 \tag{2.7}$$

Where j is the position of the harmonics at multiples of m_f and k are the adjacent harmonics.

For values of $m_f \leq 9$, the harmonic amplitude is independent from the frequency ratio, the harmonics are located at multiples of m_f:

For even multiples of the frequency ratio, j, the value of k must be odd, otherwise for odd j, k must be even. In table 2.1 are reported the normalized harmonics of $(\hat{V}_{A_0})_h/(1/2)V_d$ as function of the modulation ratio for value of $m_f \leq 9$.

Keeping in mind that the value of the voltage V_{AN} is:

$$V_{AN} = V_{A0} + \frac{1}{2}V_d, \tag{2.8}$$

The harmonic content of V_{AN} is the same of V_{A0}, so:

$$(\hat{V}_{AN})_h = (\hat{V}_{A0})_h \qquad (2.9)$$

h	m_a				
---	0.2	0.4	0.6	0.8	1.0
1	0.2	0.4	0.6	0.8	1.0
Fundamental					
m_f	1.242	1.15	1.006	0.818	0.601
$m_f \pm 2$	0.016	0.061	0.131	0.220	0.318
$m_f \pm 4$					0.018
$2m_f \pm 1$	0.190	0.326	0.370	0.314	0.181
$2m_f \pm 3$		0.024	0.071	0.139	0.212
$2m_f \pm 5$				0.013	0.033
$3m_f$	0.335	0.123	0.083	0.171	0.113
$3m_f \pm 2$	0.044	0.139	0.203	0.176	0.062
$3m_f \pm 4$		0.012	0.047	0.104	0.157
$3m_f \pm 6$				0.016	0.044
$4m_f \pm 1$	0.163	0.157	0.008	0.105	0.068
$4m_f \pm 3$	0.012	0.070	0.132	0.115	0.009
$4m_f \pm 5$			0.034	0.084	0.119
$4m_f \pm 7$				0.017	0.050

Table 2.1: Generalized Harmonics for large value of m_f [5]

Increasing the modulation ratio will reduce the harmonics content for high m_f multiples, at $m_a = 1$ and j=4, the normalized harmonic is less than the 10% of the first harmonic.

In order to reach an odd symmetry, m_f must be an odd integer. Therefore, $[\boldsymbol{f}(t) = -\boldsymbol{f}(t)]$, that results in a half period symmetry, namely $[\boldsymbol{f}(t) = -\boldsymbol{f}(t + 1/2 \cdot T_1)]$. With an odd m_f there will be the presence of only odd harmonics, since even harmonics are canceled.

2.4. Three Phase Inverter

A three-phase VSI (see fig: 2.5), has the same goal of a single phase inverter. Thanks to the use of Pulse Width Modulation, the output voltage is controlled in amplitude and in frequency with a DC voltage as input. With the objective to have a balanced three phase voltage as output, the voltage v_{tri} is compared with three sinusoidal control voltage that are 120° out of phase.
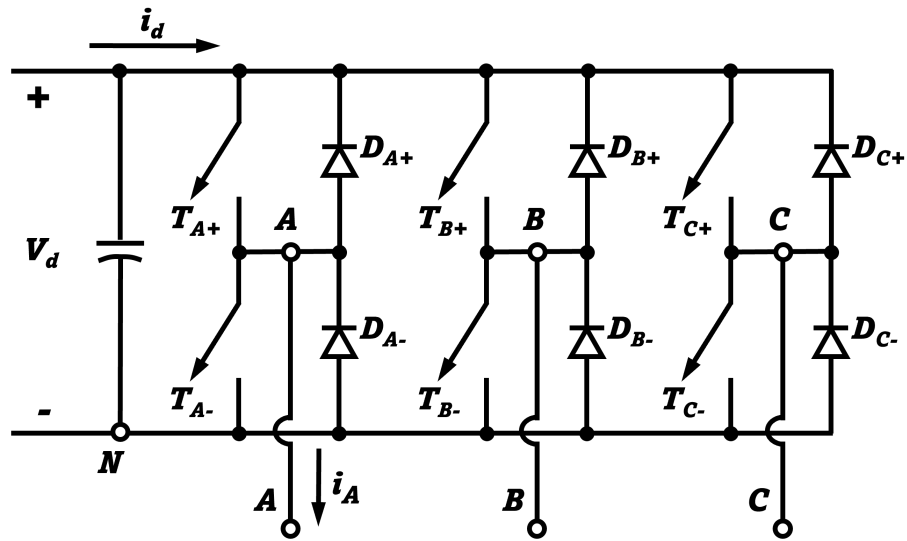
Figure 2.5: Three phase inverter [5]

The control voltages are reported in figure 2.6 where are displayed the three modulation signal as well as the carrier signal.
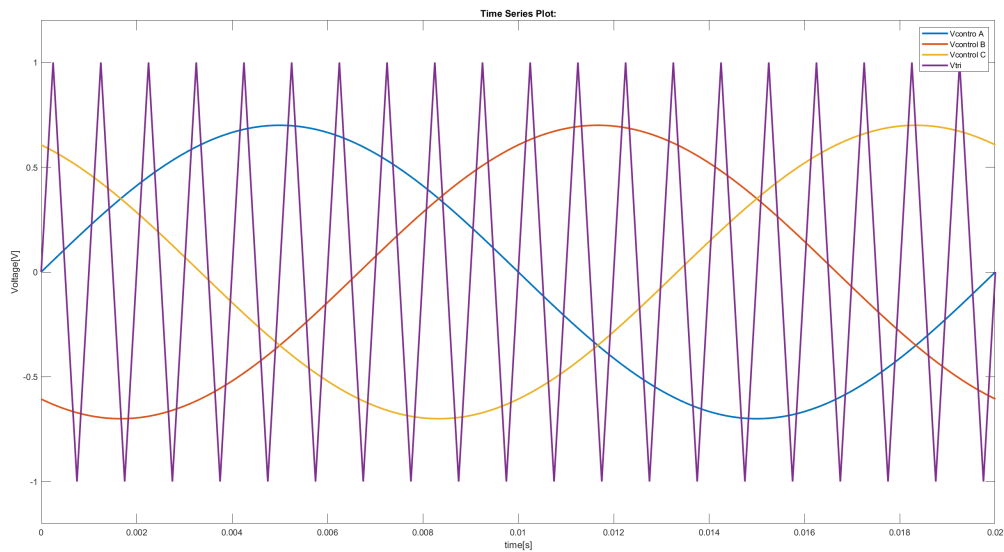
Figure 2.6: Three phase control voltage vs triangular waveform

In a three phase inverter, the harmonics content that is studied is related to the line-to-line voltage. Instead, the harmonics related to the phase voltage like V_{AN} are the same as the voltage V_{A0}: only odd harmonics are present if m_f is odd.

In this case, the harmonics of the line-to-line voltages are out of phase of $120 \cdot m_f$. For frequency ratios odd and multiple of three, thanks to the phase shift that is zero and the

phase shift between the harmonic m_f of the voltage V_{AN} and V_{BN} is equal to $120 \cdot m_f$, the harmonic located at m_f are equal to zero.

In this way the dominant harmonics, different from the fundamental, that are present in a single leg are eliminated in the line-to-line voltages of a three-phase VSI.

In order to cancel even harmonics with a low-frequency ratio, m_f must be odd and an integer if it should be synchronous, the multiple of three harmonics falls when m_f is a multiple of three.

If the m_f used is not integer, the inverter is controlled with an asynchronous PWM, in this condition there will be the presence of harmonics of order below one, which are called subharmonics.

This sub-harmonics are responsible for high currents, since the reactances are low at those frequencies, reducing the reactance will reduce the value of the impedance, in this way the circulating currents are higher. For this reason, the asynchronous PWM is avoided, also for high-frequency ratio.

2.4.1. Linear Zone and Over Modulation

The linear zone is achieved with a modulation ratio less or equal to one, in order to reach over modulation, m_a must be increased over one. The output voltage as for the single phase inverter is determined by the modulation ratio.

The voltage level is limited due to notches resulting in the output voltage, if there is the needs to increase the voltage output the modulation ratio must overcome 1. When the VSI is in this zone it is working with over-modulation, there is the presence of more side harmonics that are not present in linear zone. However with $m_a > 1$ the amplitude of the sideband harmonics is not high.

In over modulation the voltage of the first harmonics, does not change linearly with the modulation ratio.

With regard to the normalized harmonics of $(V_{LL})_h/V_d$ show an opposite behaviour with respect to the normalized harmonics of a single phase inverter, where $(\hat{V}_{A_0})_h/(1/2)V_d$ depends on m_a, here is possible to see that for a low value of the modulation ratio the m_f harmonic amplitude is lower then higher value of m_a as reported in the figure 2.7.

m_a h	0.2	0.4	0.6	0.8	1.0
1	0.122	0.245	0.367	0.490	0.612
$m_f \pm 2$	0.010	0.037	0.080	0.135	0.195
$m_f \pm 4$				0.005	0.011
$2m_f \pm 1$	0.116	0.200	0.227	0.192	0.111
$2m_f \pm 5$				0.008	0.020
$3m_f \pm 2$	0.027	0.085	0.124	0.108	0.038
$3m_f \pm 4$		0.007	0.029	0.064	0.096
$4m_f \pm 1$	0.100	0.096	0.005	0.064	0.042
$4m_f \pm 5$			0.021	0.051	0.073
$4m_f \pm 7$				0.010	0.030

Figure 2.7: Generalized harmonics of V_{LL} for large m_f [5]

The figure 2.7 shows that in the overmodulation, the losses due to these harmonics present in the linear zone could have a lower impact with respect the single phase inverter. This effect is given by the load and the switching frequency.

The figure 2.8 shows the amplitudes of the generalized harmonics, shown in the previous figure 2.7.
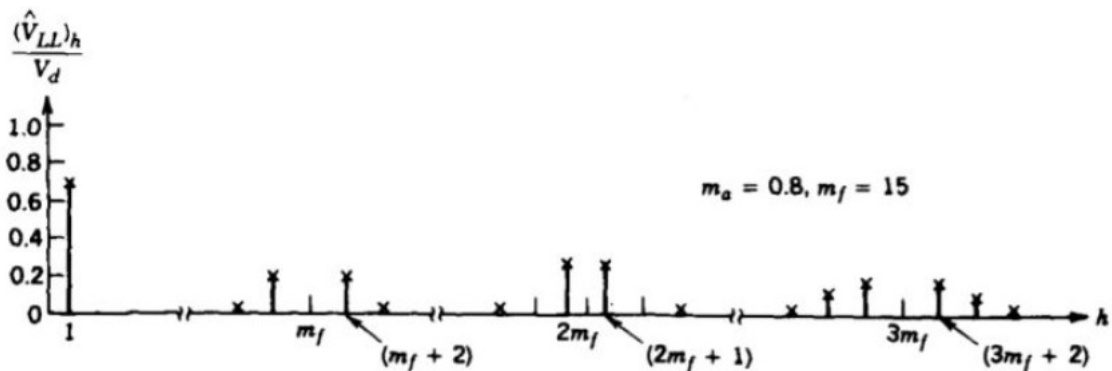
Figure 2.8: Generalized harmonics of V_{LL} for large m_f [5]

The figure 2.9 shows the graph with the zones: linear, overmodulation and square wave.
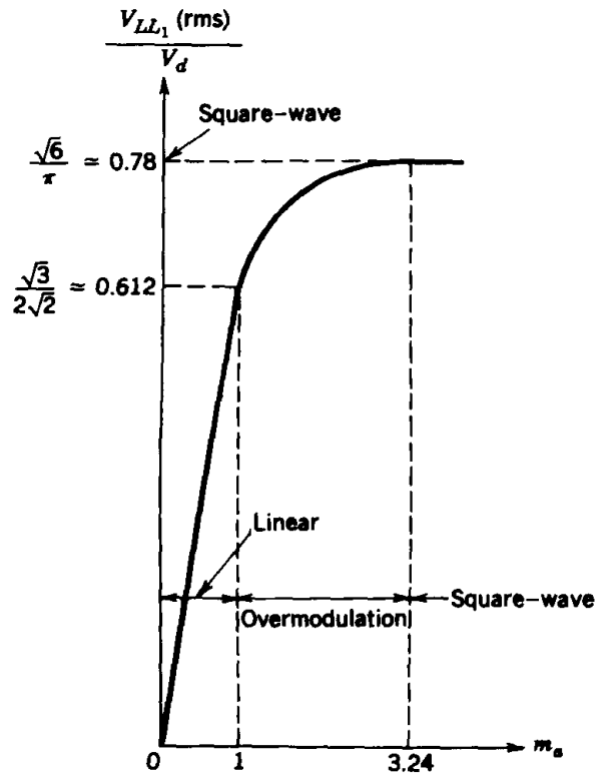
Figure 2.9: Generalized harmonics of V_{LL} for large value of m_f [5]

The values of the line to line voltage for m_a equal to one, can reaches up to $\dfrac{\sqrt{3}}{2\sqrt{2}}$, while in over modulation it can grow up to $\dfrac{\sqrt{6}}{\pi}$ with a $m_a = 3.24$.

The value reported in 2.9, in abscissa reports a value of m_a equals to 3.24. With that value of modulation ratio, the inverter is working in square wave, the intersection of v_{tri} and $v_{control}$ happens twice in a period, so the output voltage is maximum for one-half period, and minimum for the other.

As shown in figure 2.10, the maximum value of the voltage output is reached for $m_a \gg 1$.
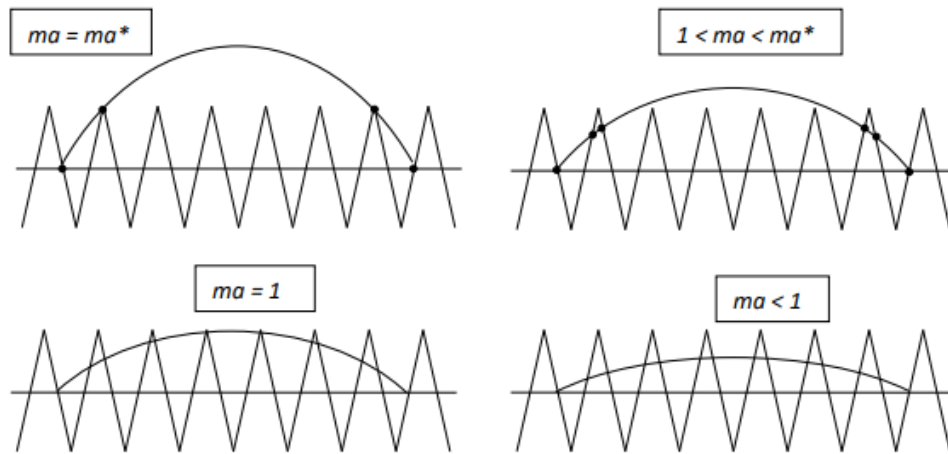
Figure 2.10: Possible scenarios for the comparison of control and carrier signals

To work in square wave m_a must be increased, up to m_a*, the value of the modulation ratio that works in square wave is as follow:

expressing v_{con} and v_{tri} in p.u. as: $v_{con} = m_a \cdot sin(\theta)$ and $\hat{V}_{tri} = 1$

the intersection of v_{con} and V_{tri} happens at:

for v_{tri} $\quad \theta = \pi \cdot \dfrac{3}{2}$

for v_{con} $\quad \theta = \pi \cdot \dfrac{3}{2} \dfrac{1}{m_f}$

considering $v_{con} = m_a \cdot sin(\theta)$

$v_{con} = m_a * \cdot sin(\pi \cdot 3/2/m_f)$,

since $v_{con} = \hat{V}_{tri} = 1$

so $m_a* = \dfrac{1}{sin(\pi \cdot 3/2/m_f)}$ $\quad$ for $m_f = 15 \quad m_a* = 3.24$

2.5. Conduction States

It has been seen that in a full-bridge converter, is important to specify the ON state phase and the conducting state phase of the MOSFET, which are two different phases. What determines the difference between the two phases is the presence of the free-wheeling Diode, placed antiparallel with the MOSFET.

The conduction of the MOSFET does not always occur when $v_{control} > v_{tri}$, but the switch

will see the current flowing from drain to source when the current is positive, in case it is negative, the current will flow through the free-wheeling Diode.

In some cases, it may happen that the current passes through two high-side MOSFETs and a high-side free-wheeling Diode, the positive current goes through the MOSFET and the negative current through the Diode (See fig: 2.11). In this case, during these periods the DC current is equal to zero because the switches are shorted. Under this condition, the output voltages are controlled acting on the duration of these short-circuit intervals.

In square-wave modulation these three-phase short-circuits are avoided.
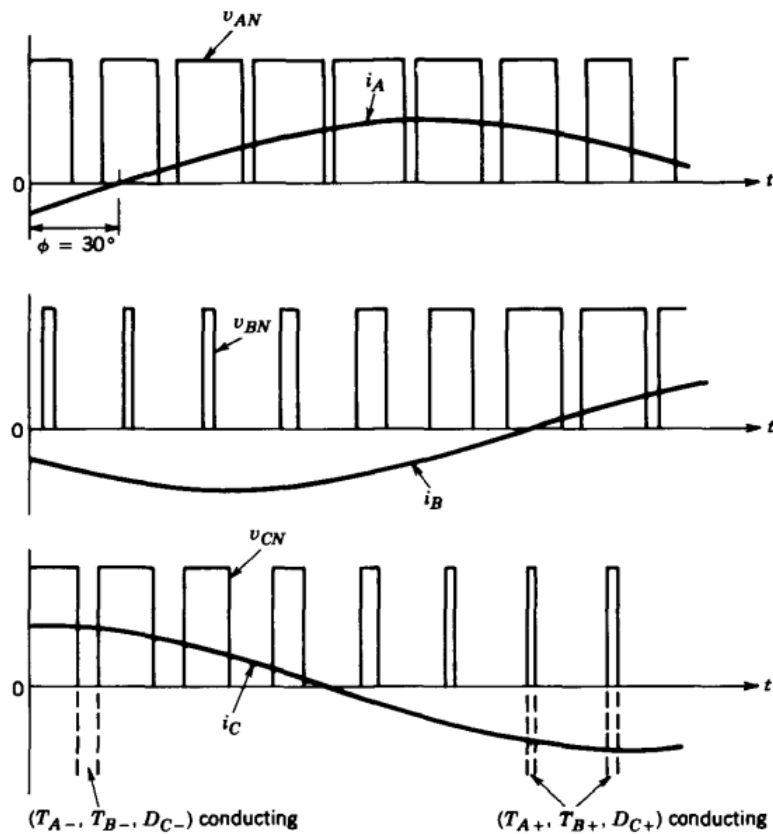
Figure 2.11: PWM three phase shorted, In the highlighted intervals, the current $i_d = 0$, the power does not come from the DC bus [5]

2.6. MOSFET Overview

In order to develop the three-phase inverter, MOSFETs were used as switches. The MOSFET together with the Diode are the basis of electronics. At the base of a electronic circuit there are other elements such as: resistor, inductor and capacitor. All these elements are included in an inverter.

The Diode is a two-terminal device and the MOSFET is a three-terminal device. A three-port device can be widely used in various fields, from signal amplification used in analog electronics to memory used and studied in digital electronics. The main groups of three-terminal devices are:

- The Metal-Oxide-Semiconductor Field-Effect Transistor, MOSFET

- Bipolar Junction Transistor, BJT

Each one has the same functions, but they offer unique features and are used in different area applications; in the last decade, the Mosfet became by far the most chosen. The MOSFETs compared to the BJTs are used for integrated circuits thanks to the smaller dimension and higher power handled. Nevertheless are more efficient, and now are widely used for analog and digital electronics.

Figure 2.12 reports the transversal section of a MOSFET.
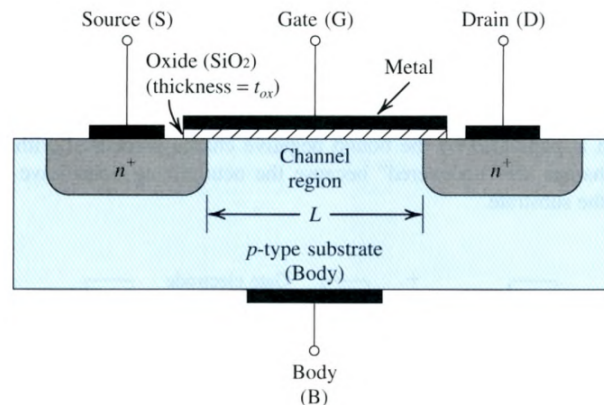
Figure 2.12: Cross section of a MOSFET transistor [8]

The structure of the transistor reported in figure 2.12, is built on a p-type substrate formed by a single crystal silicon wafer that guarantees support function. Two heavily doped n-type regions are inserted in the p-type substrate: one n-region creates the source terminal and the other creates the drain terminal.

A silicon dioxide material (SiO_2) of the thickness $\boldsymbol{t_{OX}}$ is mounted between the two n-type regions on the surface of the substrate, this oxide layer is used to insulate the two parts from the metal oxide base. On the silicon dioxide is mounted an electrode made of a metal called gate electrode. Drain, source, gate and the body have a metallic contact installed on them.

The n-region with the p-type substrate forms a $\boldsymbol{pn}$ junction: in this case, there are two

reverse junctions. The body pin is shorted with the source; for this reason, the device is named three terminal device. The body is shorted to the terminal with the lowest potential.

The gate is responsible for the current conduction between drain and source, electrons flow in a region called channel region, this path is characterized from a length and a width.

If zero voltage is applied to the gate, the two back to back Diode in series block the current, the resistance seen is infinite. In order to let the current flow in the n-channel, the channel region must be created. To this aim, a v_{gs} voltage must be applied to the gate, the electric field repels the free holes, which are the positive charge, from the substrate that is next to the gate (see fig: 2.13). The charges are attracted below the gate terminal creating a carrier depletion region, a region where the bound negative charges stand with the acceptor atoms. The charges are free because the neutralized holes are pushed into the substrate.
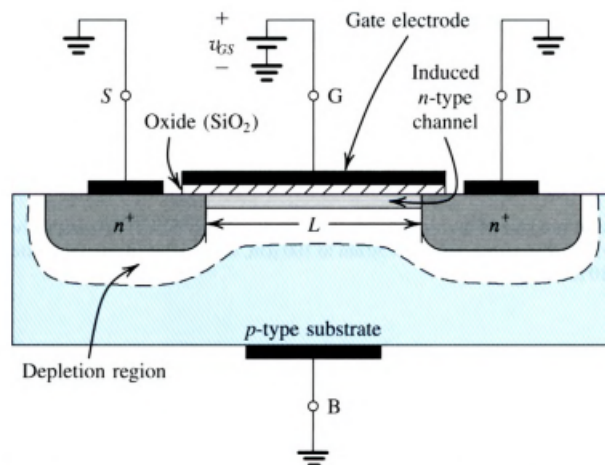
Figure 2.13: Creation of the depletion region [8]

During the operation of the device, the adjacent n-region donate the electrons in order to form the n channel, which is bounded between the silicon oxide and the p-type substrate. Thus, the path between drain and source is created. The minimum voltage applied to the gate that forms the channel is named threshold voltage V_T, which is in the range of 0.3-1 V for Si device while for the SiC is 1.8-3.6 V. The gate terminal sees a capacitor between the metal oxide and the substrate, where the silicon oxide is the medium, the metal oxide stores the positive charge, while the substrate recalls the negative charge. The electric field applied to the capacitor determines the conduction of the channel.

It is defined effective voltage, which is the voltage applied that determines the charge in

the channel,

$$\boldsymbol{v_{GS}} - V_T = v_{OV} \tag{2.10}$$

where v_{GS} is the voltage drop between Gate and Source and V_T is the treshold Voltage.

The magnitude of the charge in the n-channel is

$$|Q| = C_{OX}(WL) \cdot v_{OV} \tag{2.11}$$

Where C_{OX} is the oxide capacitance between the Metal and the substrate, W is the width and L is the length of the channel.

The electric field created by the voltage applied between drain and source is function of the length of the channel:

$$|E| = \frac{v_{DS}}{L} \tag{2.12}$$

Due to the applied elecric field, the electrons will drift with a speed determined by their mobility and by the electric field in which they are.

$$\text{Electron drift velocity} = \mu_n \cdot |E| = \mu_n \frac{v_{DS}}{L} \tag{2.13}$$

where μ_n is the mobility of the electrons.

It is clear that the materials that compose the three terminals device are connected to its performance.

The current that flows in the device is determined by:

$$i_D = (\mu C_{OX})\left(\frac{W}{L}\right)\left[(v_{GS} - V_T)v_{DS} - \frac{1}{2}v_{DS}^2\right] \tag{2.14}$$

For value of v_{DS} below V_{OV}, the MOSFET is working in Triode zone, area in which an increase of the voltage v_{DS}, means an increase of the current i_D, this is true up to $v_{DS} = V_{OV}$

If the voltage applied through the drain and source is higher than the effective voltage, the resistance increases. The curve $i_D - v_{DS}$ does not increase straightly but for values

of v_{DS} over V_{OV} the curve bends. In this portion, the n-channel is pinched-off, the shape of the channel does not change and the current does not increase. This phenomenon is called saturation, the MOSFET has entered the saturation region. The value of V_{DS} in saturation region is defined as:

$$V_{DS\,sat} = V_{OV} = V_{GS} - V_t \tag{2.15}$$

In figure 2.14 is reported the working regions of a MOSFET.
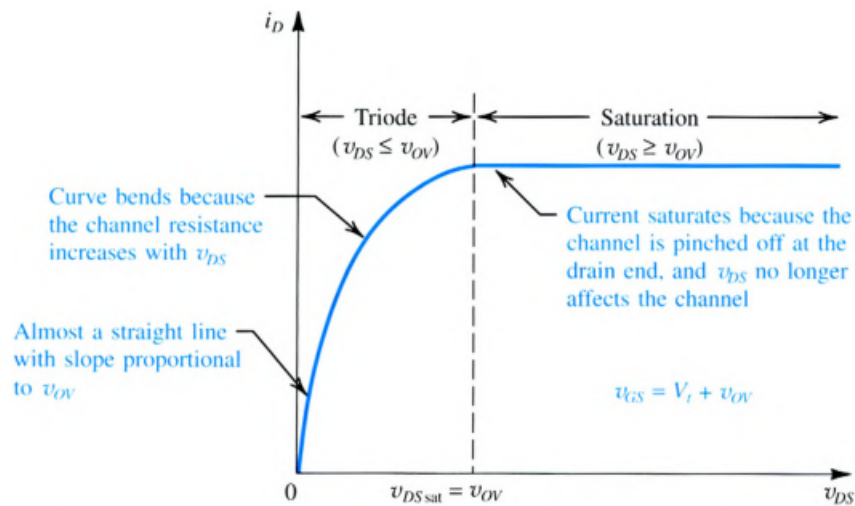
Figure 2.14: Drain current versus the drain-source voltage

2.6.1. MOSFET SiC: Advantages Over MOSFET Si

Silicon MOSFETs have been used for decades in the field of power electronics, they represent the basis of electronics. In the last fifteen years, thanks to new studies and the latest technological processes, new materials have been discovered.

In particular, Silicon Carbide, of which SiC MOSFETs and SiC diodes are made. In recent years, this new material has entered the market and is gradually taking the place of Si components. Over time, other materials such as GaN are becoming more and more popular.

Silicon carbide in the last years is the most requested material, it is replacing the Si device mostly for application in power electronics field. Nowadays it is possible to find SiC modules everywhere, in recent cars this material is found everywhere, from the microcontrollers that manage the lights to inverter for the wiper motors. This newer semiconductor

stands out because it offers more performance and facilitates some aspects that have been seen critical. Silicon carbide is becoming more and more popular and day after day it takes the place of traditional Si modules, for these reasons:

- Higher voltage rating in the same device dimension

- Wider bandgap that allows a better current conduction with reduced leakage current, the bandgap is the energy used to pass from the valence band to the conduction band

- Better thermal conductivity

- Lower level of energy losses

All these peculiarities of this material translate into the following characteristics, which traditional silicon did not have and which for years have been a huge problem to face in the design phases. SiC guarantees:

- Smaller level of switching losses

- Higher switching frequencies, that in some applications allow to avoid the use of filters

- Higher breakdown capacity, times and times higher than Si

- Higher working temperature that requests a smaller heatsink or permits higher current conduction

Since the performances are increased, also the price increase too. The cost for a single switch is ten times higher with respect to the same power characteristic of a Si MOSFET, but as previously mentioned it allowed the development of new product with higher efficiency.

The field of semiconductors is always growing, the market requests to reduce the volume of each component in order to build it always much smaller than its predecessor. Because in this way it is possible to increase the power density, especially in system-in-package products.

All the advantages described above are extremely useful in the automotive field, SiC plays a key role in particular for:

- reducing current and current ripples (meaning lower power loss)

- reducing mass (meaning, lighter vehicles)

These advantages are even more significant when the system is an electric vehicle, equipped with a battery, where energy is limited. The main goal for companies involved in the automotive field is to reduce power losses and increase the effiency, these two main characteristics make a product the best on the market.

2.6.2. SiC Manufacturing Process

All the aforementioned advantages of silicon carbide over silicon semiconductors are given by its composition. It is a rare earth material, almost scarce on the earth's surface. It is obtained chemically as follows:

- Powder preparation
  Silicon Carbide is made by Silicon and Carbon. The easiest production process request to combine silica sand and carbon in an electric furnace with graphite resistance. The oven is brought up to 2500°C. The creation of Silicon Carbide particles is achieved when the carbon excess is heated with the silica sand. The silica fume that is part of the byproduct reaction, can be turned into SiC with graphite at 1500°C. The final products are stone and grains of SiC, that are smashed in fine powder. The powder then will be purified using halogens.

- Kneading
  The fine grain powder is mixed with non-oxide sintering aids, that are non-oxide; the result of this phase is a paste.

- Shape
  The paste obtained in kneading phase, which is shaped by extrusion or with a cold isostatic process

- CNC machining
  A computer numerical control is used to machine the plates, this phase is critical due to the lower mechanical resistance of the material. The CNC will drill and mill the product giving the final shape.

- Sintering
  In this phase the machined product is sintered, at specific condition, with an inert atmosphere at the temperature of 2300° C. After the sinteresis the product volume is shrinked isostatically by around 20%.

- Lapping
  If needed after the sintering process the product could be machined again, using even finer machining, with diamond grinding or lapping techniques.

- The last part of the process is the quality check, where the characteristics of the product are evaluated in order to go further in the MOSFET and Diode production.

Silicon Carbide is the second hardest material on heart, is very difficult to machine, for the entire process advanced machine are needed, this process requests high quality equipment that are expensive.

2.6.3. Gallium Nitrate Semiconductors

In recent years another important material has been introduced gallium nitrate, which belongs to the wide bandgap family of materials.

GaN is not a new material, in fact it has been used in the past for 30 years to build bright LEDs. Before being used as a MOSFET, it was used for applications related to optical phenomena. For example, it is used in Blu Ray devices to read blue light.

Thanks to new production processes, companies have halved the costs associated with the production of this material. The new production process involves the deposition of GaN in the vapor phase, above a layer formed by aluminum and nitrate which insulates the silicon layer. This process greatly reduces costs, in this way it has been possible to increase production and therefore the use in many applications.

All of these technologies are the result of study and research. The next step is to be able to make the best use of the new technology, and herein lies the biggest challenge for the big semiconductor companies.

Gallium Nitrate semiconductor is the best material for high switching frequency applications thanks to its high electron mobility, low turn-on resistance and high switching frequency. GaN together with Silicon Carbide changing power electronics, thanks to their almost complementary characteristics.

Today they are the most demanded items on the market, since the power density is increasing day by day and the dimension of the system in package product is always lower, for some particular components there are waiting lists of more than 40-50 weeks. The biggest difference between SiC and GaN materials is certainly the thermal conductivity, Gallium Nitrate having a lower value than Silicon Carbide. GaN is in fact not used for power applications. See fig: 2.15.

Each material has its bandgap which is the energy difference between the conduction energy bands and the valence. The materials exposed before have different characteristics given by the chemical elements of which they are made.
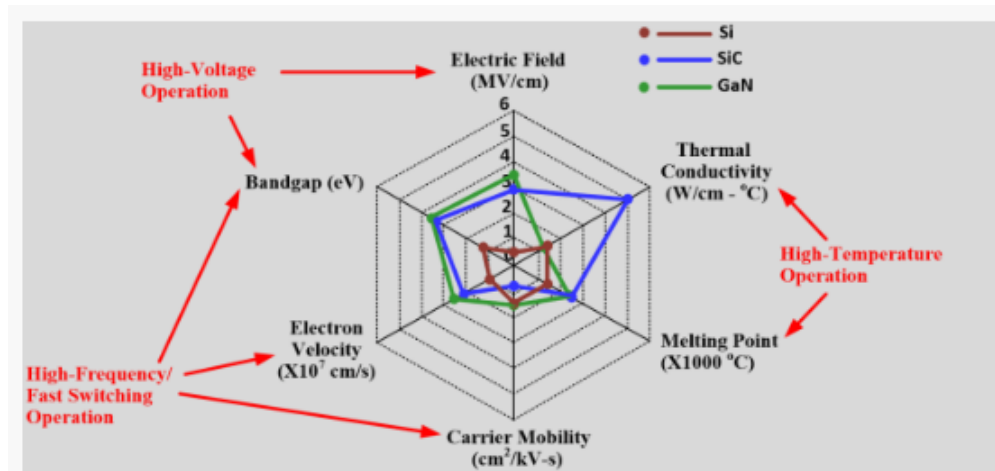
Figure 2.15: Plot comparing Si, SiC and GaN semiconductors [2]

- Band gap

  It is the energy used to pass from the valence band to the conduction band. For the semiconductor 5 eV is the maximum energy needed to tear electrons from the valence band. Insulator materials have more than 5 eV and the conductor materials do not need energy to pass from valence band to conduction band.

- Electric field intensity

  Known also as the breakdown voltage, is the maximum voltage that can be applied between drain and source. If that values is overcome avalanche breakdown occurs. From an electronic point of view, the breakdown value is the value where the valance electrons are ripped off.

- Thermal conductivity

  Express as the heat that flows in per unit time through a surface. Higher value of thermal conductivity means better heat management.

- Electron Saturation Velocity

  It is the maximum velocity of an electron, to move in a semiconductor material in presence of an electric field. High saturation velocity means high switching frequency.

- Carrier / Electron Mobility

  It is the velocity of a charge to fill a hole or viceversa pulled or pushed by the electric field.

Carrier or Electron mobility is a function of the applied voltage, while Electron Saturation Velocity is not a function of the voltage applied. In figure 2.16 are reported all the values

concerning the physical aspects of the three semiconductors material.

Figure 2.16: Principal physical characteristics comparison between Si, SiC and GaN [9]

Figure 2.17 shows a graph where are listed all the range of applications in which semiconductors perform best. It can be seen that Si is not limited in terms of demanded power, but it is limited in terms of switching frequency. Si MOSFETs are still used in many fields of application.
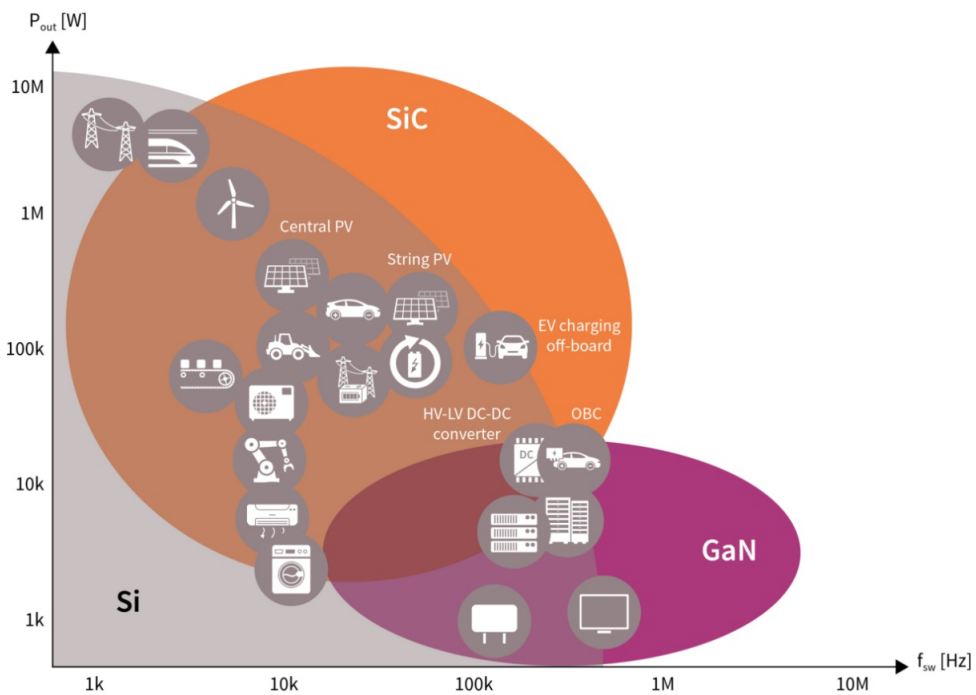
Figure 2.17: Si, SiC & GaN Application Fields [4]

Gan and SiC cover almost all the chart, and the shared area of SiC and GaN, is smaller than the shared area of SiC and Si.

Looking at the chart in fact, is possible to see that Gallium Nitrate is used for those applications that handle small power, they are more suitable for data applications, where it is required to reach very high-frequency values.

GaN reaches a switching frequency that Si and SiC couldn't explore. SiC could explore power already handled by the Si MOSFET, but GaN overcome the switching frequency used until now.

The shared area between Si and SiC represents the power electronics field moving more and more toward SiC with the need to increase the frequency of control devices(2.17).

SiC and GaN, are the key element of the rise of electric vehicles, with the same performance with a Si MOSFET, the two materials are significantly smaller in size.

To increase efficiency and reduce the total footprint of the power converter, many power converter manufacturers have turned to SiC technology.

The automotive field is the sector that is pushing the most on the use of these new materials, because they are able to guarantee unrivaled efficiency and performance.

2.7. MOSFET Used In The Three-Phase Inverter

To create this three-phase inverter, various datasheets were viewed, and the choice was immediately oriented towards a SiC module, based on the properties and characteristics already expressed in this chapter.

Different modules with different characteristics have been seen. Mainly the discriminant was the maximum current of the single MOSFET.

Subsequently, various characteristics are analysed, the main features that were taken into account were:

- The maximum allowable current of the switch, I_D

- The voltage, mainly SiC modules have a maximum voltage between Drain and Source of 650/1200/1700V

- A low value of R_{DSON}

- Low switching losses

One of the most important semiconductor manufacturers and developers of WBG is Wolfspeed, its business is mainly oriented to products using SiC and GaN materials. It offers different solutions according to the application.

Wolfspeed produces different products, providing different packages for the same component based on application and installation. It also provides support, CAD and Spice models of the products.

The choice of the MOSFET is oriented to C3M0015065, which is a Silicon Carbide MOSFET N-channel, that is available in two different packages. The first one is the C3M0015065D which is a TO 247-3L and the second one C3M0015065K which is a TO 247-4L. In fig 2.18 there is the representation of the 4 pins terminal.
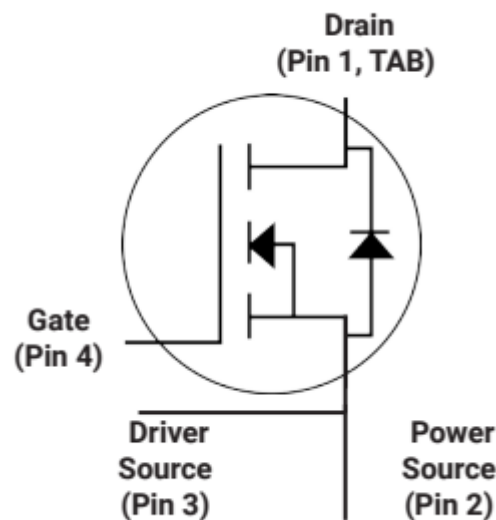
Figure 2.18: 4 pins Mosfet package

The C3M0015065 Device has the following feature:

- Optimized package with separate driver source pin

- 8 mm of creepage distance between drain and source

- High blocking voltage with low on-resistance

- High-Speed switching with low capacitances

- Fast intrinsic diode with low reverse recovery (Q_{irr})

This power module has several characteristics oriented in power application, the main features given by the use of this MOSFET are:

- Reduce switching losses and minimize gate ringing

- Higher system efficiency

- Reduce cooling requirements

- Increase power density

- Increase system switching frequency

All these features are useful in applications that requires high power densities, such as:

- Traction inverter

- EV chargers

- Solar inverters

- DC/DC power converters

The main parameters of this MOSFET have the following values:

Name	Description	Value	Unit
$V_{DS_{max}}$	Drain - Source Voltage	650	V
$V_{GS_{max}}$	Gate - Source Voltage	-8/+19	V
I_D	Continuous Drain Current, $V_{GS_{max}} = 15V$ $T_c = 25°C$	120	A
I_D	Continuous Drain Current, $V_{GS_{max}} = 15V$ $T_c = 100°C$	96	A

Table 2.2: SiC C3M0015065, main features

Another parameter that is equal for the two packages is the resistance $R_{DS_{ON}}$, which has the same behaviour when varying the junction temperature for a given current. The values are expressed in per unit, p.u. The resistance can be up to 30 % higher than its nominal value at high temperatures. It is also interesting to note that at low temperatures, the value is higher than the value in the 20-50 degree temperature range.

In figure 2.19 is reported the dependence of the $R_{DS_{ON}}$ from the junction temperature.
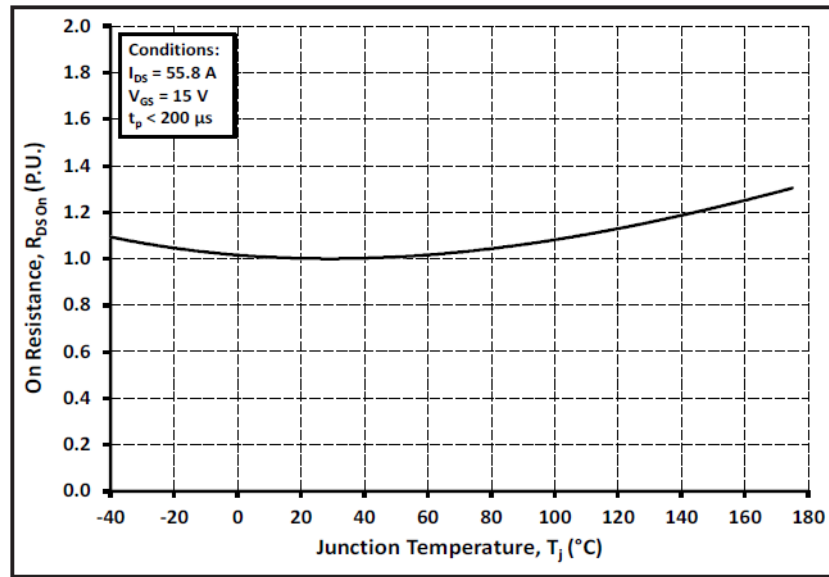
Figure 2.19: Normalized On-resistance vs. Temperature [11]

The main characteristics of the two packages are the same, but what is different is the rise and fall time of the voltage.

The difference in time between the two modules gives different energy loss during the switching transient.

Name	Description	C3M0015065K	C3M0015065D	Unit
$t_{d_{(on)}}$	Turn-On Delay Time	23	22	ns
t_r	Rise Time	32	125	ns
$t_{d_{(off)}}$	Turn-Off Delay Time	57	58	ns
t_f	Fall Time	15	25	ns

Table 2.3: C3M0015065D vs C3M0015065K Time comparison.

It is evident that the turn-On delay and turn-Off delay time is the same, but the rise time is almost four times higher for the Package with three pins, which increase the energy loss during the turning-ON.

In the datasheet is reported also the graph of Energy loss as a function of the Current, as reported in the figure below.
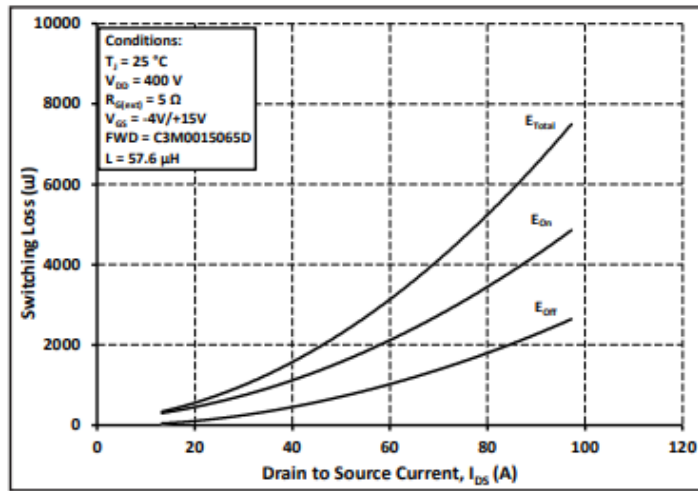
Figure 2.20: C3M0015065D Package, Energy loss by current I_{DS} [10]
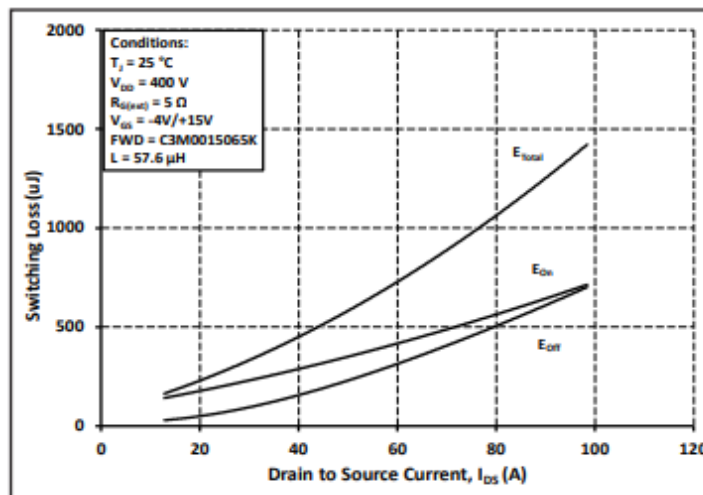
Figure 2.21: C3M0015065K Package, Energy loss by current I_{DS} [11]

From the graphs (fig: 2.20 and 2.21) it is possible to see that the condition tests are the same. The Energy loss amount is different, for series D the energy loss at 80 A reaches 5200 μJ while the K series arrives below 1200 μJ. In terms of saved energy, the series K is better.

At high current the energy saved is high, also for a medium current for example at 50 A the saved energy is considerable, for the K series the energy loss amount to 600/700 μJ, while the D series spreads 2300/2400 μJ, the relationship between them is approximately 1:4.

During estimating the losses, this Energy difference has been taken into account. Because

it's a huge difference.

If, on the other hand, one looks at the curves of lost energy as a function of temperature at a given current, one can see that the influence of junction temperature on switching losses is almost irrelevant. It can be seen that the variation is less than 10%, with 50/60% of the rated load at maximum temperature. For switching frequencies within 40 kHz there is a power loss variation of 2 W.

In figure 2.22 are reported the Energy losses at a given RMS current of 55,8 A.
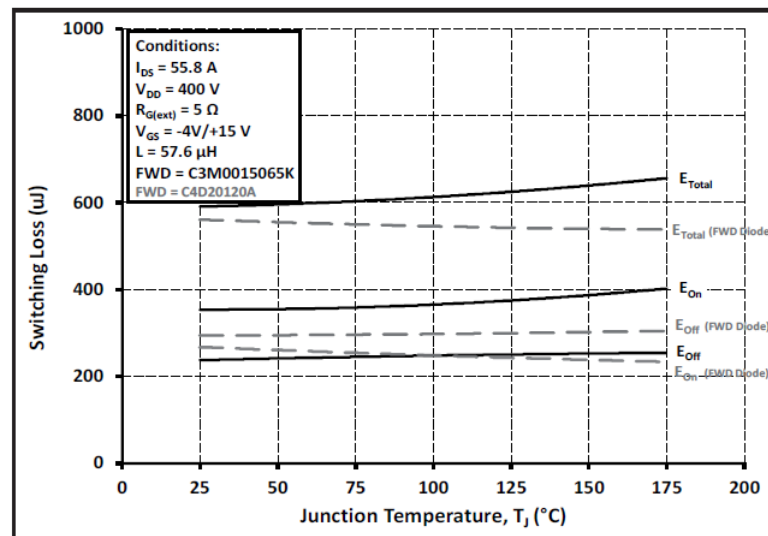
Figure 2.22: Clamped Inductive Switching Energy vs Temperature [11]

2.8. Power Losses of a MOSFET

The MOSFET and Diode are built in materials which have a resistance, the dimensions of the channel determine it. A voltage drop is formed when current flows through the channel, thus producing a loss of power which must be dissipated.

The turning on and turning off of the device is not instantaneous, it last 10/100 nanoseconds, in this period current and voltage are not zero, thus produces energy that is lost. The current takes a while when passes from zero, to the current value absorbed by the load; also the voltage takes a while when passes from U_{DC} to the voltage drop on it, thus the product of voltage and current is not zero.

This phenomenon takes place each time the switch is open or closed, in a period happens twice, so there is a loss in ON state and OFF state. The period considered is referred to the carrier signal.

2.8.1. Conduction Losses

Conduction losses occur when the device is conducting current, the flow of electrons produces heat, due to the resistance of the path, this effect is called Joule Effect.

In a MOSFET the conduction losses can be calculated with an approximation using the drain-source on-state resistance R_{DSon}.

$$u_{ds}(i_T) = R_{DSon}(T_j) \cdot i_T \tag{2.16}$$

Where u_{DS} is the voltage drop between the drain and the source, and i_T is the load current, the value of $R_{DSon}(i_D)$ is a function of the temperature: it has a nominal value which can vary due to the junction temperature. The current passing through the switch produces a Joule effect due to R_{DSon}. Therefore, the power loss can be estimated as:

$$p_{CM}(t) = u_{DS}(t) \cdot i_T(t) \tag{2.17}$$

$$= R_{DSon}(i_T) \cdot i_T^2(t) \tag{2.18}$$

By integrating the power over the whole period it is possible to evaluate the power losses during a period of the fundamental. The result is the average conduction loss.

$$P_{CM} = \frac{1}{T} \int_0^T p_{CM}(t)\, dt \tag{2.19}$$

$$= \frac{1}{T} \int_0^T R_{DSon} i_T^2(t)\, dt = R_{DSon} \cdot I_{TRMS}^2 \tag{2.20}$$

where i_T is the instantaneous current and i_{TRMS} is the root mean square value of the current over a period during the ON-state current.

For these calculations, the variation of $R_{DS_{ON}}$ as a function of temperature has not been taken into account.

MOSFET allows current to flow in one direction, but since the current is alternating, the conduction period is halved. Since conduction occurs for a period equal to T/2, it is possible to evaluate the integral over T/2.

The previous formula considers the load current, since the losses are considered only in one MOSFET, it is necessary to consider the duty cycle δ.

It is therefore possible to express the losses on a single MOSFET, considering the duty cycle and the load current in the following way:

$$P_{CM} = \frac{1}{T} \int_0^{T/2} p_{CM}(t)\, dt$$

$$= \frac{1}{T} \int_0^{T/2} \delta(t) \cdot V_{DS} \cdot i_L(t)\, dt$$

$$= \frac{1}{T} \int_0^{T/2} \left[\frac{1}{2} + \frac{1}{2} M \cdot sin(\omega t + \phi)\right] \cdot \left[V_{DS} \cdot i_M \cdot sin(\omega t)\right] dt$$

$$= \frac{1}{2} \cdot V_{DS} \cdot I_M \cdot \frac{1}{T} \int_0^{T/2} [1 + M \cdot sin(\omega t + \phi)] \cdot sin(\omega t)\, dt$$

$$= \frac{1}{2} \cdot V_{DS} \cdot I_M \cdot \frac{1}{\omega T} \int_0^{\pi} [1 + M \cdot sin(\omega t + \phi)] \cdot sin(\omega t)\, d\omega t]$$

$$= \frac{V_{DS} \cdot I_M}{4\pi} \left[\int_0^{\pi} sin(x)\, dx + M \cdot \int_0^{\pi} sin(x + \phi) \cdot sin(x)\, dx\right]$$

$$= \frac{V_{DS} \cdot I_M}{4\pi} \left[\int_0^{\pi} sin(x)\, dx + M \cdot \int_0^{\pi} \frac{1}{2}[cos(x + \phi - x) - cos(x + \phi - x)]\, dx\right]$$

$$= \frac{V_{DS} \cdot I_M}{4\pi} \left[\int_0^{\pi} sin(x)\, dx + \frac{M}{2} \cdot \left[cos\phi \int_0^{\pi} dx - \int_0^{\pi} cos(2x + \phi) \cdot dx\right]\right]$$

The third term is equal to zero due to the considered period:

$$\int_0^{\pi} cos(2x + \phi) \cdot dx = 0 \tag{2.21}$$

The presence of the cosine introduces an element that depends on the phase shift of the load: if the load is purely inductive the cosine is equal to zero. This case gives low losses, but the load is purely inductive. Instead a load without the presence of the inductance has a cosine equal to one, which is the worst scenario with high losses.

So the conduction losses of the MOSFET are equal to:

$$P_{CM} = \frac{V_{DS} \cdot I_M}{4\pi} \left[2 + \frac{M}{2} \cdot cos\phi \cdot \pi\right] = V_{DS} \cdot I_M \cdot \left(\frac{1}{2\pi} + \frac{M}{8} \cdot cos\phi\right) \tag{2.22}$$

It is possible to see that the losses also depend on the modulation ratio; for high values of m_a around one or higher the contribution is maximum.

With this formula is possible to see that the losses are function of:

- Maximum current I_M

- The voltage drop v_{DS}

- Modulation ratio

- The load angle

While the conduction losses related to the free-Wheeling Diode are:

$$P_{CD} = \frac{1}{T} \int_0^{T/2} p_{CD}\, dt$$

$$= \frac{1}{T} \int_0^{T/2} [1 - \delta(t)] \cdot V_d \cdot i_L(t)\, dt$$

$$= \frac{1}{T} \int_0^{T/2} \left[1 - \frac{1}{2} - \frac{1}{2} \cdot M \cdot sin(\omega t + \phi)\right] \cdot \left[V_D \cdot i_M(t) \cdot sin(\omega t)\right] dt$$

$$= \frac{1}{T} \int_0^{T/2} \frac{1}{2} V_D \cdot I_M \cdot sin(\omega t)\, dt - \frac{1}{T} \int_0^{T/2} \frac{1}{2} \cdot M \cdot V_D \cdot I_M \cdot sin(\omega t + \phi) \cdot sin(\omega t)\, dt$$

$$= \frac{V_D \cdot I_M}{2T} \int_0^{T/2} sin(\omega t)\, dt - \frac{M \cdot V_D \cdot I_M}{2T} \int_0^{T/2} sin(\omega t + \phi) \cdot sin(\omega t)\, dt$$

$$= \frac{V_D \cdot I_M}{2T\omega} \int_0^{\pi} sin(x)\, dx - \frac{M \cdot V_D \cdot I_M}{2T} \int_0^{T/2} \frac{1}{2}\left[cos(\omega t + \phi - \omega t) - cos(\omega t + \phi + \omega t)\right] dt$$

$$= \frac{V_D \cdot I_M}{2T\omega} [-cosx]_0^{T/2} - \frac{M \cdot V_D \cdot I_M}{4T} cos\phi \int_0^{\pi} dt + \frac{M \cdot V_D \cdot I_M}{2T} \int_0^{T/2} \frac{1}{2} cos(2\omega t + \phi)\, dt$$

$$= \frac{V_D \cdot I_M}{T\omega} - \frac{M \cdot V_D \cdot I_M}{4T\omega} cos\phi \frac{T}{2}$$

$$= \frac{V_D \cdot I_M}{2\pi} - \frac{M \cdot V_D \cdot I_M}{8} cos\phi$$

The third term is equal to zero due to the considered period:

$$\int_0^\pi cos(2x + \phi) \cdot dx = 0 \tag{2.23}$$

So it is possible to express the conduction losses relative to the Diode with:

$$P_{CD} = V_D \cdot I_M \cdot \left(\frac{1}{2\pi} - \frac{M}{8} \cdot cos\phi \right) \tag{2.24}$$

It is possible to see that there is a difference between the two terms, if the cosine is equal to zero, the power loss is maximum. The inductive load asks for a continuous drain current in order to maintain the energy continuous, the current can not go to zero in an instant.

2.8.2. Switching Losses

Switching losses depend on the component; it was briefly mentioned at the beginning of the section how this energy is lost during the transition phase from the On to Off state and vice-versa. Regardless of the component, there will always be energy lost because voltage and current rising edges have no infinitesimal time. The rise and fall times depend on the component, its turn-on response, its characteristics, and also the drive circuit.

Calculation Switching Losses

Switching losses, are calculated on the basis of the switching frequency, because the on-off phase of the switch happens twice in a switching period.

There are two state transitions, that are an ON-phase and an OFF-phase of the switch.

$$\boldsymbol{P}_{ON} = \frac{1}{T} \int_0^{T_{ON}} u_{DS}(t) i_D(t) \, dt \tag{2.25}$$

$$\boldsymbol{P}_{OFF} = \frac{1}{T} \int_0^{T_{OFF}} u_{DS}(t) i_D(t) \, dt \tag{2.26}$$

where:

- T - switching period,

- $u_{DS}(t)$ - drain-source voltage drop during the transistor conduction,

- $i_D(t)$ drain current,

- t_{ON} mosfet turning ON time,

- t_{OFF} mosfet turning OFF time.

With the data taken from the datasheet is possible to quantify the losses through the aforementioned formula using voltage drop on the Switch, the rise time and the fall time. Alternatively, is possible to use the test condition reported in the datasheet, where there are the calculations done by the manufacturer. The rigorous calculation is done by performing the integral of the energy that passes through the switch, because it is load dependent.

In figure 2.23), are reported the voltage and current of the gate, while in the second chart of 2.23) are reported the voltages and currents flowing through the drain and source.
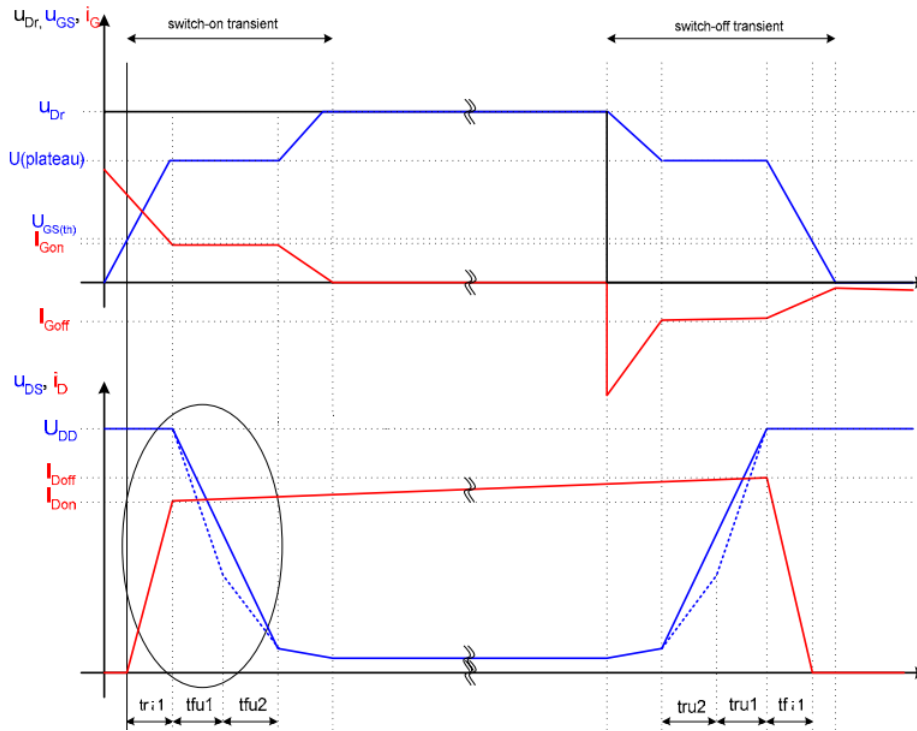
Figure 2.23: Turning ON and Turning OFF transients [1]

In figure 2.23 are reported the following quantities:

- t_{ru} is the rise time of voltage

- t_{fu} is the fall time of voltage

- t_{ri} is the rise time of current

- t_{fi} is the fall time of current

Figure 2.24 shows the rise and fall times of the current and voltage, where the transient

period is highlighted. In figure 2.24
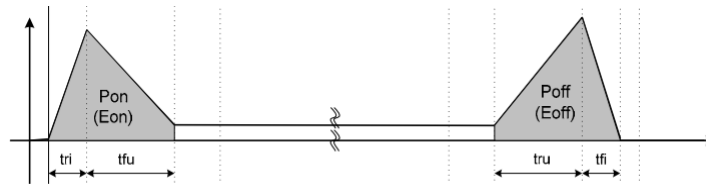
Figure 2.24: Turning ON and Turning OFF Power losses [1]

During the switch-on phase, the freewheeling Diode increases the current in the switch, releasing a peak current that flows through the MOSFET. This current comes from the inductance of the circuit; increasing the current means increasing the energy flowing through the junction. (see fig: 2.25)
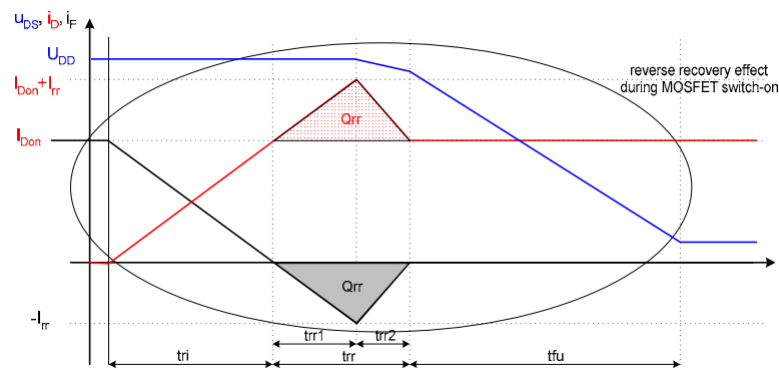
Figure 2.25: Diode recovery current delivered to the Mosfet [1]

2.8.3. Switch-On Transient
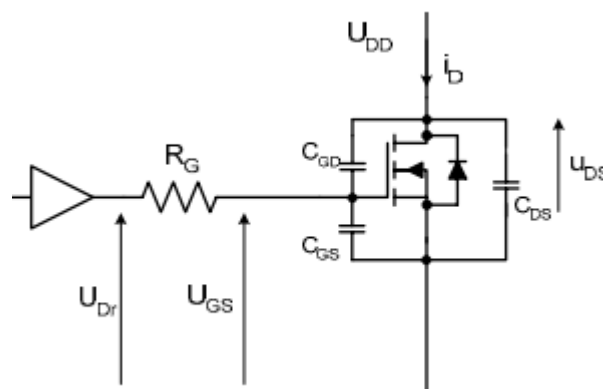
Figure 2.26: MOSFET + Free-Wheeling Diode [1]

The driver circuit (see fig: 2.26) supplies a voltage from 0 to u_{Dr}, with a time constant defined by the gate resistance and the input capacitance of the MOSFET. The input capacitance is defined as: $C_{iss}=C_{GD}+C_{GS}$, respectively C_{GD} is the capacitance between gate and drain and C_{GS} is the capacitance between gate and source.

The output of the MOSFET doesn't change until the voltage reaches the value of $U_{GS(th)}$. At this point the transient starts the current rise period $\boldsymbol{t_{ri}}$. The current I_D passes through the MOSFET while the free-wheeling Diode is conducting too, as reported in the figure of the Diode (see fig: 2.25). The Diode conducts until the voltage reaches the value of U_{DD}.

The Diode conduct until it removes all the stored carrier, the recovery current of the Diode will be absorbed by the MOSFET increasing the power losses. The amount of the stored carrier of the Diode is defined by Q_{rr} and the transient of discharge last for t_{rr}.

2.8.4. Swtiching Off Transient

The switching OFF process is similar to the switching ON transient, but the order of the phenomena is reversed. Moreover, during the turning OFF there is not the presence of the reverse recovery current caused by the Diode. In fact in the figure of the Diode 2.25 is possible to see that the effect of the current release happens once in a carrier period.

2.8.5. Switching Losses Calculation

Typically the switching losses are expressed in Energy lost, they are calculated for the MOSFET in both transitions and for the Diode only the energy lost at turn-on is considered.

They can be calculated in the following way.

$$E_{onMOS} = \int_0^{t_{ri}+t_{fu}} u_{DS}(t)i_D(t)\,dt = U_{DD} \cdot I_{Don} \cdot \frac{tri + tfu}{2} + Q_{rr} \cdot U_{DD} \qquad (2.27)$$

$$E_{offMOS} = \int_0^{t_{ru}+t_{fi}} u_{DS}(t)i_D(t)\,dt = U_{DD} \cdot I_{Doff} \cdot \frac{tru + tfi}{2} \qquad (2.28)$$

$$E_{onDIODE} = \int_0^{t_{ri}+t_{fu}} u_D(t)i_F(t)\,dt = E_{onDIODErr} = \frac{1}{4} \cdot Q_{rr} \cdot U_{Drr} \qquad (2.29)$$

The switching losses in the MOSFET and in the Diode are the product of the energy and

the carrier frequency, that is the frequency at which the reverse recovery occurs.

$$P_{swMOSFET} = (E_{onMOSFET} + E_{offMOSFET}) \cdot f_{sw} \tag{2.30}$$

$$P_{swDiode} = (E_{onDIODE} + E_{offDIODE}) \cdot f_{sw} = E_{onDIODE} \cdot f_{sw} \tag{2.31}$$

Since the manufacturer does not state the value of t_{ri} and t_{fi} on the data sheet, but only the rise and fall time of the voltage, it is not possible to do these rigorous calculations, so another approach has been used.

An alternative to the method just described, is to consider energy loss curves. With the curves of E_{ON} and E_{OFF} given on the data sheet, it is possible to calculate the energy loss considering:

- I_M the maximum value of current for the application

- V_{DS} value of the voltage applied on the MOSFET

- V_{OFF} value of the voltage applied on the MOSFET when it is reverse biased, equal to the voltage applied to the DC bus

- E_{ONM} and E_{OFFM} the maximum Energy loss with I_M

- $i_l(t)$ drawn current

From the lost energy curves, the maximum current value is fixed, from which the maximum lost energy values are derived.

$$E_{ON}(t) = E_{ONM} \frac{V_{DD}}{V_{DS}} \frac{i_t(t)}{I_M} \tag{2.32}$$

$$E_{OFF}(t) = E_{OFFM} \frac{V_{DD}}{V_{DS}} \frac{i_t(t)}{I_M} \tag{2.33}$$

Since E_{ON}, E_{OFF}, V_{CE} and I_M are constants, it is possible to seen K_{ON} and K_OFF as two time constants:

$$K_{ON} = \frac{E_{ONM}}{V_{CE} \cdot I_M} \tag{2.34}$$

$$K_{OFF} = \frac{E_{OFFM}}{V_{CE} \cdot I_M} \tag{2.35}$$

The two constants are seen as time intervals, which expresses how long a current is applied.

$$E_{ON}(t) = K_{ON} \cdot V_{DD} \cdot i_t(t) \tag{2.36}$$

$$E_{OFF}(t) = K_{OFF} \cdot V_{DD} \cdot i_t(t) \tag{2.37}$$

Multiplying the energy by the switching frequency is possible to obtain the power losses during the switching phase.

$$p_{ON}(t) = E_{ON}(t) \cdot f_s = K_{ON} \cdot V_{DD} \cdot i_t(t) \cdot f_s \tag{2.38}$$

$$p_{OFF}(t) = E_{OFF}(t) \cdot f_s = K_{OFF} \cdot V_{DD} \cdot i_t(t) \cdot f_s \tag{2.39}$$

In order to obtain the power loss over a period of the fundamental, a suitable integration should be performed.

$$P_{ON} = \frac{1}{T} \int_0^{T_{ON}} p_{ON}(t)\, dt, \tag{2.40}$$

$$P_{OFF} = \frac{1}{T} \int_0^{T_{OFF}} p_{OFF}(t)\, dt \tag{2.41}$$

3 | Thermal Analysis

3.1. Thermal Model

The thermal model is the representation from a thermal point of view of the system, it is a very useful tool used to determine the heat exchange from the heat source to the environment. Each element considered in the system has its own resistance, which can be connected in series or in parallel. A standard thermal model is represented by resistance, capacitance and heat source; there is a duality between the electrical and thermal circuits.

The thermal network in figure 3.1 represents the heat path from the chip, which is the power source, to the surrounding environment; similarly to the electrical circuit, the parameters such as thermal Resistance and thermal Capacitance can be expressed in per unit length. This makes it possible to parameterise these values exactly. Furthermore, infinite lumped volumes can be combined to derive the equivalent elements.
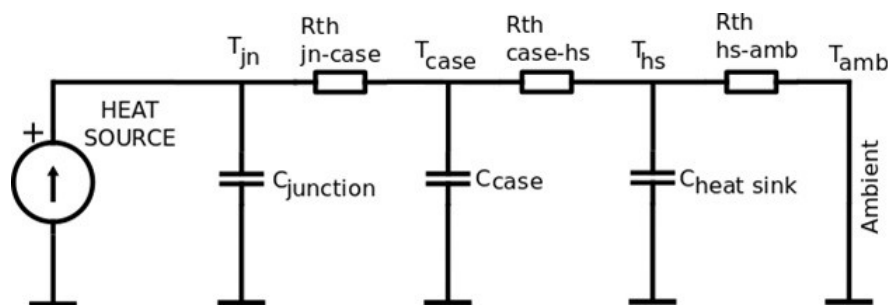
Figure 3.1: Heat sink properties windows

With this model, it is possible to consider a one-dimensional heat flow and perform the same calculations used to find similar quantities in an electrical circuit.

- Resistance

  Thermal resistance is defined as the inability to conduct heat through a material. Instead, thermal conductivity is defined as the ability of a material to conduct heat and it is denoted by λ. In nature, there are materials that have higher values

of conductivity and others that have lower values. Higher level of conductivity belongs to those materials such as metals, while lower level of λ belongs to insulating material. Resistances represent the thermal resistance between two elements.

- Capacitance

Due to elements such as capacitance, transients will occur. The mass of the heat sink represents the capacitance, and it is the largest capacitor in the circuit. It is charged until the transient is complete, it works like an electrical capacitor that stores electric energy, storing charges, whereas for a thermal circuit, the stored energy is heat. In the system studied, it is considered only the capacitance of the heat sink, the capacitance of the junction and heat plate is not considered, because the capacitive effect is minimal. The fins are used because they increase the heat exchanger surface. In some applications, the base alone is not able to dissipate all the heat produced by the system.

- Current source

On the other hand, the current source is the heat that needs to be dissipated; the MOSFET will produce heat depending on the current flowing through it. The current source injects the power loss of the system.

- Nodes

At each node it is possible to measure the temperature of a particular element. For example, to measure the junction temperature, one should measure the temperature before the junction resistance.

- Ambient temperature

The ambient temperature is taken as the reference temperature of the environment. In the system it is imposed using a DC voltage source.

Given the elements used in a thermal circuit, one can understand how a duality arises between the two circuits.

The table 3.1 shows the duality between the thermal and electrical elements of a system.

Thermal		Electric
R_{th} [°C/W]	$\rightarrow$	R[Ω]
C_{th} [Ws/k]	$\rightarrow$	C[A/Vs]
P_c [W]	$\rightarrow$	I[A]
T [°C]	$\rightarrow$	V[v]

Table 3.1: Thermal-Electric Analogy: Quantity Map

3.2. Heatsink

The most important element in the thermal network is the heat sink, it is responsible to take under maximum value the junction resistance of the devices attached to it.

There are different shapes of heat sinks, the shape varies according to the place of installation, the type of fluid, if it is air-cooled it can be forced or natural. Depending on the application there are different shapes and geometries of the fins.

Mainly it could be made with aluminium or copper, each one has its properties, but aluminium is the most chosen.

In the table 3.2, are reported the main characteristics that are taken in care in the design process.

Quantities	Aluminium	Copper
Thermal conductivity [W/(mK)]	203	395
Density [kg/m^3]	2712	8940
Cost \$/tonn	2,463.00	6,939.00

Table 3.2: Comparison between Aluminium and Copper

Table 3.2 shows the main advantages of aluminium over copper. It is evident that although copper conductivity is higher, it is more expensive and has almost three times the density, which means more mass for the same volume. In applications where weight is crucial, aluminium is preferred due to its weight, but also the economical aspects are kept care.

These properties of aluminium are directly related to its use, there are also mechanical and industrial reasons that make it the most suitable material for this type of application.

From a manufacturing point of view, it is easier to extrude, cast, scratch or mill with respect to the copper. For these reasons, the manufacturer opt to build heat exchangers made of aluminium, because it requires less expensive processing techniques, which further reduces the price of the final component.

The dissipator is a metal structure formed by the base and a set of fins; the base is connected directly to the heaters, while the fins are arranged on the base generally on the opposite side from the heat source. The base is responsible for heat conduction, as the energy is transmitted directly to the thicker plate. While fins are directly related to convection, which is concerned with the process of removing energy through a fluid flowing through thin plates arranged parallel to the fluid flow. The fins are used to extract energy from the larger mass so that heat can be exchanged to achieve thermal equilibrium.

3.2.1. Conduction

Conduction is a physical phenomenon whereby heat transfers from a hotter temperature to a colder one. In this case the base of the heatsink is the first element that sees the incoming heat. The base accumulates heat due to its capacity, acts as a heat reservoir. Also try to disperse it by transferring it to a lower temperature element such as fins. By increasing the exchange surface, the exchanger will take less time to disperse energy into the environment. This role is given to the fins.

3.2.2. Convection

Convection is that phenomenon that transfers heat from a system and brings it to the surroundings thanks to the movement of a fluid, it could be natural or forced, it is natural when the heat is extracted without the help of a pump or a fan, instead, it is forced when uses a device that stirs the air.

The effect of convection in the case of a heat sink occurs more on the fins. Fins have the task to make a wider surface of the object, the heat exchange depends by the surface in contact with the air. For this reason, the radiator are developed in volume, with long parallel plate surface. In this way the surface portion in contact with the air is higher. Increasing the surface area while keeping the same base dimensions may have disadvantages. Increasing the number of parallel faces is not always optimal because placing too many elements close together the convection effect begins to decrease. In this way the time taken to extract heat increases, decreasing the efficiency of the exchanger.

Since convection use always a vector to exchange energy with the surrounding volume of

air, it is important to define the correct spacing between two parallel faces. Because the element used as a vector could have particles larger than the distance between the two plates, in this way the surfaces are not touched by the fluid. Furthermore, the speed at which the fluid moves could also cause problems with a space between two fins that is too small.

The minimum dimensions regardless of the inlet fluid and its speed are:

- Natural convection need a minimum fins spacing of 6mm

- Forced convection need minimum fins thickness of 2mm

In forced convection the minimum distance between two parallel faces is smaller than natural because the air is pushed or pulled, with a fan. The fan introduces work in the system, it pulls air with an external source of power. However, if the gap is too thin the effect of the forced air is as previously mentioned counterproductive because there will be the presence of turbulent flow that have a chaotic effect. The effect that occurs is studied in fluid dynamics, a turbulent regime produces an irregular flow, with the presence of swirls and flow instabilities. The results is a non uniform flow of the fluid in the fins, so that it is impossible to extract heat from them.

It is possible to determine if the flow is turbulent or not computing the Reynolds number, that is a formula developed by Stokes and named in honour of Osbourne Reynolds. The Reynolds formula is:

$$\boldsymbol{R}_e = \frac{\boldsymbol{\rho u d}}{\boldsymbol{\mu}}, \tag{3.1}$$

where:

- ρ is the density of the fluid in interest

- $\boldsymbol{u}$ fluid velocity

- $\boldsymbol{d}$ diameter of the channel

- $\boldsymbol{\mu}$ viscosity of the fluid

The convective heat exchange interest mostly the parallel plates in this case, for this system the whole analsys on CFD has been computed with a specific Software.

3.3. Ansys Icepack

In order to study the thermal system, it has been used Ansys Icepack, a software based on Finite Element Analysis. F.E.A. uses for finite element method, it solves differential equation, with a numerical method. With this method it is easy to calculate and study the effect of some phenomena, which require the resolution of differential equations to be studied, such as:

- Mechanical stress

- Mechanical vibration

- Fatigue

- Motion

- Fluid flow

- Heat transfer

- Electrostatics

This kind of software are used to predict the behavior of a system, thanks to a set of parameters of the objects and the boundary conditions it can solve the problem.
The method that F.E.A. uses is simple, it makes a discretization of the object, it divides the object under test in thousand and thousand of finite volumes. The product is called mesh, that is a set of three dimensional small objects, that will be solved with algebraic equations.

This kind of software are powerful, because they doesn't need to solve differential equation of one volume, which are very complex even for a computer to solve. This method with the right parameters and the right conditions, can give excellent results using simple algebraic equations, in a short time.

The object to be studied must be designed with a CAD software, that could be Autodesk or others, but most of the software have them CAD section. After the CAD design, follows the parameters set, where the properties of the materials are set. Nevertheless it is important to define the boundary conditions, that are all the settings that define the whole system.

The quality of the mesh determines the result, if it is well done the solver can easily return a solution, taking fewer iterations, and for large systems with good quality this aspect is crucial. This software uses a numerical method to solve each element of the system, with

a large number of small elements it could quickly arrive at the solution.

In order to evaluate the quality mesh there are parameters in project design, that shows the number of elements that have been decomposed well. The parameters are:

- Face alignment
  Face alignment evaluates the alignment between two adjacent elements, it is the vector product between the two centroids $\vec{c}_0$ and $\vec{c}_1$ and the normal vector $\vec{f}$: if the result is one, the alignment is perfect, values below one indicates a distorted mesh. Values below 0.15 are given for completely distorted element.

$$\boldsymbol{Face \quad alignment \quad index} \quad = \quad \vec{c_0 c_1} \cdot \vec{f}, \tag{3.2}$$

- Volume
  Volume indicates the size of each finite element, if there are solids very small the mesh could lead to an unsolvable system, and elements of the order of $\mathbf{10^{-12}}$ are difficult to be evaluated.

- Skewness
  Skewness evaluates the geometry of each element, if the volume or faces are similar to an equilateral triangle or a square, the skewness volume is equal to one, otherwise, the value decreases. Asymmetry values of 0.02 represent an incorrect decomposition of the entire element.

If the lower limits of the three aforementioned quantities are never reached the quality of the mesh is good enough to find results, if there are many elements that present lower values of the aforementioned variables, the software may not give solutions. The most important thing is that the number of items below the acceptable values is small.

3.4.   Setting Parameters in Ansys Icepack

In order to build a complete model it is necessary to define each element used in the system. There are elements that already have a definition and can be customized, others that need to be defined from scratch. Elements that are not defined correctly will not be seen by the solver and therefore will not be part of the solution.

The heat sink is the subject of this part, it is studied, improved and needed to launch several simulations in order to be defined. The heat exchanger settings screen is shown in figure 3.2, where the various dimensions of the different parts can be set.
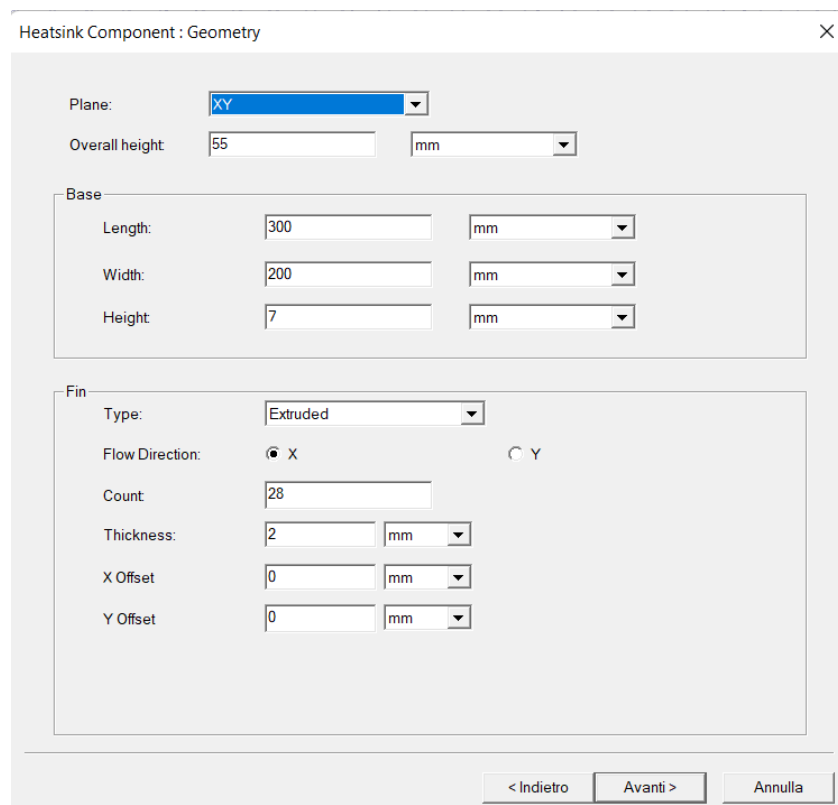
Figure 3.2: Heat sink properties windows

On the heat sink there is the focus of the thermal design, it is studied in order to keep the junction temperature under the limits.

Icepack allows to implement different elements easily. Heatsink and fans have their library and configuration windows where is possible to set different parameters, which makes the design process faster.

The fans that have been used are the ones installed on the previous inverter, for the air speed have been set a CFD curve, that is reported in the datasheet of the constructor.

Figure 3.3 shows the pop-up with the dimensions of the fans; these settings are related to the dimensions, while the CFD settings are derived later.

In this case the fans were not designed, but were chosen from existing ones. As can be seen from the datasheet curves see figure 3.4, it is possible to define different working curves depending on the type of control chosen. For this application, the one with 100% PWM control was chosen.
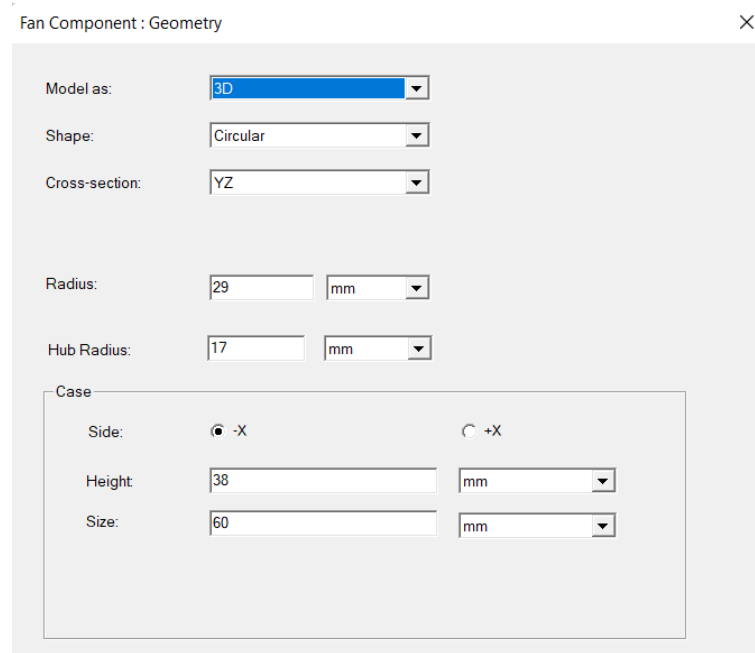
Figure 3.3: Fan properties windows

In figure 3.4 are reported the CFD curves related to the fan already used for the previuos inverter.
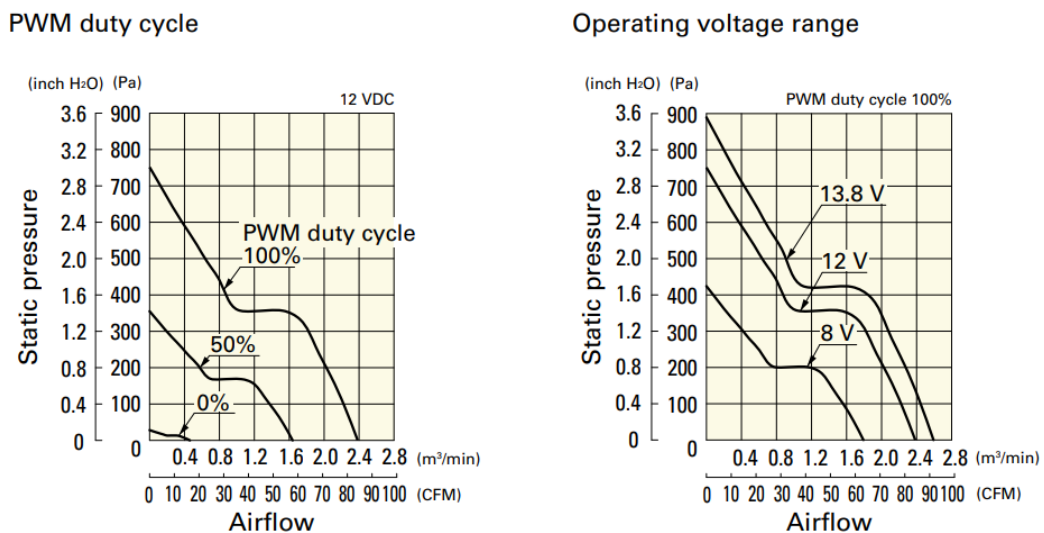
Figure 3.4: CFD curves of the used fan [7]

The three fans are set in extraction mode are used to extract heat from the heat sink.

The inverter is placed under the saddle, in that position the air is not conveyed pushed towards the fins, but is extracted, the fans are installed so as to extract the air and throw

it out of the compartment.

3.4.1. Thermal Network of the MOSFET

The thermal path of the MOSFET has been implemented in the thermal network section; in this section of the software, the thermal resistance and the heat source can be defined. The junction represents the source from which heat is produced, while the two resistances represent the resistance between the case and junction and between the junction and the ambient. The values of the two resistances are entered in the resistance symbols, while the power to be dissipated is set in the junction symbol.

The resistance values are:

- R_{jc} is set to 0.35°C/W

- R_{ja} is set to 40°C/W

In figure 3.5 it is drawn the thermal path of the junction set in Ansys Icepack.
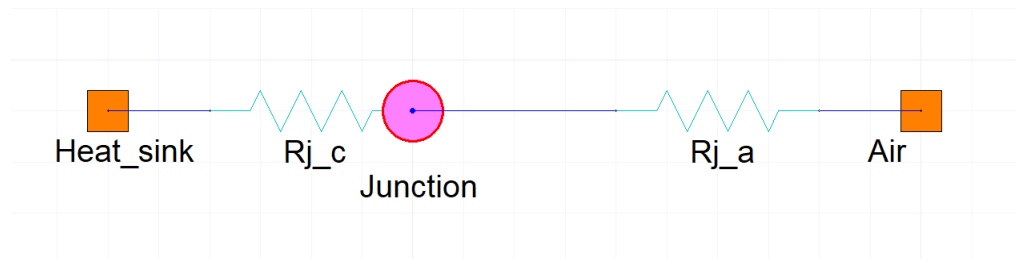
Figure 3.5: Mosfet thermal network

3.5. Thermal Design

The first approach to the design phase started with the construction of a small and simple system. In this way it was possible to learn the first steps and to understand how to use the various functions that the program makes available.

Becoming familiar with this software, a more complete configuration was realised, a heat sink for a single leg consisting of two switches in series. Initially, only the maximum temperature at the junction was taken into account. Since the module had a rated current of 100A, six modules were initially considered. Ideally, the current carried by the six MOSFETs in parallel is 600A, which with the chosen number of elements could be achieved, it was noted that the temperature was well above the maximum permissible value.

At this point, the design process of the heat sink starts.

Several tests were carried out in order to define the number of switches in parallel that could withstand a high current for an indefinite time. From an operational point of view, an attempt was made to verify that the system could withstand the losses that occur with such currents. When the maximum junction temperature was exceeded, an additional parallel element was inserted.

For these tests, the system is very simple:

- the air flow is set in one of the side of the air region with low air speed values, not taking into account the distance to the heatsink

- the dimensions of MOSFET are supposed considering standard MOSFET dimension, since the package was not define yet

- the dimension of the heat sink was in working progress

Even if all these specs are not completely defined or defined correctly, the system reaches a high temperature. Acting on the number of fins, the height of the fins and the height of the base can reduce the temperature by a few degrees.

Since the temperature is still high, the number of switches has been increased by step, from six switches in parallel to the final number until the temperatures on the junctions are just a little bit higher than the maximum tolerated.

At this point, the proper sizing of the heat sink was done, taking care of few quantities that are important in automotive solutions such as:

- the weight

- the volume

Both of these quantities are decisive in an application where dimensions are limited, since the bike is already made, there are limits on maximum volumes.

The defined volume of the heat sink is:

- length 300mm

- width 200mm

- height 120mm

It is also important to define the volume of air available, since as mentioned above, the air under the saddle is not infinite, a region of air equal to that available was set, with distances from the saddle walls of ten millimetres.

3.5.1. Heatsink Design Process

The first designed part was the base plate of the heat sink, which accounts for most of the mass, thus determining the thermal capacity, that is the thermal inertia. A very thick base gives to the system a large inertia, so it may not be optimal. It must not be too thin because it would risk not being able to exchange enough energy with the fins. It is necessary to find the right value to determine the right trade-off.

In the process of finding the best conformation of the heatsink, a lot of testing was done to achieve the lowest possible temperatures. To find quantities such as:

- height of the base

- number of fins

- fin dimensions

a lot of analysis were carried out scoring all the results and evaluating the best performance.

The final result was arrived at by defining the parameters:

- height of the base is set equal to 7mm

- number of fins is set equal to 28

- fins dimensions is set equal to 43mm

The model that was created is shown in the figure 3.6
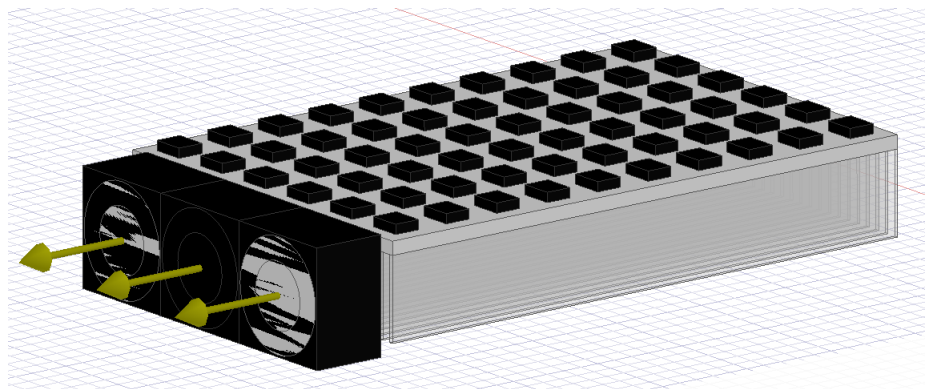
Figure 3.6: First complete model in Ansys Icepack

Together with the PMF team, it was decided that the height of the heat exchanger could be increased by a further 10mm, so that a new system could be made and studied, which will be reported in the following section.

3.6. Last Improvement

An idea came from looking at the heatsink catalogue, where there are different shapes of heatsinks, in particular, some are square with an additional backplate on the other side of the fins, in order to confine the airflow into the fins.

Seeing these models it was decided to insert a backplate in order to close the fins from the bottom.

With this improvement, it has seen in the simulation, that it is possible to reduce the depression of the flow already seen in the previous models.

In figure 3.7 is reported the last version of the model seen by three different observation points.
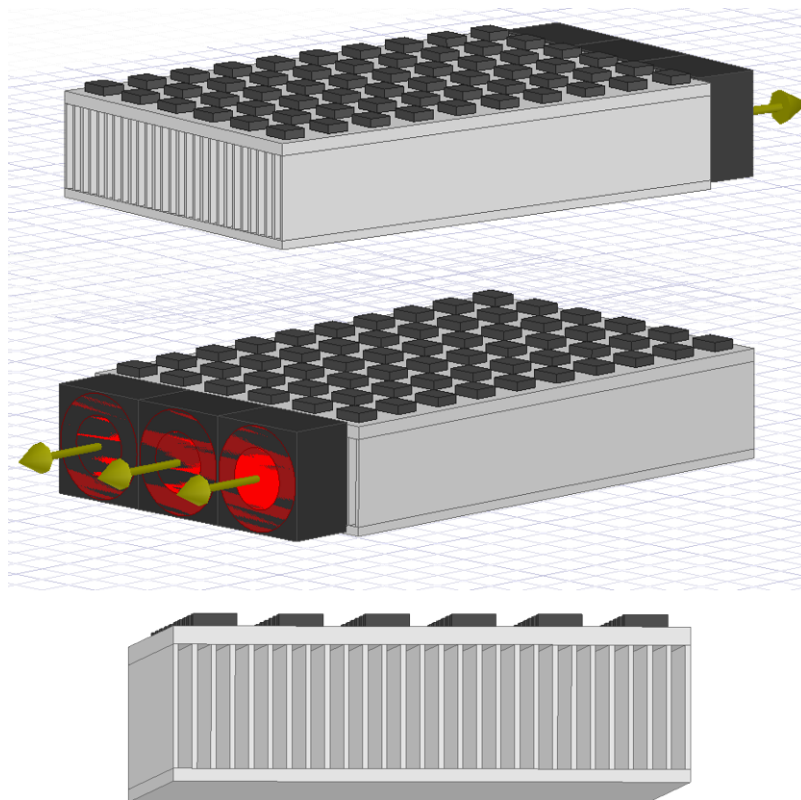
Figure 3.7: Heat sink point of views

The added base has identical dimensions to the main one, but is 5mm thick, it is less thick than the base where the switches are attached. This improvement allows power losses to be pushed up to 70 W per MOSFET, from the previous model losses can be increased by 17%.

3.7. Steady State Condition

The steady state in an electrical system is the equilibrium condition of the circuit in which transient effects are no longer relevant. Currently the dynamic components do not influence the physical quantities. The system no longer changes and the behavior of the network remains constant. This condition is reached when the partial derivative of the quantities is 0.

3.7.1. Steady State Study

In Ansys Icepacl from the field overlay menu, it is possible to select the variables whose magnitudes one wants to see and they will be plotted directly on the drawn object.

One can see the temperature of the air, the pressure developed within a volume of air, and the temperature of an individual element. It is also possible to make several layers, highlighting individual elements and displaying their steady-state quantities.

The result shown by the field overlay shows the steady-state magnitude value. The solver will report a magnitude that no longer depends on time. It is important, however, to take into account what settings are given to the simulation, each simulation is launched with a setup. In the setup section, one will find several settings useful to the solver in order to find a solution that converges. The first thing to set is the number of iterations one gives the solver in order to find a solution. It is recommended to set a minimum number of iterations for the system to always converge. Usually, a high value is set because there are some circumstances where the system takes really long to converge, if the system does not find a solution an error will be reported. In general, poor-quality meshes require many iterations to fix.

The values of the residuals, i.e., the error one is willing to accept in order to find a solution, are also specified; the smaller the error allowed, the longer the simulation will take. Typically, tests are done with values that are not too small at the initial stage, later if one wants to have a more accurate result to report certain quantities it is recommended to reduce the value.

In the setting section, one can set the type of problem is going to be study, whether flow or temperature. Since this is software for CFD studies, it is necessary to specify the type of flow being studied. The modifiable residuals are:

- Flow is set generally from 0.001 to 0.0001

- Energy is set generally from 1e-7 or 1e-8.

In Ansys Icepack is possible to simulate the steady state and the transient, the steady state can show a list of different quantities such as:

- Pressure

- Temperature

- Velocity

- Turbulence

- Thermal conductivity

- EM Mapping

- Joule heating

3.7.2. Steady State Simulation

The stationary regime is the scenario on which the study of the system was most heavily based. It was important to check the quality of the exchanger, to find out what temperatures the MOSFETs were reaching. For a large part of the simulations, the focus was on the worst case, the goal was to achieve the maximum power dissipation from each switch. As already mentioned, the steady state was studied in the design stages of the exchanger.

3.7.3. Steady State Results

The steady-state results were helpful in understanding how the system behaved. The most important result is certainly the one that records the maximum permissible temperature with the highest power dissipation, but remains below the threshold value, which for a SiC MOSFET is 175°C. It is considered that the temperature is recorded between the switch and the heatsink. To find the junction temperature, the power dissipation and the resistance between junction and MOSFET case should be added to the value.

Shown in figure is the test done with a power loss on each valve of 60W. The surface temperatures and air velocity vectors are shown.

In the figure 3.8 is reported the simulation of the first model of the heatsink with the power loss for each MOSFET equal to 60 W.
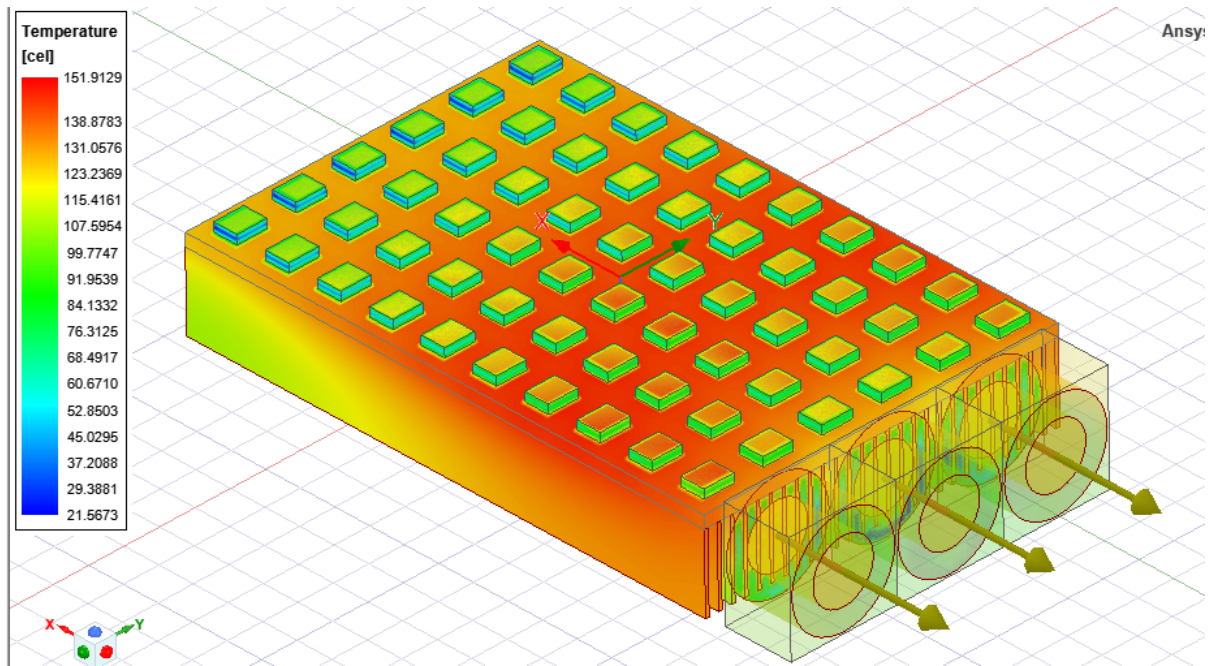
Figure 3.8: First version Heatsink with 60 W per MOSFET power losses

Before making the final model, the height of the fins was increased slightly from 43mm to 48mm. With this upgrade the results are slightly better.

In the last result, shown in figure 3.9, is reported the model with the fins height increased by 5 mm, with a power dissipation per module of 60 W.
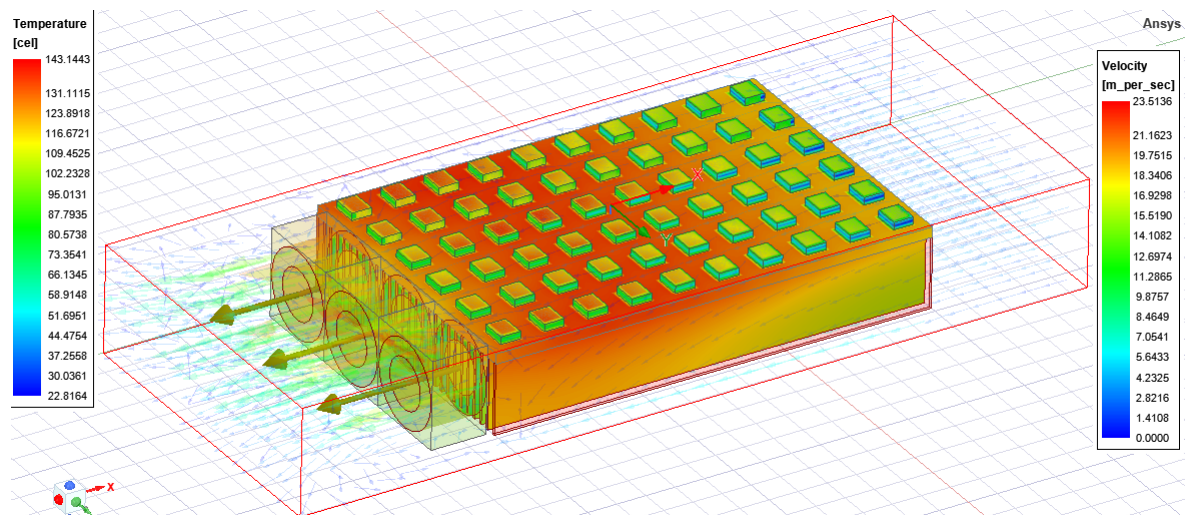
Figure 3.9: Intermediate version Heatsink with height fins of 48 mm with 60 W per MOSFET power losses

The intermediate model does not bring a large reduction in the recorded temperature, it

shows a reduction on the maximum measured value of 7 degrees. This solution allows the system to have more leeway, but not so much to allow it to increase the power dissipation.

In the figure 3.10 is reported the simulation of the last model of the heatsink with a power loss for each MOSFET equal to 60 W.
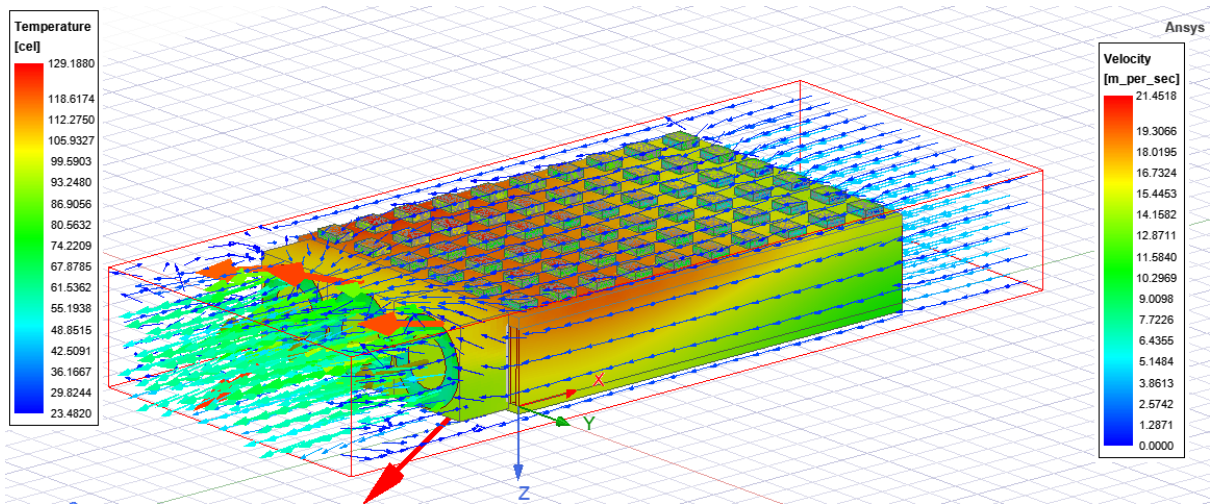
Figure 3.10: Final version Heatsink with height fins of 48 mm and back plate of 5 mm with 60 W power loss per MOSFET

Comparing the first heatsink model with the final set at the same power losses, the maximum temperature reached is now more than 20 degrees lower for the final version. This temperature reduction allows power to be pushed beyond the previous limit set in the first version.

This result is useful because it shows how much power can be increased. These results are from tests and conditions that may differ in the real world. Such a lower operating temperature allows the system to actually work with such high power. In the dimensioning phase, the worst case is always considered, and based on that, certain adjustments are made.

Looking at the temperatures measured on the heat sink, one can see that the added base has a completely different temperature distribution. The first prototype shows a temperature distribution that appears more homogeneous, in particular in the center of the base toward the fans, but reports significantly higher temperatures. Together with these results, an analysis of the variation of power dissipated by each module in parallel will be useful to verify the goodness of the exchanger.

A further consideration could only be made in retrospect once the model has actually been made. Considering the temperature of the first model is higher, in fact the second

version is an improvement on it, one can see that indeed the temperature is lower over the entire surface even on the fins, but is still high.

It is interesting to analyse the air surrounding the aluminium structure. The heat of the air could be completely different from that described, there could be an additional influence of hot air. A mass of almost one kilogram with such high temperatures could show far worse behaviour and negatively influence the system temperature.

In the final version, the air speed was also displayed, and it can be seen that the air does not reach high speeds. The speed on the outside of the impeller is driven at very high speeds, while at the centre of the shaft the speed is much lower. On the side opposite the impeller, the speed is lower only near the inlet. The air at the inlet has a speed of 3 and 4 m/s, while at the outlet of the fans it reaches 6 and 7 m/s.

The vectors representing the velocity are confined between the two plates and the fins, the air is channelled in this way and is therefore faster and absorbs more heat, reducing the maximum temperature. This is due to the fact that the plate enclosing the fins from below prevents air dispersion and also allows it to receive the heat exchanged by the air.

The lower plate acts as a heat reservoir, albeit smaller than the upper one, but which allows the heat extracted from the upper plate to be absorbed. In this way, heat is partially exchanged between the two bases, with the lower one absorbing the energy contained by the upper one.

The new base increases the thermal inertia of the model and, having a greater mass, increases the thermal capacity of the system.

3.8. Power Dissipation Limit

Since it was seen that the maximum temperature reached by the last model with a power loss per MOSFET of 60 W was below the limit temperature, a test was performed with a higher power dissipation. A test was performed imposing losses of 70 W per MOSFET; the result, as expected, was satisfactory because the recorded temperatures were below the limit.

The temperatures measured at a power dissipation of 70 W per module are shown in the figure 3.11.
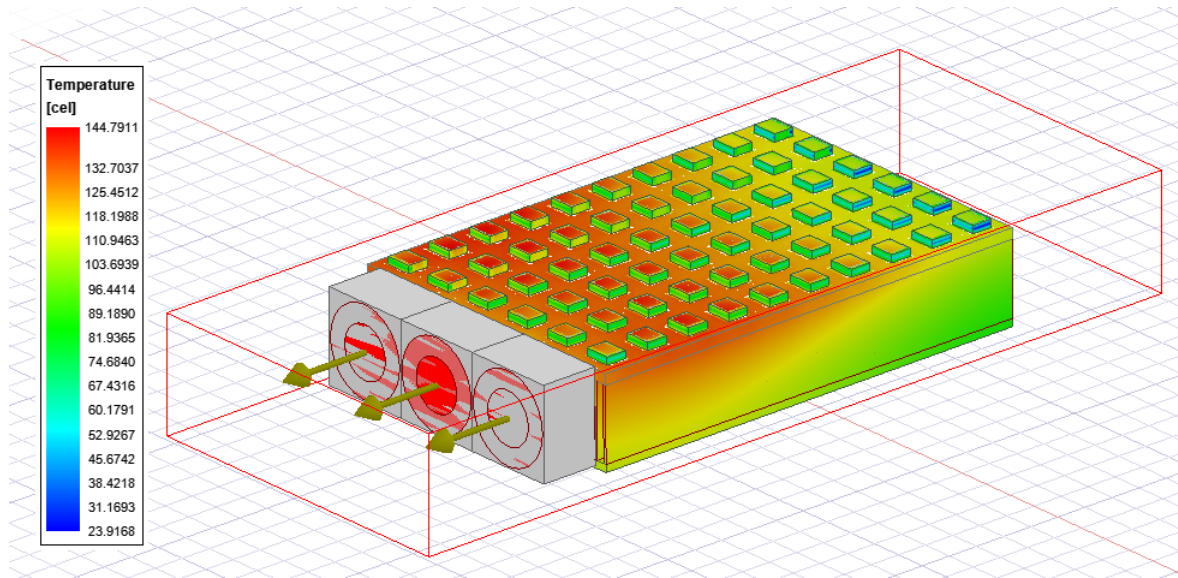
Figure 3.11: Last version of the heatsink with a power loss of 70 W per module

As can be seen, the temperature is at a maximum of 144°C. It should always be considered that the measured value is taken below the MOSFET. The maximum temperature recorded is therefore 144°C, the product of power and resistance must be added to find the junction temperature, the final value being 169°C. The heat is not evenly distributed in this case either, for the reasons already mentioned above. In the following chapter, a thermal model temperature dependent is created to study the temperature distribution.

3.9.   Transient Simulation

Transient is the phenomenon observed in systems where disturbances occur, such as in a network when small-signal disturbances occur. Transient analysis is useful to study the dynamics of the system and to see what happens after the fault. Another important aspect is the time taken to reach the equilibrium condition again, if it is reached. In this case, transient analysis is done to visualise how quantities change over time and especially the time constants to determine how long it takes to reach the steady state.

In Icepack transient tests require to use monitors, which are nothing more than probes that detect the quantities one wants to display. The monitors are placed punctually or on sides; the object must have "solver inside" checked in order to display the value of the selected quantities.

Through the monitor placed on the faces is possible to determine:

- Mass Flow

- Volume Flow

- Temperature

- HeatFlowRate

Through the monitor placed on the object faces is possible to determine the:

- Speed

- Pressure

- Wall YPlus

- Temperature

- Heatflux

It is also possible to visualize other quantities but these are the ones used for the studies

With point monitors it is possible to measure those precise quantities, such as speed for example, because it is possible to place the monitor on any point. While with the monitors positioned on the faces it is possible to see those quantities that concern an exchange.

In transient mode it is possible to define how long the simulation must last, and determine how long each time step must be. The iterations for each step to find the solution are also defined. If the convergence is not reached and therefore the residuals do not drop under the threshold value, during each step the system will not give useful results.

The residuals shown in the figure show the trends, at the first steps, the residuals have gross errors. In fact, in the figure, it can be seen that just before the 10 iterations the curve shows some inflection points, which will lead to temperature values not in line with the expected results. In these inflection points, the temperature graphs report an overshoot that still 10 iterations. This happens because, in the first steps, the error can be accentuated, only after a few iterations the residuals value decrease, if the solution is found. If the solution is not found, the value of the residuals diverges following an increasing trajectory.

The figure 3.12 shows a curve of the residuals which reaches convergence. One can understand the threshold values set, the iterations used and the inflection points previously discussed.
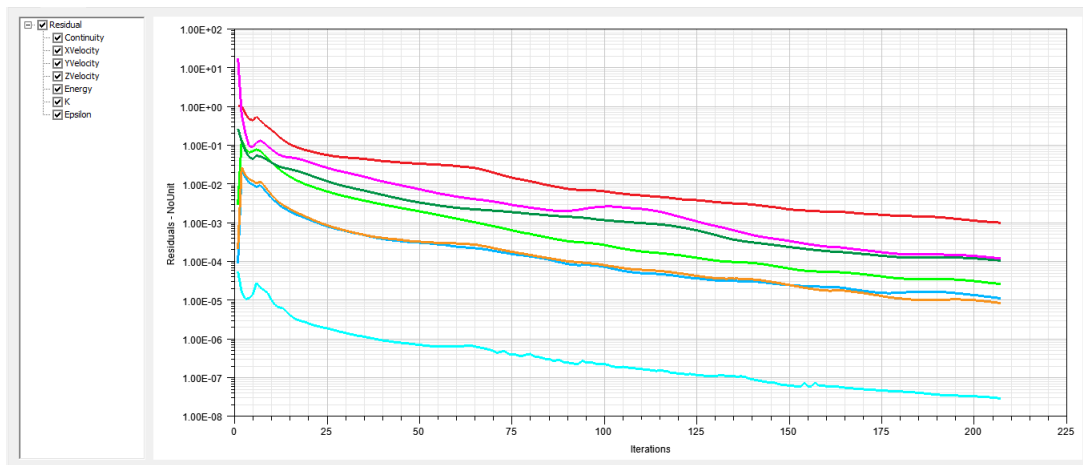
Figure 3.12: Residuals

The transient test was performed with the same maximum power settings as the steady-state results. Care was taken to provide the right number of iterations per step for the simulation to converge.

3.9.1. Transient Results

As previously reported, in this case the transient test was used to estimate the time to reach the steady-state. An attempt was made to obtain enough time for the temperatures to reach the equilibrium point. The maximum value recorded is 133°C, in analogy with the steady state test. It is essential to perform this test in order to understand the dynamics of the masses, as it can be seen that the steady state is reached in about 600 seconds. This gives the possibility to make an initial assumption on the time required to heat the heat sink.

Only 10 temperatures were measured; monitors were placed only on one column, high side switches of phase A, one per switch in parallel. Since the temperatures as seen in the previous tests are quite constant at each row, and not in column, it did not make sense to measure 60 different values by inserting too many values within the same graph. If 60 temperature curves are plotted in the same graph, 6 curves will be obtained superimposed on 10 different temperature values. So it's better to display only 10 curves related to one of the six columns.

The figure 3.13 shows the temperatures detected in the MOSFET column of the high side of phase A.
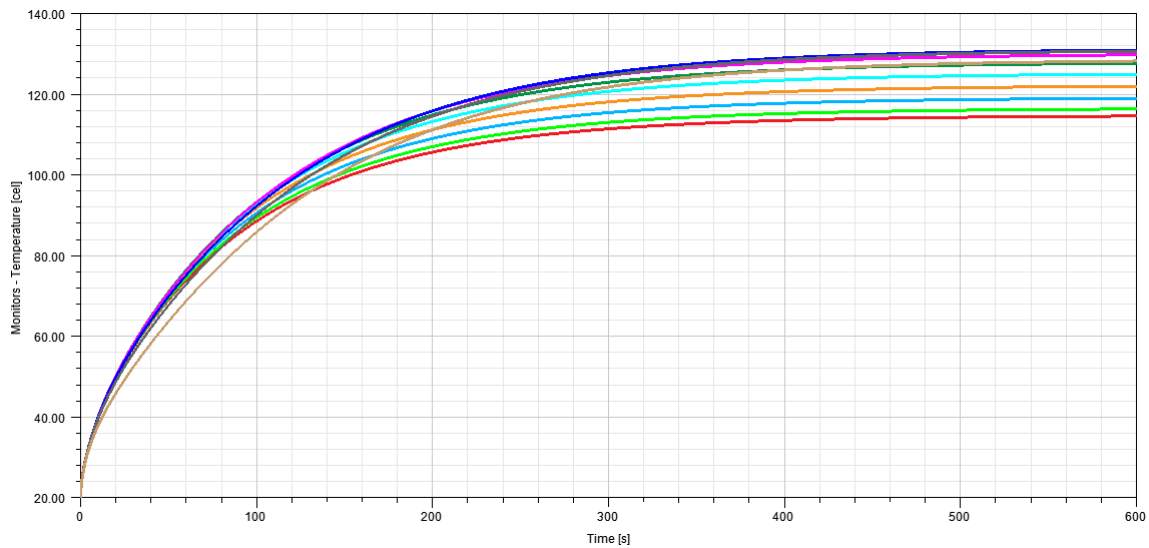
Figure 3.13: MOSFET Temperature in Transient test

It can be seen that the temperatures measured between the highest and lowest of the same column differ by almost 20 degrees. At transient complete, the coolest MOSFET reports 112°C, while the highest is at 129°C. Respectively, the highest one is measured near the fans, while the lowest one is measured away from the fans, where the taken air is at ambient temperature and has not yet come in contact with the heat from the heat exchanger.

3.10. Estimation of the Thermal Resistance

Icepack as previously said uses finite element method. It can analyze a system with a right set of parameters and boundary conditions.

In order to evaluate the resistance value of the heat sink, have been done a set of analysis at different conditions. The characterization of the heat exchanger has been done setting different power loss and different air speed.

3.10.1. Constant Air Speed, Different Power Setting

This test was done by setting a power value to be dissipated for each MOSFET, different for each test. While the air velocity is kept constant using the fans with their CFD curves, the power losses is changed for each simulation.

On Icepack it is possible to do a single simulation with a rated power, which is set constant. It is not possible to vary the power in real time or use a vector of power that

change dynamically. Each simulation is performed with a specific power, it has been tested with a maximum power that does not bring the junction to the limit temperature.

This test was done in order to see how the heat produced by the 60 sources affects the resistance estimated. With the values obtained, it is possible to see what effect this has and how much the effect of excessively heated air increases the resistance of the system.

In table 3.3 are reported the test names with the used power losses, instead in figure 3.14 the plot of temperatures reached by junctions at different power losses.

TestName	Power [W]
TEST 1	10
TEST 2	20
TEST 3	30
TEST 4	40
TEST 5	50
TEST 6	60
TEST 7	70

Table 3.3: Seven test carried out with the same air speed, but different power losses

In figure 3.14 are reported all the results of the test. In abscissa are reported the value of power used for each test, and in ordinate are reported the measured temperatures.
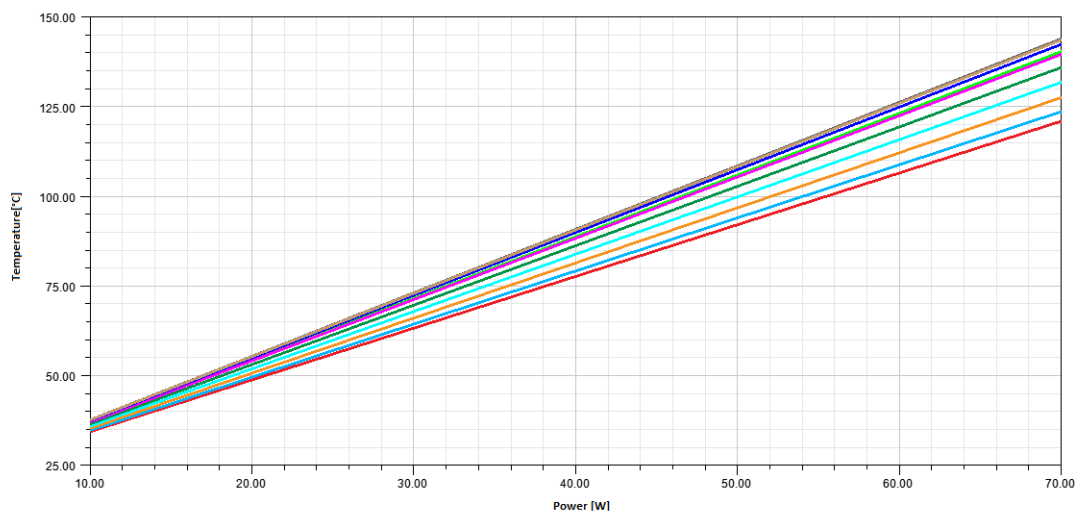
Figure 3.14: Test Results with different power losses and fixed air speed

3.10.2. Constant Power, Different Air Speed Setting

While for testing at different air speeds and constant power, the process is pretty much the same. To obtain the same effect produced by the fans, the air opening has been moved towards the heat sink at a distance such as to simulate the same vortex produced by the fans. At the air opening, an air speed was set at different values, one for each test. The direction of the air is the same as for the fans. In table 3.4 list the test used with related air velocity used.

TestName	Air velocity [m/s]
TEST 1	0.5
TEST 2	1.5
TEST 3	3
TEST 4	5
TEST 5	7
TEST 6	9
TEST 7	11
TEST 8	13

Table 3.4: Eight test carried out with the same power, but with different air speeds

These tests measured the temperatures between the MOSFET and the heat sink base, as it was impossible to measure junction temperatures directly.

The maximum temperature value is recorded directly under the MOSFET, the data log which contains all parameters, shows the minimum, maximum and average value. At the edges of the MOSFET the temperature is lower than that measured at the centre. Being the junction contained inside the MOSFET, it is not possible to obtain its temperature directly, for this reason a post processing operation was carried out.

3.11. Matlab Data Processing

The data taken on Ansys Icepack are exported on MATLAB where an equivalent network has been created in order to compute the junction temperatures.

The strongest hypothesis is to consider the worst case, i.e. the maximum temperature

recorded in a single point and extend it to the entire surface.

Since the adjacent area around the case is equal for each modules, it is possible to state that the portion of heat sink seen by each modules is the same. Each Mosfet sees the same mass of the heat sink and it is subjected to the same power losses in a first approximation. So it is possible to consider them connected to the same resistances, in this way it is possible to create a network of sixty power generator, connected to sixty equal elements of the heat sink.

The network created in Matlab is composed by sixty branches, each one has:

- P Power source

- R_{jc} Junction to case resistance

- R_{ja} Junction to ambient resistance

- R_{ch} Case to heat sink resistance

- R_{ha} Heat sink to ambient resistance

- Connection to ground - Ambient temperature

The R_{ch} has not been described yet: it is the resistance between the MOSFET case and the heat sink and it represents the thermal paste used in order to improve the adherence among the faces, reducing possible gaps. Moreover, the heat produces expansion and shrinkage of the MOSFET that could increase the contact resistance.

In figure 3.15 there is a cross view showing the effect of adhesion between two surfaces.
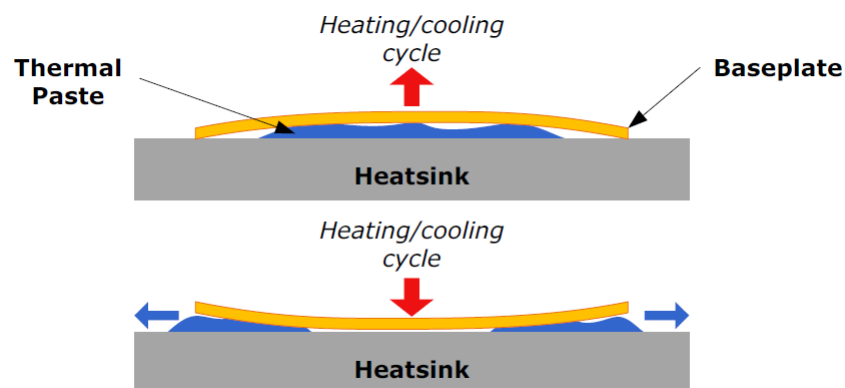
Figure 3.15: Thermal paste effect [3]

It is assumed that a thermal paste with thermal resistance equal to 0.4°C/W is used. This value was taken as a value to consider that in some places the thermal paste may be

missing and not uniform.

Each branch of the circuit is connected in parallel with the others: the common node is the earth connection, which represents the ambient temperature.

On Matlab has been developed a script that computes the junction temperature, using the dual thermal version of the Ohm law.

$$T_j = (R_{jc} + R_{ch} + R_{ha}) \cdot P + T_a \tag{3.3}$$

In figure 3.16 is reported a surfplot done in Matlab, with the results of Ansys Icepack, it report the temperature between each MOSFETs and the heat sink.
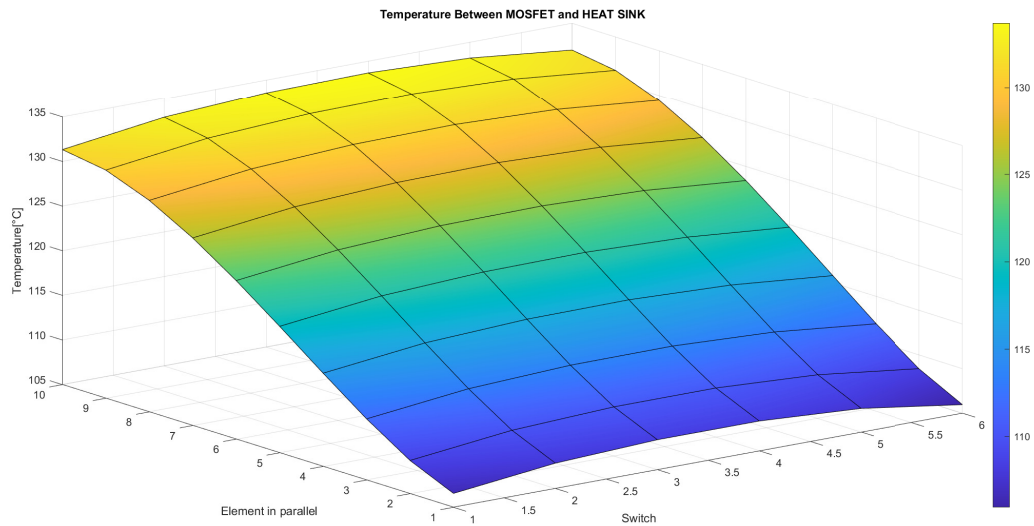
Figure 3.16: Temperatures between MOSFET and heat exchanger

With the result obtained from Icepack, the formula has been modified, since the junction temperature is not directly measurable, so it is added the contribution of ΔT to the temperatures obtained from Ansys Icepack, this variation considers the temperature losses on the junction resistance. This procedure is correct because the power in a thermal network corresponds to the current in an electric network, the product with the resistance gives the temperature at a higher step of the branch.

$$\Delta T = P \cdot R_{jc} \tag{3.4}$$

$$T_{junction} = T_{measured} + \Delta T \tag{3.5}$$

On the graph 3.17, the results of Icepack are shown as Matlab surface plot. The blue part represents the lower temperature, where the air enters, while the yellow part is the part close to the fans. One could see how the temperature increases almost linearly. One can also notice how the temperature at the boundary of the surface is slightly lower, more over this behavior is not so clear in Ansys. This phenomenon is due to the fact that the heat sources in the centre influence the temperature of the central part. Instead, the outermost switches are in direct contact with the air and do not experience mutual heat from both sides.
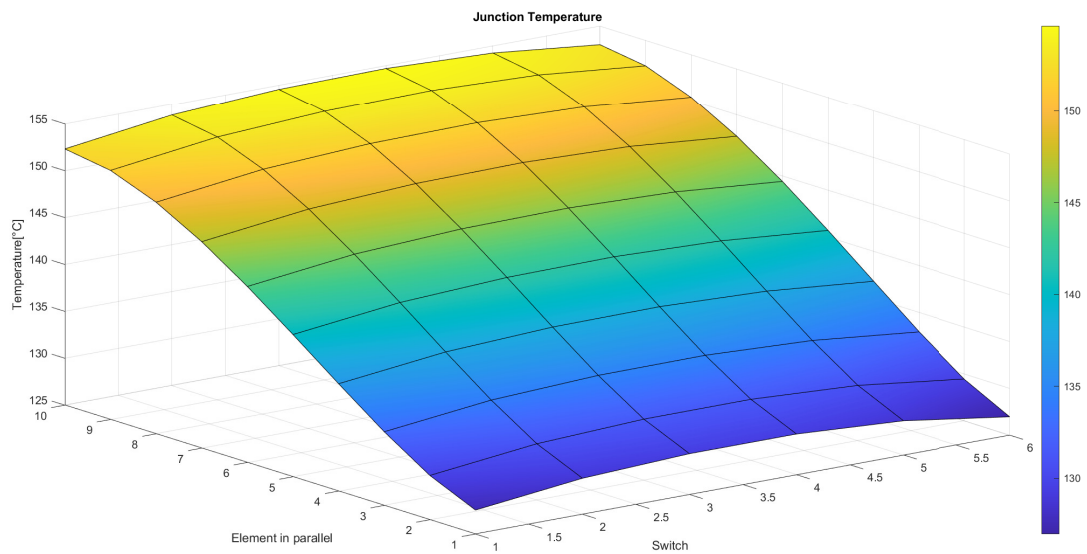
Figure 3.17: Junction temperature

The following formula was used to calculate the heatsink resistance:

$$T_j = (R_{jc} + R_{ch} + R_{ha}) \cdot P + T_a \tag{3.6}$$

$$T_j - T_a = (R_{jc} + R_{ch} + R_{ha}) \cdot P \tag{3.7}$$

$$\frac{T_j - T_a}{P} = (R_{jc} + R_{ch} + R_{ha}) \tag{3.8}$$

$$R_{ha} = \frac{T_j - T_a}{P} - (R_{jc} + R_{ch}) \tag{3.9}$$

All the branches give a different value of R_{ha} since T_{j_i} is different for each power module.

This is predictable since on the heat sink the temperature registered is different at each point.

In order to calculate each element of the discretized heat sink the following formula has been used, it uses 60 different values of the temperature taken from Ansys Icepack.

$$R_{ha_{[i]}} = \frac{T_{j_{[i]}} - T_a}{P} - (R_{jc} + R_{ch}) \tag{3.10}$$

In order to compute the total resistance of the heat sink has been performed a parallel of the sixty values of R_{ha_i}.

$$R_{heatisink} = \frac{1}{\sum_{i=1}^{60} \frac{1}{R_{ha_i}}} \tag{3.11}$$

Performed the parallel of the sixty elements of the heat sink, each tests gives its $R_{heatsink}$.

Now it is possible to define a curve where on the Y-axis there are the values of the Resistance computed, in the other hand on X-axis there are different values of the quantity under test.

3.11.1.   Constant Air Speed, Different Power: Results

The figure 3.18 shows the resistance values as a function of power losses.
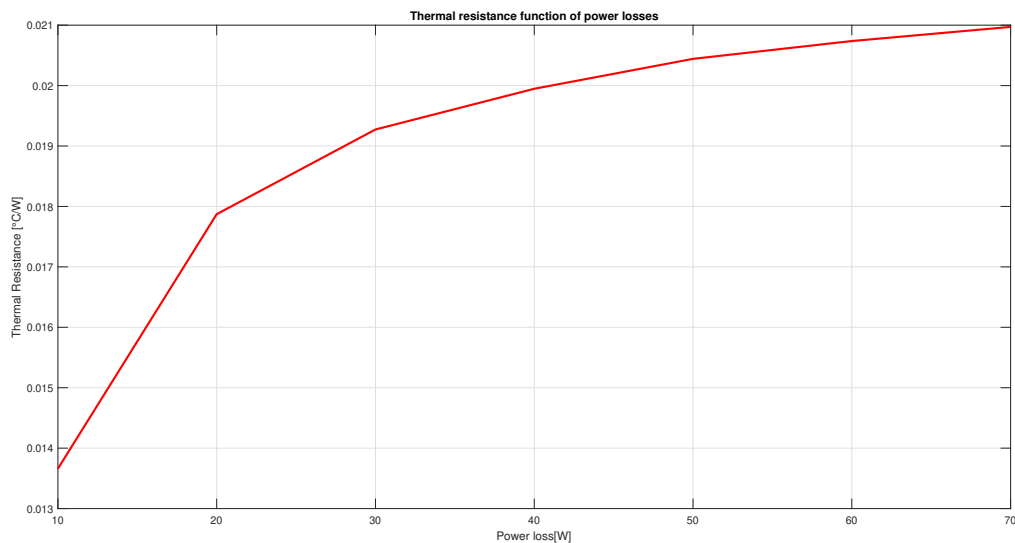
Figure 3.18: Thermal resistance as function of the power losses seen by the MOSFET

It is interesting to see what was explained in the previous paragraph: the heat sink, as already mentioned, was tested at different powers, i.e., from 10 W to the maximum allowed. The simulations show that an increase in power leads to an approximately linear increase of the temperature. This is interesting because it is easy to predict the temperature of the modules.

By doing the same calculations made before, it is noted that it is something different from expectations. The values of $R_{heatsink}$ are not constant, at low power the resistance value is low at about 0.014 °C/W. Instead, by increasing the dissipated power, the calculated resistance increases and grows until it becomes more or less constant, with a variation of less than 3% at each test.

In this test, a constant resistance value should be calculated. What you can see is that as you increase your losses, your resistance also increases. Going from 10W to 20W of losses, one notice how the resistance changes by almost 30%. With values lower than 20 W of loss, it is noted how the thermal inertia of the system does not make the calculated value appreciable. Significant values are seen above 20 W.

3.11.2. Constant Power, Different Air Speed: Results

In this case the two variables are the thermal resistance and the air speed, like a CFD curve of a datasheet.

In the table 3.5 are reported all the Thermal resistances calculated at different air speeds.

TestName	Air Speed m/s	Thermal Resistance °C/W
Test 1	0.5	0.125
Test 2	1.5	0.0508
Test 3	3	0.03
Test 4	5	0.0198
Test 5	7	0.0147
Test 6	9	0.0116
Test 7	11	0.0096
Test 8	13	0.0082

Table 3.5: The different thermal resistance calculated at different air speed

In figure 3.19 are reported the different values of $R_{heatsink}$ as function of the air speed.
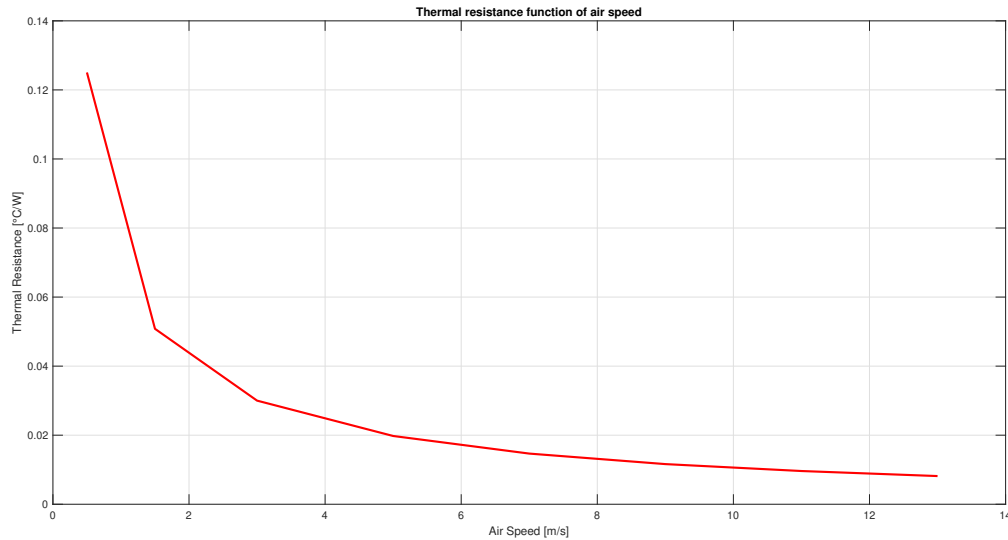
Figure 3.19: Thermal resistance as function of the air speed seen by the MOSFET

From the curve 3.19 with different air speeds, it is possible to see what happens if the air velocity increases: at low speed the air flux is not enough. Air speed below 0.5 m/s does not bring solid results, because the system is not stable. The convergence of the system is not reached, continuity parameter does not reaches the desired residual value of 5e-3. So the result is not reliable, it needs to change the solver but this invalidate the following test. For air speed above 0.5 m/s, all the residuals reach the expected value, so the results are reliable.

Considering the curve 3.19 it is possible to say that increasing the velocity of the fluid, the resistance decrease. Speed over 6 m/s does not report a better improvement of the resistance values. Moreover, it could be difficult to push a fluid at those speeds, resulting also in useless power absorption from the fans.

Thanks to the correct fins spacing, the fast air speeds do not result in burdensome turbulence effects or swirls that could worsen the heat extraction from the lower part of the base.

3.11.3. Surface Plot of the Heat Sink Resistance Discretization

Using test junction temperatures at different air speeds and constant power, it is possible to derive the resistance that each MOSFET sees. These resistance values, as expected, are different. The lowest values are where the recorded junction temperature is lowest, while the highest values are found near the fans. Observing the curve showing the resistance

as a function of the air speed, it can be seen that the resistance measured at a speed of 5m/s compared to 13m/s is substantially double.

In the surface-plot reported below the angles created by the intersecting lines are the resistance values obtained at that precise point of the heatsink.

In figure 3.20 are reported the 60 values of the resistances calculated at 5 m/s.
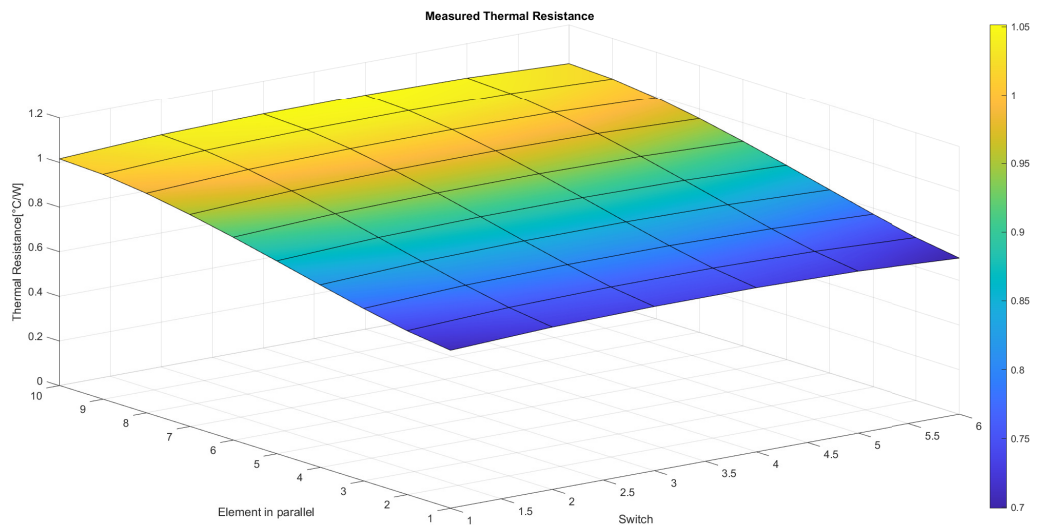
Figure 3.20: Thermal resistances measured at 5m/s

In figure 3.21 are reported the resistances calculated at 13 m/s.
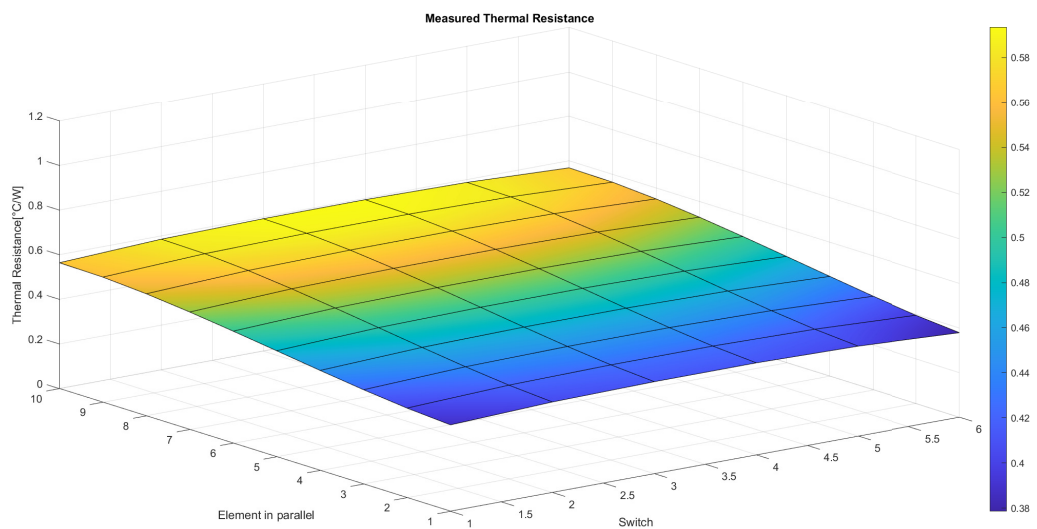
Figure 3.21: Thermal resistances measured at 13m/s

It can be seen that the resistances calculated considering an air flow at 13m/s are very similar and do not differ much, as can be seen from the Ansys Icepack graph. The surface obtained by Matlab is therefore almost parallel to the plane, unlike the case at 5 m/s which shows an increase towards the fans. Obtaining an air velocity of 13m/s is not trivial, since it would require very special fans. An alternative to the fans is possible to fit air conveyors that draw air at a high speed and convey it directly into the inverter compartment.

3.12. Capacitance

To determine the capacity of the heat exchanger the volume of the structure was computed. The volume considers only the base and fins. Having found the volume, the mass of the exchanger was calculated from the density of the aluminium.

- Base volume $= height \cdot lenght \cdot thickness$

- Fins volume $=$ number of fins $\cdot height \cdot lenght \cdot thickness$

The volume of each element is:

$$Volume_{Base1} = 200 \text{ mm} \cdot 300 \text{ mm} \cdot 7 \text{ mm}$$

$$Volume_{Base2} = 200 \text{ mm} \cdot 300 \text{ mm} \cdot 5 \text{ mm} \tag{3.12}$$

$$Volume_{Fins} = 28 \cdot 2 \text{ mm} \cdot 300 \text{ mm} \cdot 48 \text{ mm}$$

The total volume is $1.5264 \cdot 10^{-3}$ m^3

The final model with the two bases has a volume of $1.5264 \cdot 10^{-3} m^3$, while the first version was $1.226 \cdot 10^{-3} m^3$. The first model is less than 30% volume.

$$C = Volume \cdot Density \cdot ThermalCapacitance$$

$$= 1.5264 \cdot 10^{-3} m^3 \cdot 2700 \frac{kg}{m^3} \cdot 900 \frac{Ws}{kgK} = 3709 \frac{Ws}{K} \tag{3.13}$$

4 | Functional Simulation

4.1. Matlab Initialization

In the previous chapters, the thermal model of the system has been studied. A few critical points were noted in the Ansys Icepack results, one of which is the temperature distribution across the heat sink surface. Since the temperature is not distributed uniformly on the aluminum base, it can lead to unwanted effects such as a different wear of the switches. It can be seen that there are MOSFETs at higher temperatures than others, with a difference of up to 30 degrees. This effect leads to consumption and degradation of the materials of which the switch is made, which reduces its service life.

On Ansys Icepack, it was not possible to impose different powers on the switches in order to test the impact on the temperature distribution, while keeping the power handled by the system unchanged. However, it is possible to study this effect in Matlab;

Up to now the simulations done on Ansys Icepack have been useful for calculating the parameters of the heat exchanger. With these calculated parameters it is possible to create a model using temperature dependent resistance values of $R_{DS_{ON}}$.

The resistance $R_{DS_{ON}}$ of the switch is temperature-dependent as discussed in Chapter 2.

When the junction temperature increases, the resistance increases in value, the behaviours is reported in figure 2.19. Since there are 10 MOSFETs and therefore 10 resistors in the each high side, or low side of any phase. If some of these switches have a higher resistance, the other elements in parallel will draw a higher current than those with a higher temperature.

This model is useful to see if this phenomenon actually occurs and, if so, how hot the junction of each individual switch gets. The desired result is that there is a redistribution of the current so that there are no very hot elements and no cold ones, in order to obtain a more constant temperature between the junctions.

The electrical and thermal models have been merged together, up to now the two models that have been seen independently. Now instead the two different model have been united

by a single element, that is the resistance $R_{DS_{ON}}$ between drain and source.

In the electrical model, the current flowing through the MOSFET and the body Diode, is calculated. The current passing through a resistor produces heat, the power loss produced is used to feed the thermal model.

Initially, the junction is at ambient temperature, so the starting value is known; as the junction heats up, the temperature will vary, varying the junction temperature, the $R_{DS_{ON}}$ varies too, so the power injected in that thermal network vary accordingly.

This will be the phenomenon that will be studied in this chapter.

4.2. Electric Model

To simulate the electrical model, was made a circuit that produces the same current waveform as a single MOSFET and Diode.

Both MOSFET and Body Diode are modelled with resistances, more precisely the resistances between drain and source for the MOSFET and the resistance of the Diode for the Body Diode.

For the electrical model, the main elements are:

- controlled voltage source

- variable resistors

- ideal switch

4.2.1. Voltage Source

The controlled voltage source was used in order to directly set as an input a current value which, will determine the voltage needed to run the desired current value, when multiplied by the resistance of the channel between the drain and the source.

The voltage source is driven by a sine wave of amplitude one multiplied by the input current, which can easily be changed; the sine is multiplied by the value of the parallel of the ten resistance, thus producing the desired alternating current. The resistors in parallel, impose in the circuit the total current that passes inside a column of switches, of the high side or low side of one of the three phases.

Having built a model with 10 modules in parallel, the current will split into 10 different paths. As the resistance varies, the current in that path will also vary.

The input current can be a constant or dynamic value; for testing a steady state condition, a constant current is set, while for dynamic testing a current array is set. For example, for the variable load test it is possible to simulate a lap of the track or an acceleration test.

4.2.2.   Ideal Switch

In order to model the opening and closing of the switch, an ideal switch was inserted for the MOSFET circuit and another for the Diode.

4.2.3.   Variable Resistance

The $R_{DS_{ON}}$ resistance is temperature-dependent and it is modelled using a variable resistance, whereas a constant resistance is used for the free-wheeling Diode; since losses on the diode are low for high values of m_a, as explained in the conduction loss formulas in chapter 2, the temperature dependence of the Diode resistance is not taken into account. For this reason, the Diode current is set equal for the 10 switches in parallel.

Figure 4.1 shows the total resistance value calculated from the measured junction temperatures of the thermal models. This value is multiplied by the desired current value to impose the applied voltage.
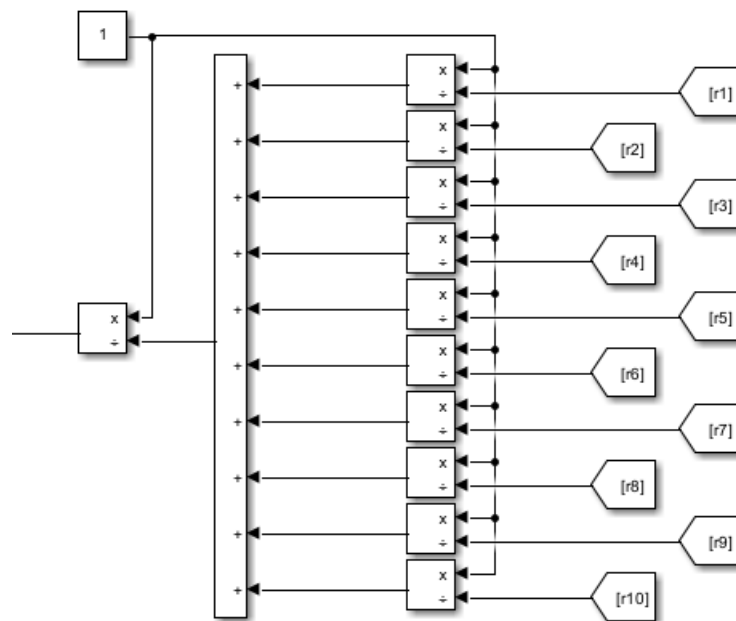
Figure 4.1: Calculation of the equivalent resistance of the 10 MOSFETs

With these elements, it is possible to simulate and control the switch and the Diode, creating the same behaviour that the power module has.

Current sensors are used to calculate power losses using the RMS value of the current; The goal of this test is to study whether the temperature dependence of $R_{DS_{ON}}$ will record junction temperatures different from those calculated on the Ansys Icepack.

What is expected is a redistribution of the current in the ten switches in parallel, so as to obtain a uniform distribution of heat, which will save the life of the components.

The figure 4.2 shows the detail of one of the 6 switches used in the three-phase inverter. The model consist of 10 variable resistors connected in parallel, one circuit for the body Diode. The switch is arranged to interrupt the conduction of the modules and it is controlled by a PWM control.

Figure 4.2: Electric Model of one column of switches

The following circuit is used for single MOSFET loss calculations. Conduction losses are calculated with RMS current squared, times the resistance of $R_{DS_{ON}}$. While the switching losses are calculated with the datasheet curves. In a lookup-table two vectors are inserted, one of the currents and the other of energy losses. The curve of the energy losses during the switching transient is reported in fig 2.22.

The value given at the input is the RMS current and the output is the value of lost energy, multiplying the latter by the switching frequency the power losses are obtained.

$$P_{CM} = R_{DS_{ON}} \cdot I^2_{M_{RMS}} \tag{4.1}$$

$$P_{SWM} = E(I_{M_{RMS}}) \cdot f_{sw} \tag{4.2}$$

$$P_{M_{tot}} = P_{CM} + P_{SWM} \tag{4.3}$$

In figure 4.3 are reported the Power losses calculation of the MOSFET that will be injected in the thermal model. In the same scheme, there is the calculations of $R_{DS_{ON}}$, it is calculated from the curve of the datasheet. The junction temperature enters in a lookup table where there are the values of $R_{DS_{ON}}$ as a function of temperature. The output of the lookup table is given to the variable resistance that represents the MOSFET.

Instead the diode conduction losses are given by:

$$P_{CD} = R_D \cdot I^2_{D_{RMS}} \tag{4.4}$$
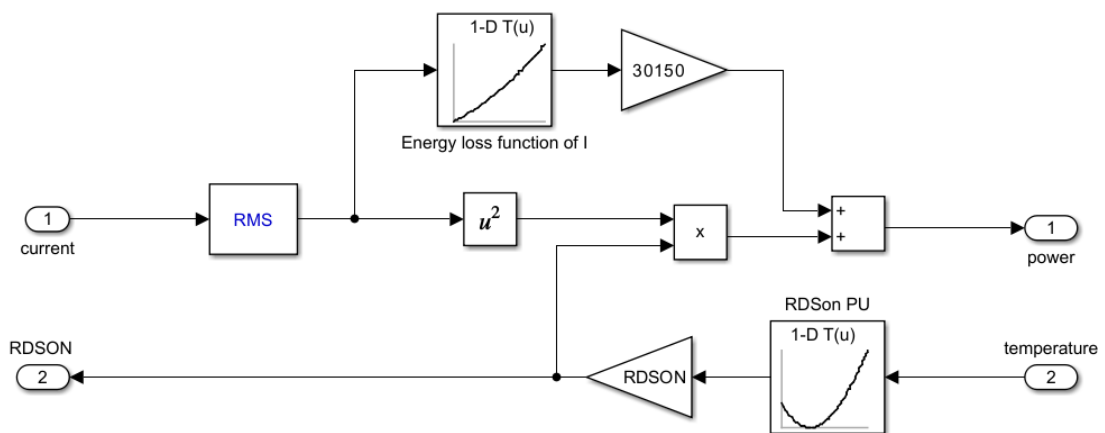
Figure 4.3: MOSFET power losses calculation

The resulting electrical model is arranged as shown in figure 4.4; to control the circuit, it is enough to define the PWM control and the input current. For the steady state test, the current is set using a constant, while the PWM is obtained from the comparison of the carrier and modulating signal. In the steady state case, the PWM has a modulation ratio of 1.
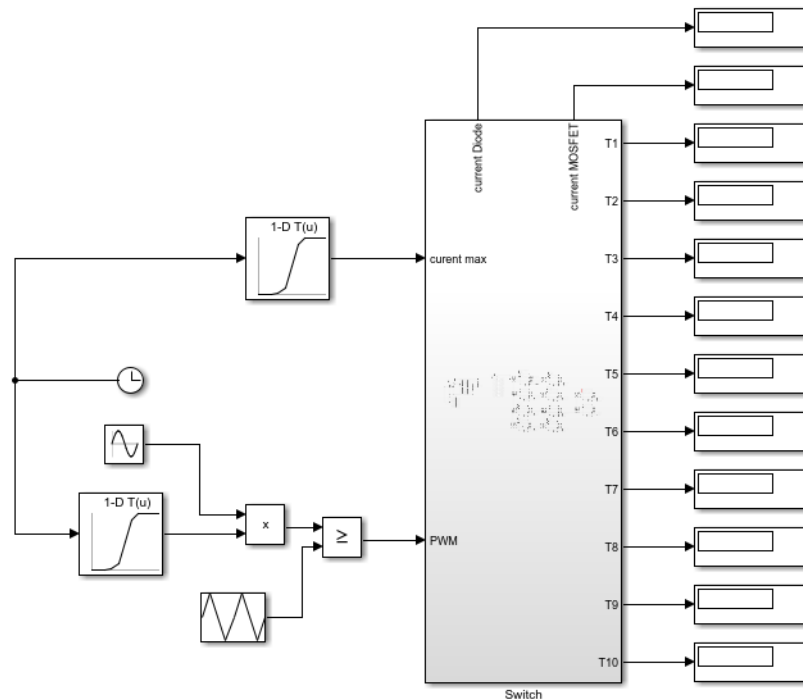
Figure 4.4: Input element of the electric Model

4.3. Thermal Model

Using the results obtained from Ansys Icepack, a 'mesh' of sixty heatsink elements were created, with each element being used for a single thermal network, in order to obtain separate models connected to the same source. The heat sink is no longer seen as having lumped parameters, but is now seen as having distributed parameters.

The idea is to make a model of the heat sink by dividing the heat exchanger as if it were a chessboard, each heat source with its own portion of the base and its own portion of fins. Each thermal network is then connected to an element of this chessboard. This procedure considers the thermal influence of adjacent elements in the calculation of heat sink resistance, which was discussed in chapter three.

It will be simulated that as the temperature increases, the current distribution will not be equal in each switch. One wants to see that hotter switches draw less current than cooler ones.

The exchanger has been divided as shown in the figure 4.5.
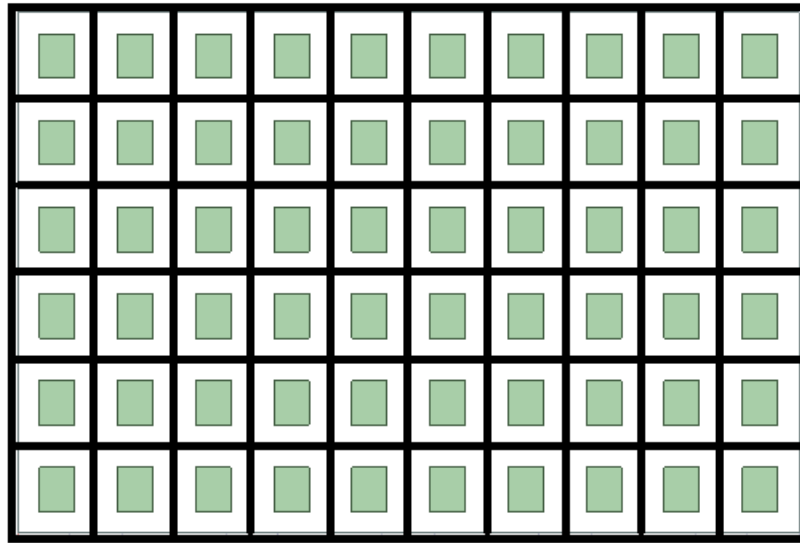
Figure 4.5: Splitting the inverter in 60 equal elements

The Thermal circuit of each MOSFET and Diode is heated by three current sources that inject the Power losses, contributions are made by conduction and switching losses of the switch and the conduction losses of the Diode, this power flows in all the elements already discussed in chapter three.
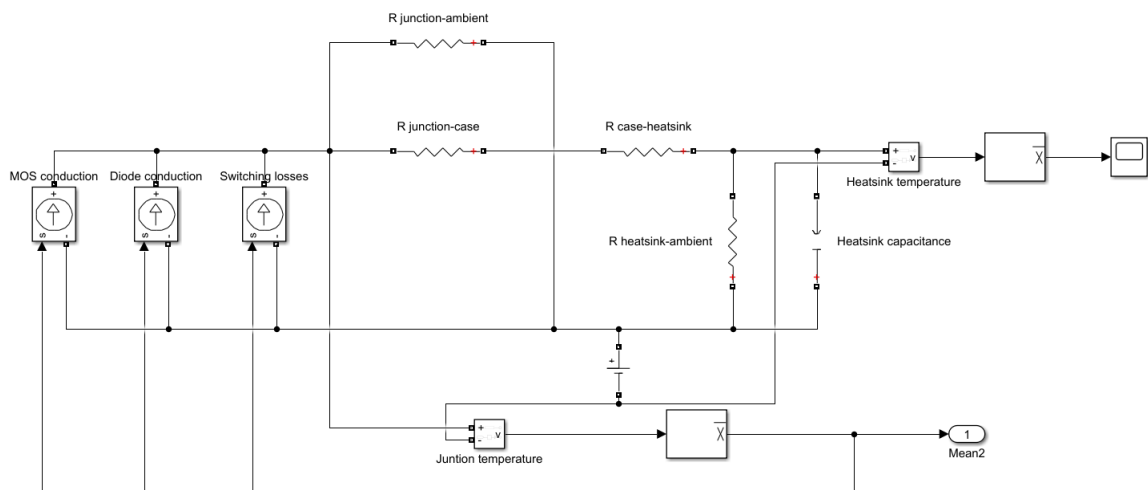
Figure 4.6: Thermal part of the thermal-electrical model

The DC voltage where the voltage measurements are connected represents the Ambient temperature, which is set at 25°C. In this way it is possible to take this value as a reference.

To measure the junction temperature, a voltage measurement must be connected between the junction resistance and the negative pole of the DC source.

From the voltage measurement, the temperature of the junction is measured, this is then sent as input in the block that calculates the losses of the MOSFET, explained in the electrical model.

4.4.   Simulation of the Electro-Thermal Model

To carry out these simulations, once the model has been defined, it is sufficient to define only two parameters which are:

- Value of current for constant power or dynamic test.

- PWM in order to control the Switch and the Diode.

For this test some considerations are needed, the model created gives an alternative test considering the one done on Ansys Icepack.

The test is done considering the steady state condition, a period where the temperature of the MOSFETs are constant, and the system reaches 160°C at the maximum power. On the CFD software is not possible to measure and observe all the aspects, on Matlab it is possible, so it is carried out a test where the parameters of the electronic devices are dependent on the temperature.

The system takes a long time to calculate all the parameters and the quantities involved. In order to increase the accuracy it is required to reduce the sampling time, which means to lengthen the simulation time again.

The solver is set with a sampling time of 50e-6s, which is not enough to see all the switching intervals of the MOSFET and Diode, because the switching frequency is set to 30150Hz. When the control voltage is at its maximum value, the switch and Diode are closed for a while which is less than the sample time. This leads to seeing the MOSFET in continuous conduction and the Diode is never activated for a few milliseconds. This condition has led to a worst case for the MOSFET and best case for the Diode; for this reason further losses due to the Diode are added.

In this type of analysis, it is important to explain how the model has been studied for a long time, an attempt has been made to recreate two different current paths, one for the MOSFET and the other for the body Diode. Thus dividing the two streams it was possible to study the losses in a precise way. It is not possible to calculate the losses when using the MOSFET block, because the current seen has the component going to the load and the other returning from it. Furthermore, the period in which the current is negative and therefore passes through the recirculation diode varies starting from the modulation

ratio m_A.

With modulation ratio values higher than 0.5 and a switching frequency of 30150 Hz, the Diode conduction has a very low T_{ON} time. Since the conduction time of the Diode is so short, the missing current in the power losses does not greatly affect the result.

Instead with very low m_a values, below 0.5, the Diode has a longer conduction time. Since the Diode has a resistance R_D three times higher than the MOSFET, this effect cannot be overlooked.

For this reason, since the modulation ratio is always over 0.5, it is assumed that the current reading imbalance in the two devices balances out.

Since it was not possible to increase the resolution by decreasing the sampling time, otherwise the simulation would have lasted too much time, 20 hours of simulation saturated all the memory available to the computer.

To be able to get results without the computer crashing, different models were made, but memory problems always occurred. The model had to be scaled down to 10 MOSFETs of one columns to be able to simulate the model.

Could be interesting to simulate the system with a server, in order to consider all the variations and to avoid compromise given by the sample time.

4.4.1. Steady State Test

The steady state condition is reached in about six hundred seconds, the thermal network has a large time constant, and the system continuously changes until the temperature is around the steady state value. Taking in consideration the transient analysis, done in Ansys Icepack, before the knee the temperature has a higher slope, while after the knee the temperature is almost constant.

The simulation time is 600 seconds, and the actual time it takes to calculate the whole test is completely different, with a standard computer and the whole inverter consisting of 6 subsystems it takes more than four days.

Given the complexity of the system, a single subsystem representing the 10 switches in parallel was considered to carry out these tests.

The steady state test was done to partially verify what was seen on the Ansys Icepack. The intention was to verify a redistribution of the current in the colder and the hotter switches, and in fact this behavior is present.

Looking at the currents, it can be seen that the current in the last switch in the row shows a modest reduction in current, and the blu one report an increase of current. The cooler MOSFET draws more current, so the hotter MOSFET may be less loaded. This is the first goal achieved.

Figure 4.7 reports the current measurements of the coldest and hottest MOSFETs.
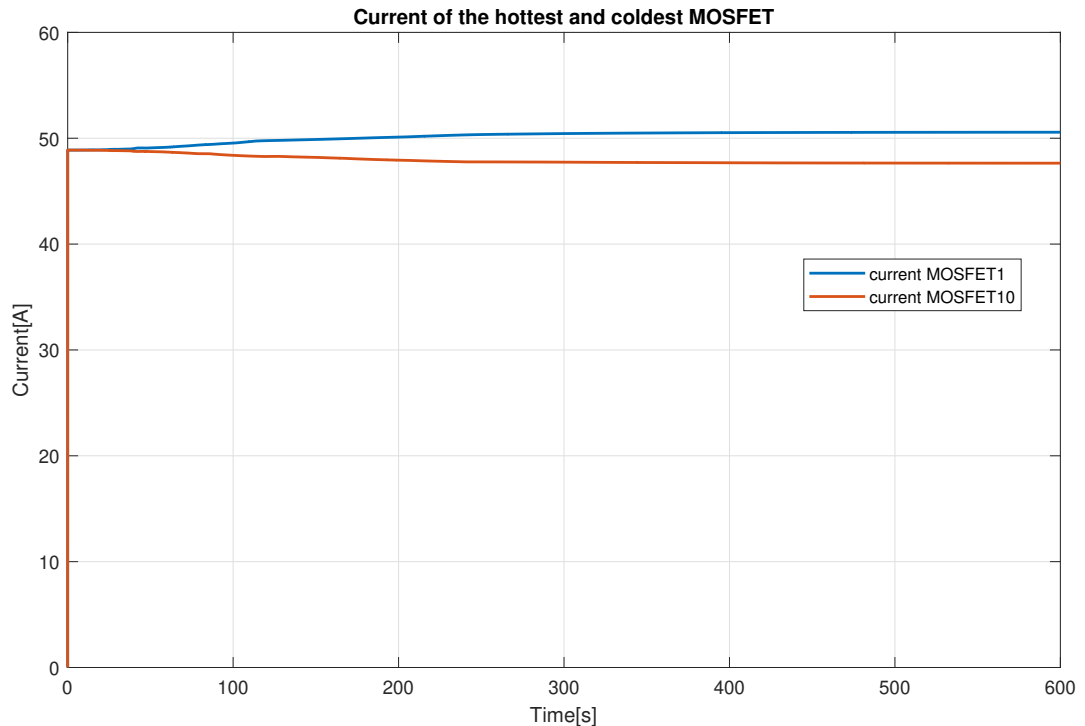
Figure 4.7: Current drawn by the hotter and colder MOSFET

Proof of what has just been said is also given by the power circulating within the thermal network of the coldest MOSFET, it can be seen that it is being loaded more. With regard to this graph, it can be seen that the increase in current results in an increase in its power.

The increase in power given by increasing the resistance $R_{DS_{ON}}$ is not appreciable, because the variation in resistance is maximum at 175 °C. Since the variation between the two values of $R_{DS_{ON}}$, even if one is found at 150 °C and the other at 170 °C degrees, they will still have a very similar resistance value. While a reduction of more than 4 A with a 50 A load, will have a more marked difference in terms of power.

It can also be seen that the power is at a higher value than that tested with the F.E.M. software. The test at the maximum power in Ansys, is done with 70 W of loss per switch, here the system overcomes 70 W.

A graph of the power dissipated by the first switch is shown in the figure 4.8.
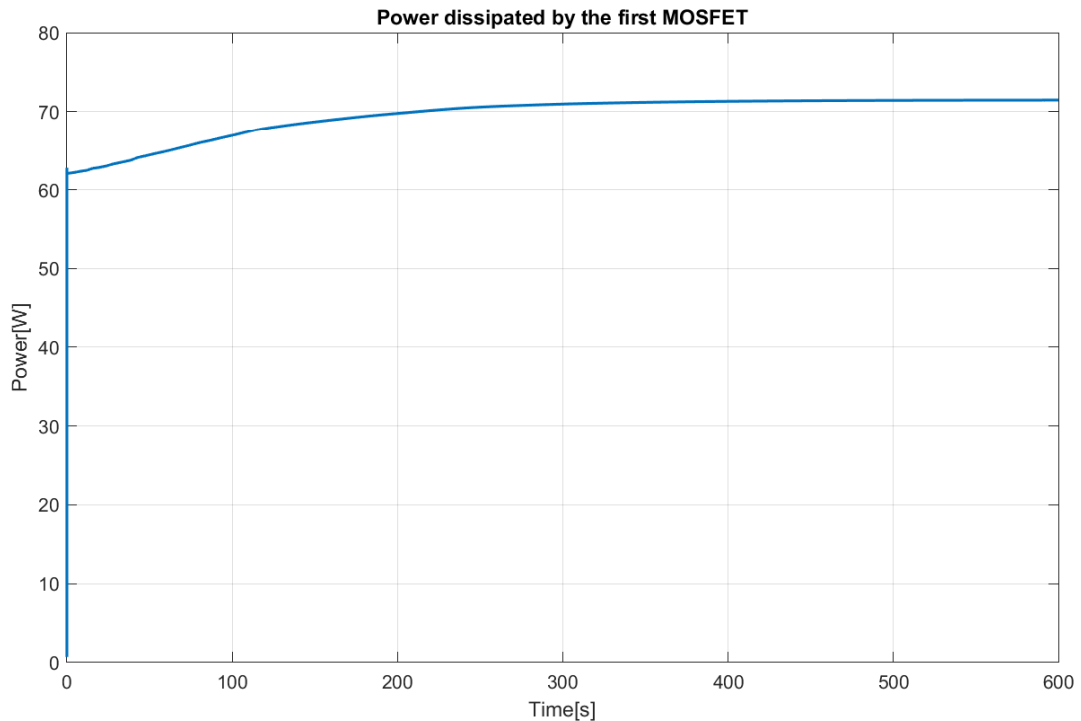
Figure 4.8: Power loss measured on the colder MOSFET

From the junction temperature results you can see the maximum values recorded. It is possible to see how they are lower than the values reported on Ansys Icepack. This behaviour is given by the fact that now, the heat sources, the MOSFETs no longer have a fixed power loss, but vary, how and why it has just been explained.

The ΔT of temperature between the hottest and the lowest MOSFET has been reduced, the thermal simulations reported a much higher temperature difference on the heat sink. Now the difference is less than 20°C.

The temperature at the beginning immediately goes to a very high value and then grows following the transient, as if there is a very small capacitance that immediately brings the system to a temperature of 70°C. On the other hand, one can see how the time constants of the two systems seen on Ansys Icepack and this one are similar. It takes 600 seconds to reach the steady state values.

The temperatures of the MOSFETs in a single row for the high side of phase A are shown in figure 4.9.
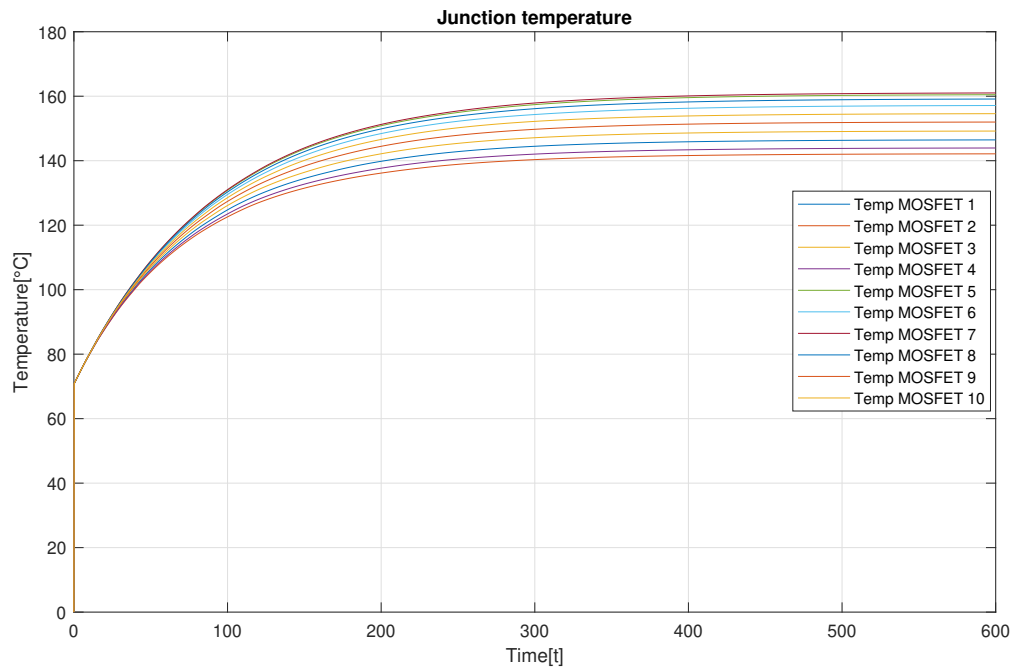
Figure 4.9: Junction temperatures of the first MOSFET column

4.4.2. Dynamic Test

The telemetry given by the team is used in order to do the dynamic test. The figure 4.10 plots the speed curve registered during a lap track.
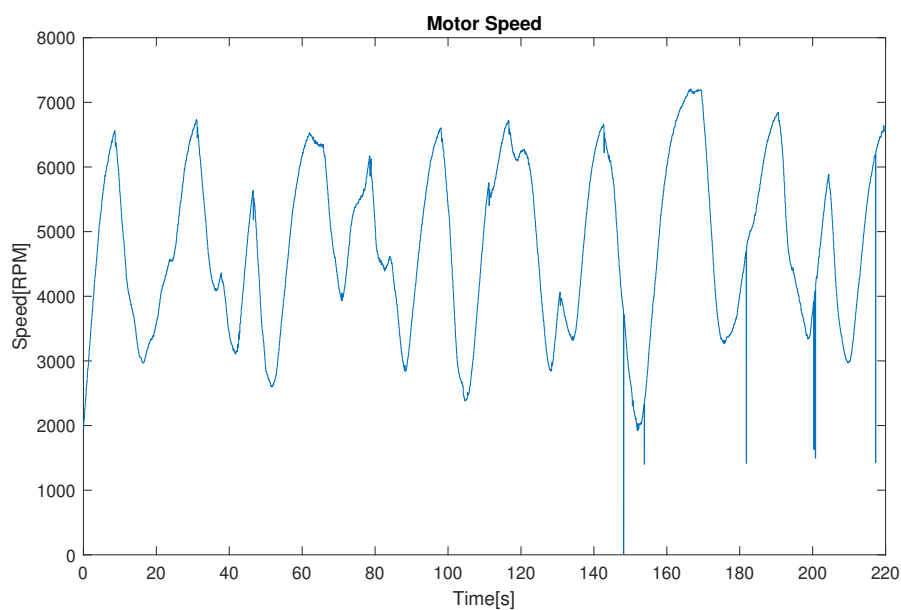
Figure 4.10: Motor speed expressed in RPM

Once the data was taken, it was verified that the values are correct, sometimes the data reported values that were incomplete or wrong. The values reported are the peak values of the following quantities.

The main quantities available from the telemetry are:

- DC Current

- AC current

- DC voltage

- AC voltage

- Speed

The values useful for dynamic testing of the electro-thermal model are the phase current, the DC-side voltage and the ac-side voltage. The AC-side current is used to impose a circulating phase current. With the help of the saturation block it is possible to impose conduction only for a certain half-period, in order to simulate the conduction state of the switch, which is different from the ON state.

The two voltages are useful because by seeing them, it is possible to determine the type of modulation. By calculating the modulation ratio $m_a = V_{AC}/V_{DC} \cdot 2$, it is possible to say what kind of relationship exists between the two voltages. In this case, m_a reaches value over the unity, this means that the control sometimes works in square wave. So it is possible to say that there is not the use of the third harmonic injected in the $v_{control}$ signal.

Looking at the output voltages and the battery voltage (fig: 4.11), which are shown in maximum value, it can be said that the control voltage v_{con} is obtained from a single sine wave, the addition of the third harmonic is not noticeable.
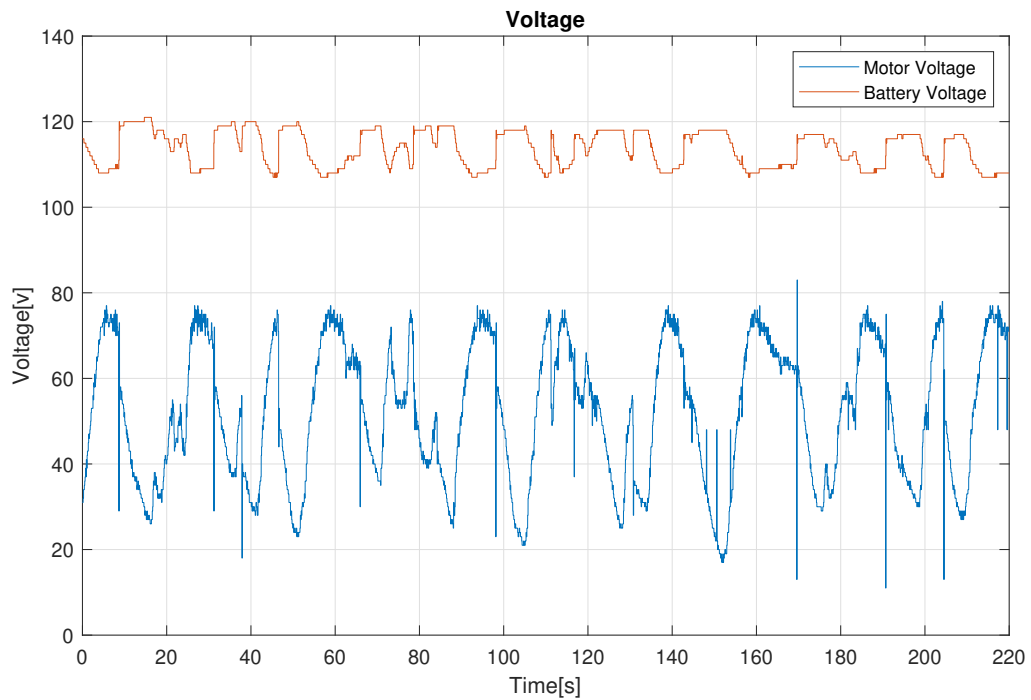
Figure 4.11: DC voltage and AC voltage relative to the phase A

Figure 4.12 reports the AC phase current and the DC current.

Although the phase current turns out to be higher than the DC current, the power balance must always be taken into account, which is always useful as a check.

The AC phase current has been used to fix the current reference of the model; the current record in this circuit is very low compared to that recorded on other tracks. The data recorded on the track was taken at the Imola circuit, it appears to be the most complete data, because them are read with an acquisition time of 100Hz and the AC voltage and speed reported correct values.
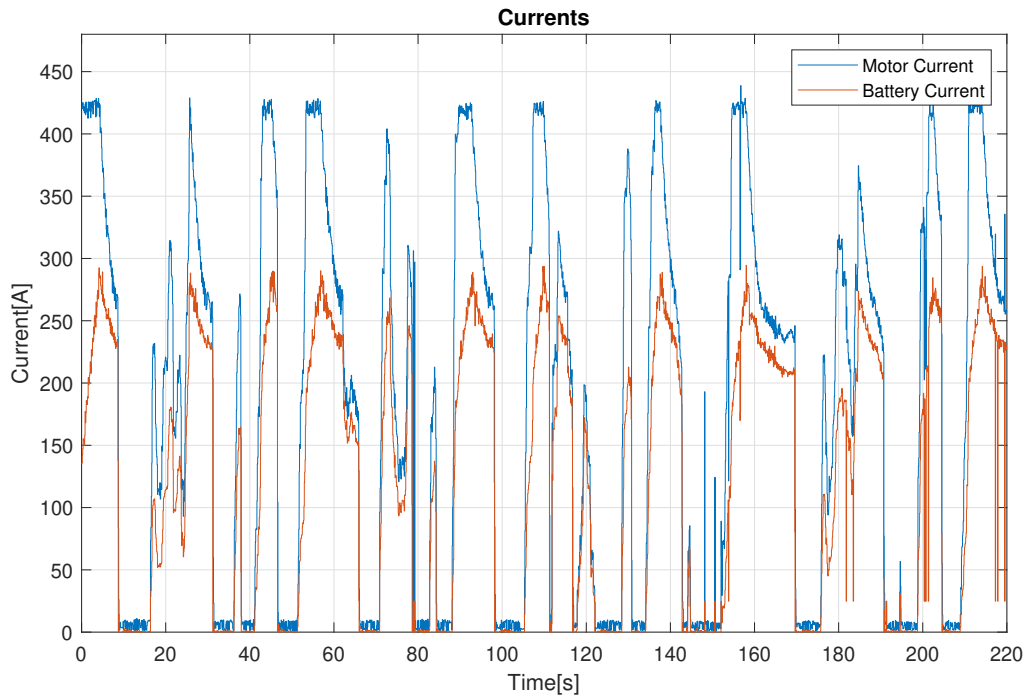
Figure 4.12: Motor and Battery Currents

Looking at the modulation ratio, it is possible to see, that when the speed is increasing the m_a is increasing too, over the base speed of the motor, the control is working in over-modulation. It is known that square wave produces bad harmonics.

Better results could have come out with the addition of the third harmonic with an amplitude of $1/6$ of the first. The results would have been better because the motor does not behave well with the presence of harmonics given by over-modulation. With the third harmonics injection, is possible to avoid over modulation.

Figure 4.13 reports the modulation ratio calculated with $m_a = V_{AC}/V_{DC} \cdot 2$, the horizontal line located at Y=1 represents the border where the over modulation occurs.
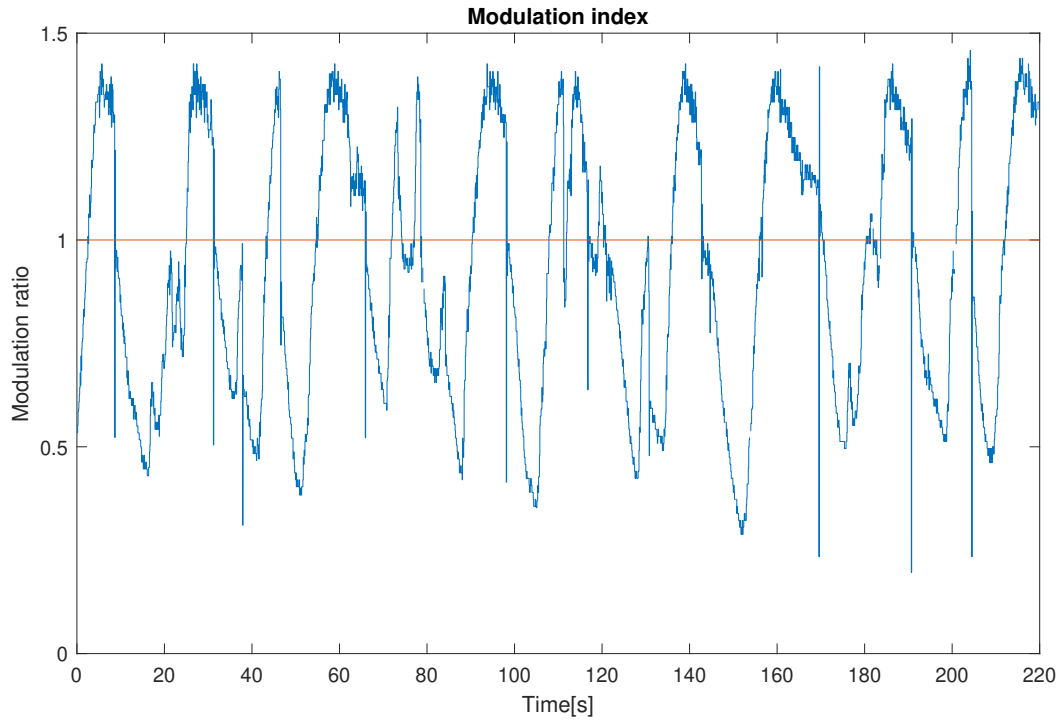
Figure 4.13: Modulation Ratio

With this data, it is possible to conduct the dynamic test, since a current reference value and a modulation amplitude index value are found. The results obtained from this test are very important, they are very useful to validate the model and start building a model of the heat exchanger.

A very low RMS current circulates in each MOSFET, because the back electromotive force, BEMF, reduces the current in the circuit if one considers the Behn-Eschenburg construction where:

$$V_s = E + L_s \cdot I_s + R_s \cdot I_s \tag{4.5}$$

It can be seen that with a non-zero BEMF, the current is limited. Nevertheless, a fair amount of power is needed to transfer torque, because the load angle increases when the torque is needed and so the current rises.

In this case, the currents drawn by the two hottest and coldest switches are shown in Figure 4.14. As can be seen that the currents are almost overlapping, one will see why by looking at the temperatures recorded.
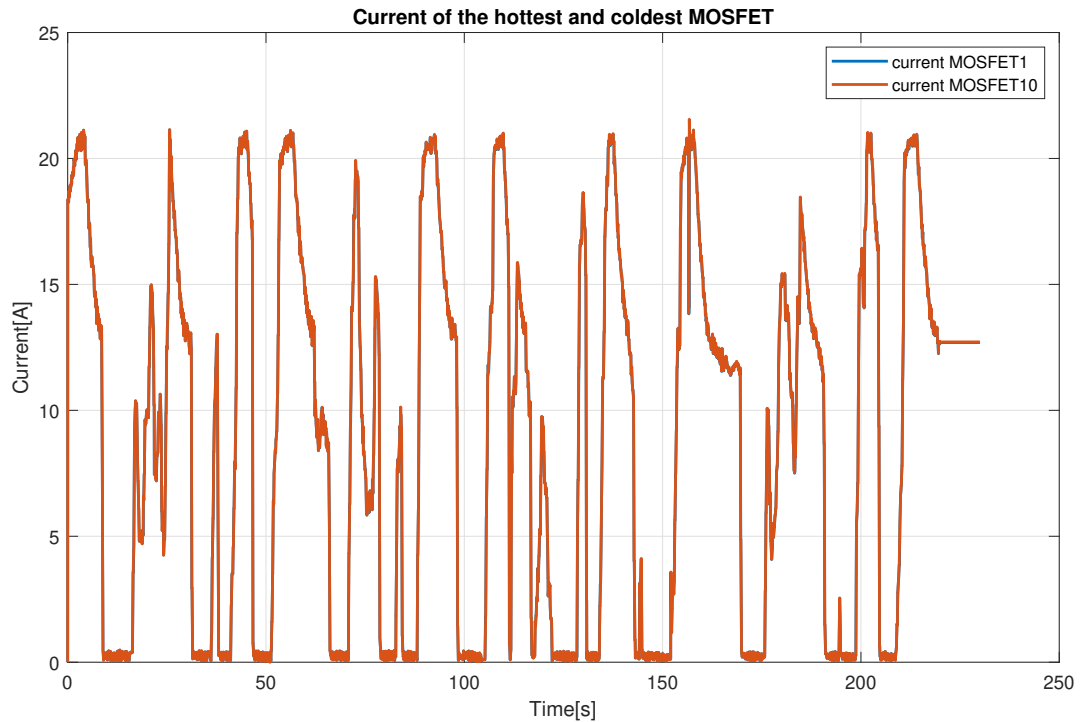
Figure 4.14: MOSFET Currents of the hotter and colder module

As far as power loss is concerned, it can be seen the maximum value recorded is well below the power measured in the test at maximum power (fig: 4.15). The maximum value is below 20 W, which compared to the 60/70 W simulated in the previous test is much lower, but it should be considered that power goes with the square of the current, the current handled by the MOSFET is small. This test is different from the steady state one, it has been done in order to see the temperature involved during the competition.

With this application, most of the losses come from the MOSFETs, because with a modulation index greater than one, the action of the freewheeling Diodes is reduced.
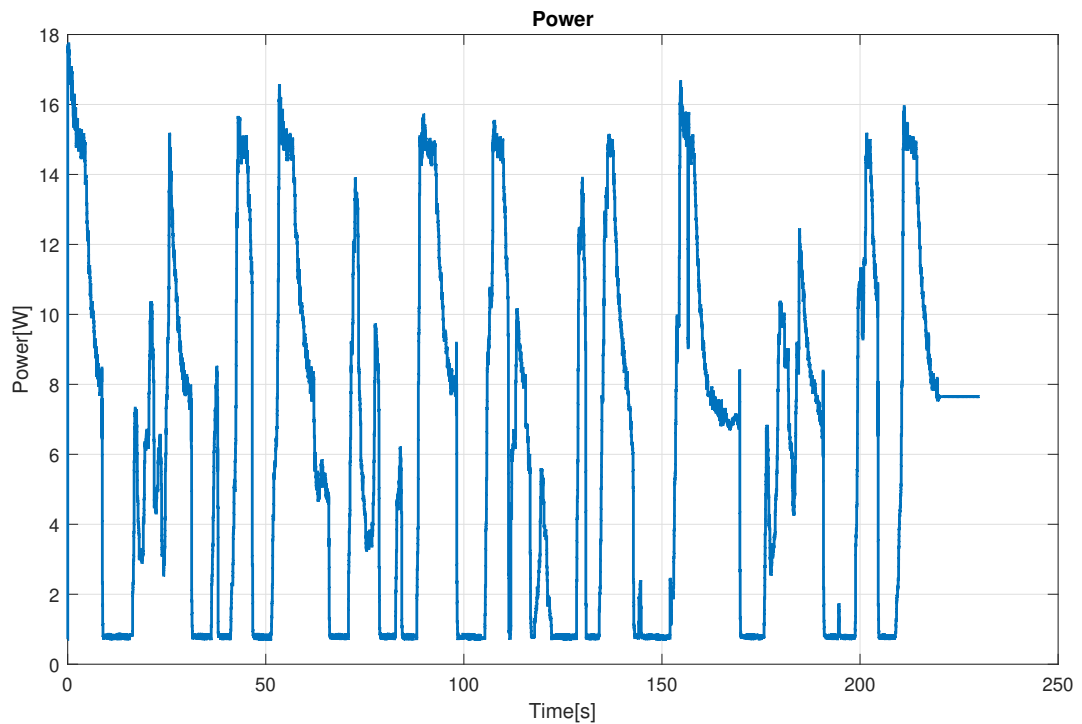
Figure 4.15: Power loss on each single MOSFET

Considering the results obtained, very low temperatures can be noted, compared to those obtained in the previous test. This is given by the lower imposed current and by a variable load. If one considers the results obtained on Icepack, in the 20 W test, which report a maximum temperature measured of 50° C, where the temperature drop on the junction must be considered considering $50C + 20W \cdot 0.35C/W$. The junction temperature on Icepack reaches 57° C, here instead the maximum temperature is 45° C with a much lower dissipated power.
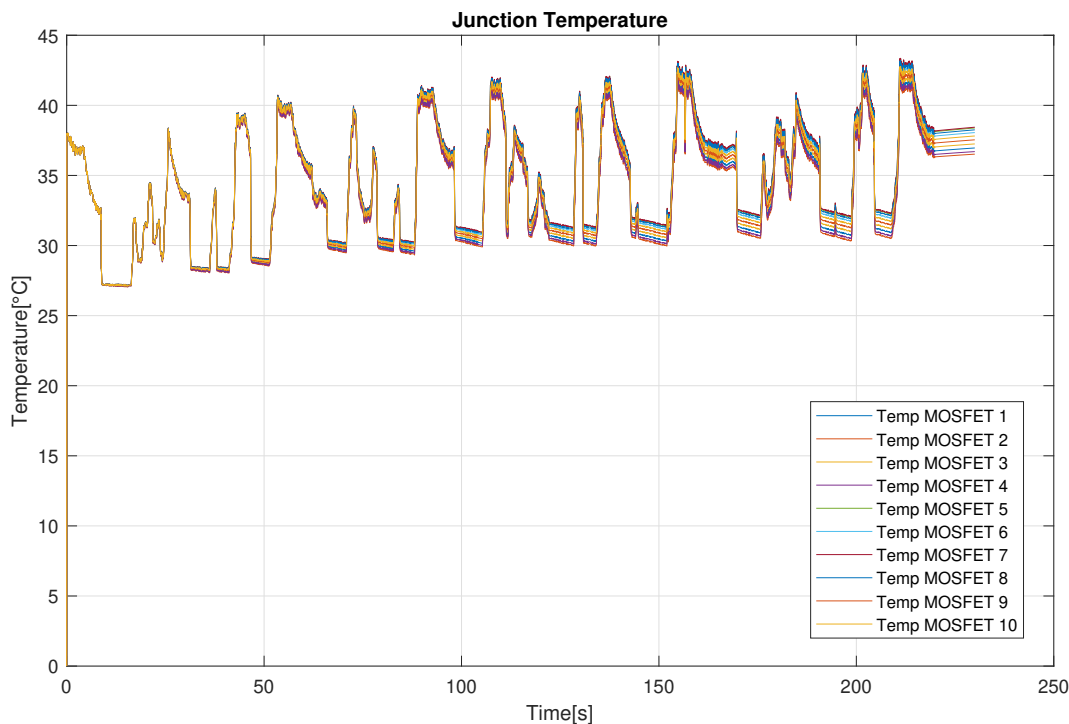
Figure 4.16: MOSFET Junction temperatures

In the instants when the load is zero, the effect of the heat exchanger capacity can be seen. The energy absorbed by the aluminium structure in the dynamic test does not reach temperatures higher than 35 degrees. This effect can be seen by considering the graph of current and temperature; when the current is zero, the temperature detected at the junction depends only on the heat exchanger temperature.

Since the load is variable, the heat exchanger does not continue to absorb energy that increases the system temperature, but remains almost stationary when the power to be dissipated is 0. In fact, it can be seen that the temperature decreases before the absorbed current goes from 0 to a higher value. The temperatures measured on the row of MOSFETs are not equal, but the difference is small when considering the value of the magnitude by division.

Another important element to see is how the junction temperatures vary so quickly, they heat up immediately. This effect is given by the absence of a thermal capacitance of the junction and the thermal paste, but there is only the capacitance of the heat sink.

Both simulations have been very helpful in understanding the reliability of the system. The first at steady state was a test that determined the quality of the calculations performed, the model passed from a circuit with lumped parameters to distributed ones,

nevertheless it has been seen the effect of having dynamic losses. The system was tested at maximum power, beyond that value it was not possible to go up. As for the second test, the purely dynamic one, excellent results were obtained, which will leave a lot of margins, moreover it will give to the team the possibility of having more power available and will avoid overheating problems.

4.5.   Electrical Test of the Three-Phase Inverter

The last test was done to define the power involved in the inverter.

Until now, to study the thermal part, the motorcycle absorption current peaks have been taken as references. Based on these values, the heat exchanger was sized and the number of switches in parallel was defined.

Now it is useful to understand how the converter behaves. It is useful to evaluate the output power and check the power lost on each module as well.

The two-level inverter consists of 6 switches, each of which has its own gate command, thus 6 different gate signals. The sized inverter foresees that in place of each switch there are 10 modules in parallel, 10 for the high side and 10 for the low side of each phase, for a total of 60 modules.
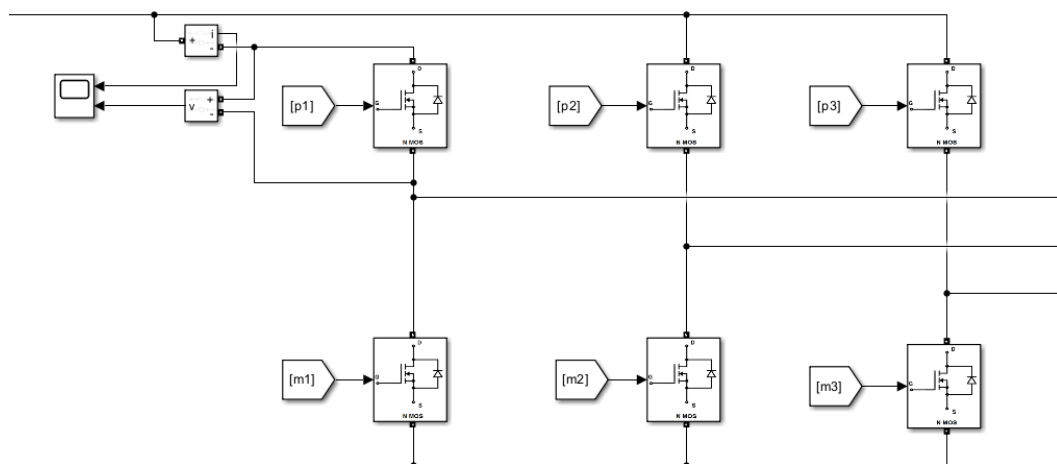
Figure 4.17: Three phase inverter, used for the pure electrical test

The scheme of the inverter (fig: 4.17) is made by sixty modules C3M0015065K, each leg has ten switches in parallel for the high side and ten for the low side. Each of the 6 MOSFETs shown in the schematic has 10 switches connected in parallel (fig: 4.18).
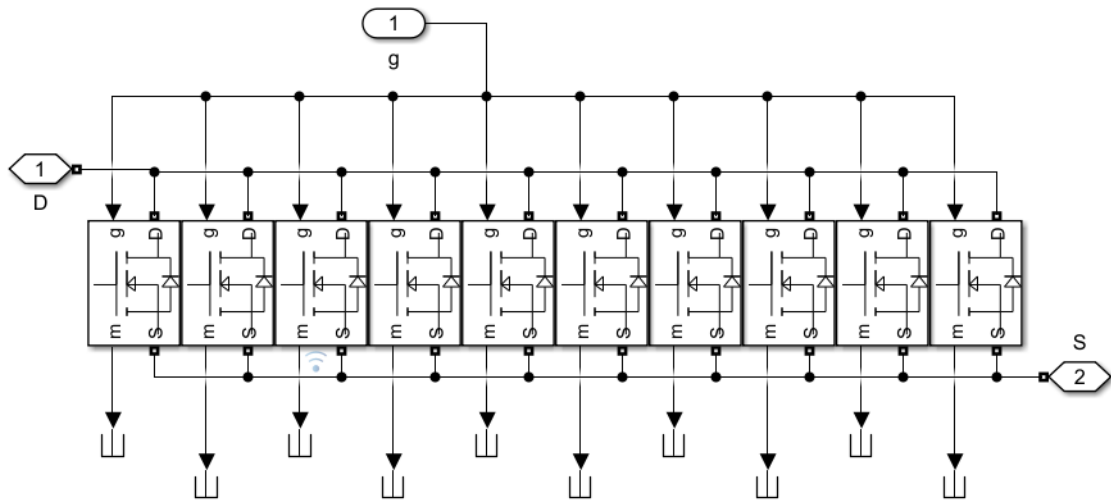
Figure 4.18: Each single MOSFET subsystem contains ten power modules

The block of the MOSFET in the Specialized Sower System has already the free-wheeling Diode, the setting parameters of this block are essential, such as

- The Threshold Voltage

- $R_{DS_{on}}$

- Forward Voltage of the Diode

- Snubber Parameters

It is majorly used for electrical tests in the study of waveforms.

For the control, it was assumed to use a modulation ratio equal to 1, so as to remain within the base speed range and to use both MOSFETs and Diodes.

The control signal (fig: 4.19) is done with three sine waves out of 120° phase that are compared with a triangle wave, the comparison return:

- 0 when $v_{con} < v_{tri}$

- 1 when $v_{tri} \leq v_{con}$
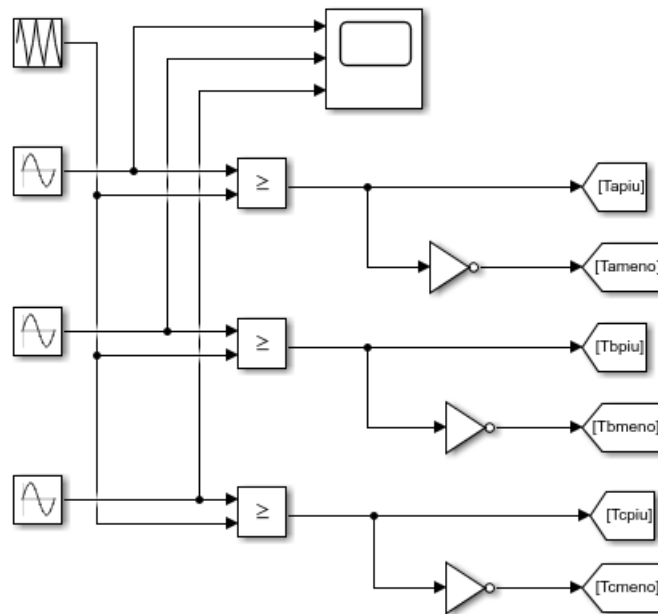
Figure 4.19: PWM for a three phase inverter

The MOSFET is controlled without a specific value of v_{GS}, but it is logically controlled.

In this simulation, the focus is on the magnitudes of the quantities under test.

The specialized power system does not need a dead time that avoids the short circuit of the DC link when the high and low side switches are both closed, because the slope of current or voltage is considered infinite, there is no energy loss due to switching transient. So for the sake of simplicity, it is not considered.

The signal compared without the not port goes directly to the high side switches, while the negate one goes to the low side, the switches in parallel are controlled from the same v_{con} signal.

The load was assumed to be an RL load with the value of the inductance and resistance of the permanent magnet synchronous machine, the parameters are:

The values of the resistance and the inductance are:

- Resistance equals 0.046 Ω

- Inductance equals 96 μH

Using this load, the short-circuit test is performed, which for an electrical machine is equivalent to the locked rotor test. The applied voltage is different from that used for the short-circuit test since the nominal voltage is applied in this case.

In order to display the different quantities involved in the inverter, such as Root Mean Square, peak value, first order harmonic RMS, instant values and the phase an ad hoc block is done with the following calculation (fig: 4.20). The quantities that can be seen with this block are:

- Peak
  The peak value is computed directly from the Fourier block that finds the Absolute value of the first harmonics

- Rms of the first harmonics
  The root mean square of the first harmonics is calculated from the Peak value dividing it by the square root of two

- Instantaneous value
  Uses the Peak value, as the amplitude, while the phase and the clock are used for the sine arguments.

- Phase
  The phase of the first harmonic derives from the Fourier block

- Rms
  Evaluates the Rms with all the harmonics content

This block needs only to set the fundamental frequency for the Fourier block and the RMS.
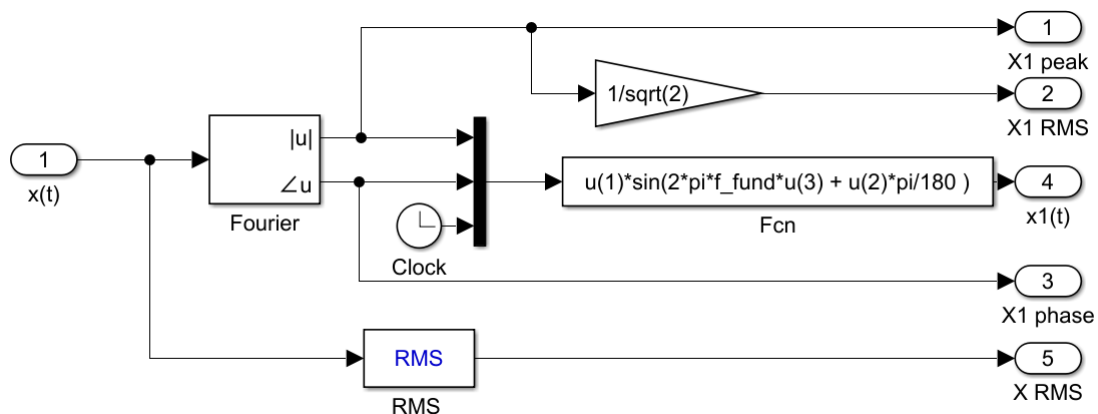
Figure 4.20: Scheme used to calculate the first harmonic voltage and current

4.6. Results

The phase currents reported in figure 4.21 as can be seen are very high, the peak overcomes 1000 A, reaching precisely 1068 A, each module handling an RMS current of 49.4 A.

In the figure 4.21 are reported the three-phase currents full of the harmonics content, evaluated without filters, this results is very impressive.
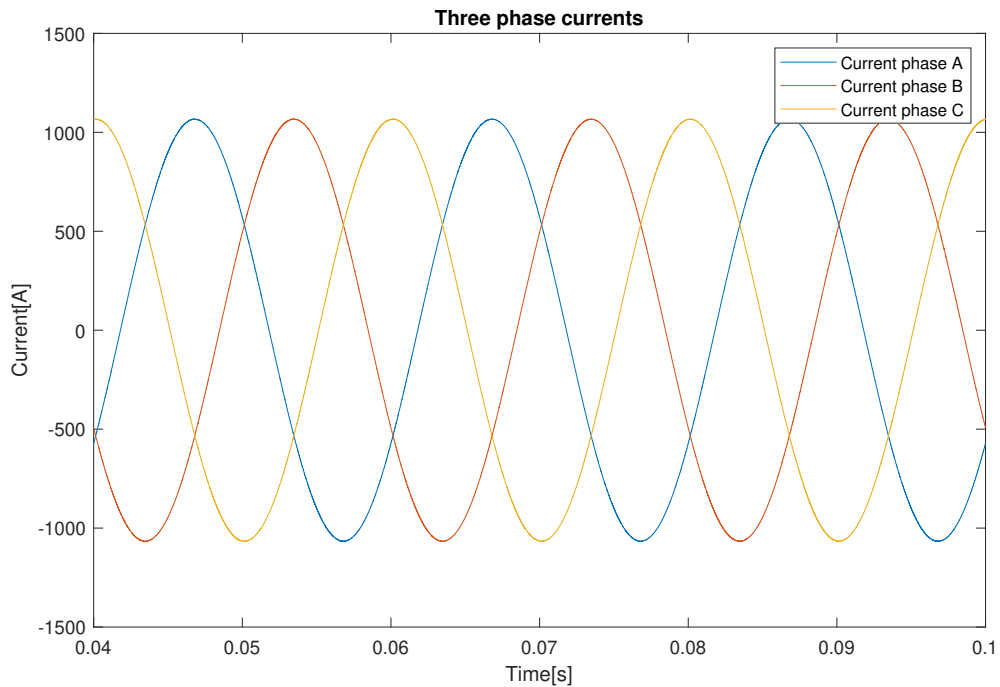
Figure 4.21: Output phase currents

It is emphasised that dead time has not been considered in this type of circuit.

The ripple is the difference between the total current and the first harmonic current, the current ripple depends on the voltage ripple and the inductance value. Furthermore, having such a high switching frequency, the distortion is infinitesimal, the registered total harmonics distortion, THD is lower than 1%.

As can be seen, the current don't have much ripple so the total component differs little from the first harmonic current.

The current ripple is equal to:

$$i_{ripple} = i_o - i_{o1} \tag{4.6}$$

In figure 4.22 is reported the current ripple of the phase A.
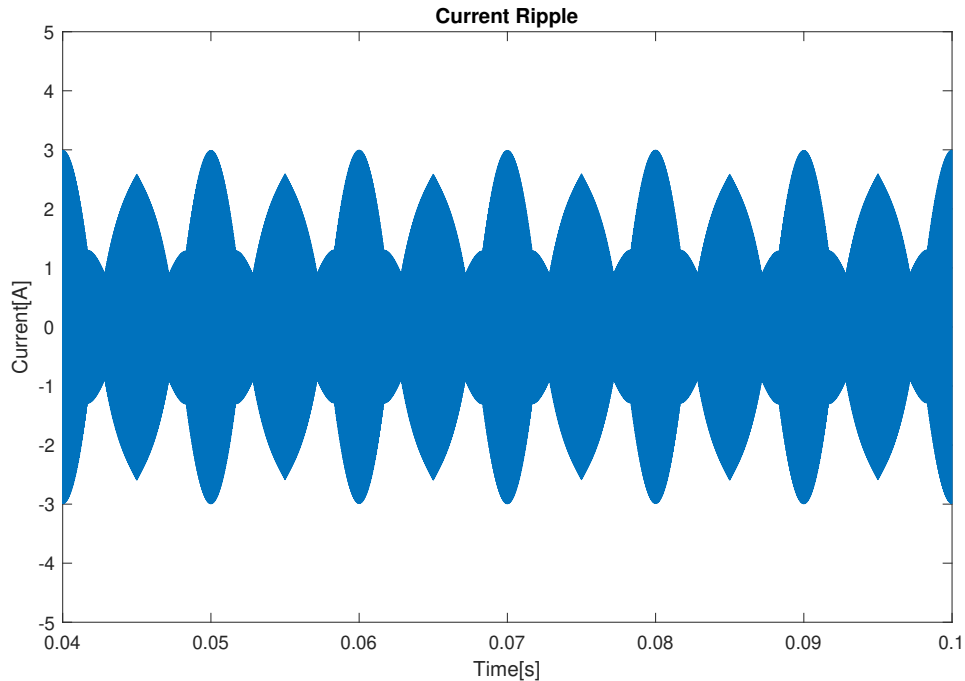
Figure 4.22: Current ripple

As for the ripple, the measured value has been reported starting from 40 ms. Because the RMS block during the first period referred to the first harmonic frequency, takes information about the signal, so the it will display the right value after one period.

The ripple current is limited to 3 A, with 754 A RMS as the first harmonic phase current, so it is possible to understand how the phase currents which contain all the components have a pure sinusoidal shape.

The phase shift between the current and phase voltage is reported in the figure 4.23, they are reported in different scales, because it is easier to see the angle between them. The angle included between the phase voltage and the phase current is 31.58°
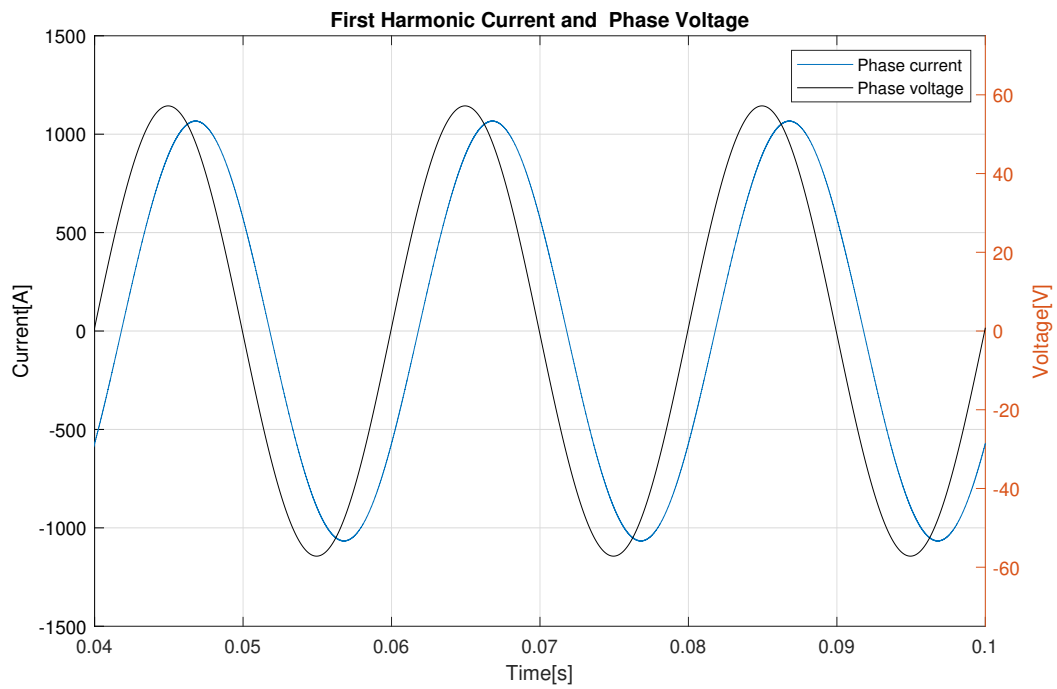
Figure 4.23: Phase current and voltage
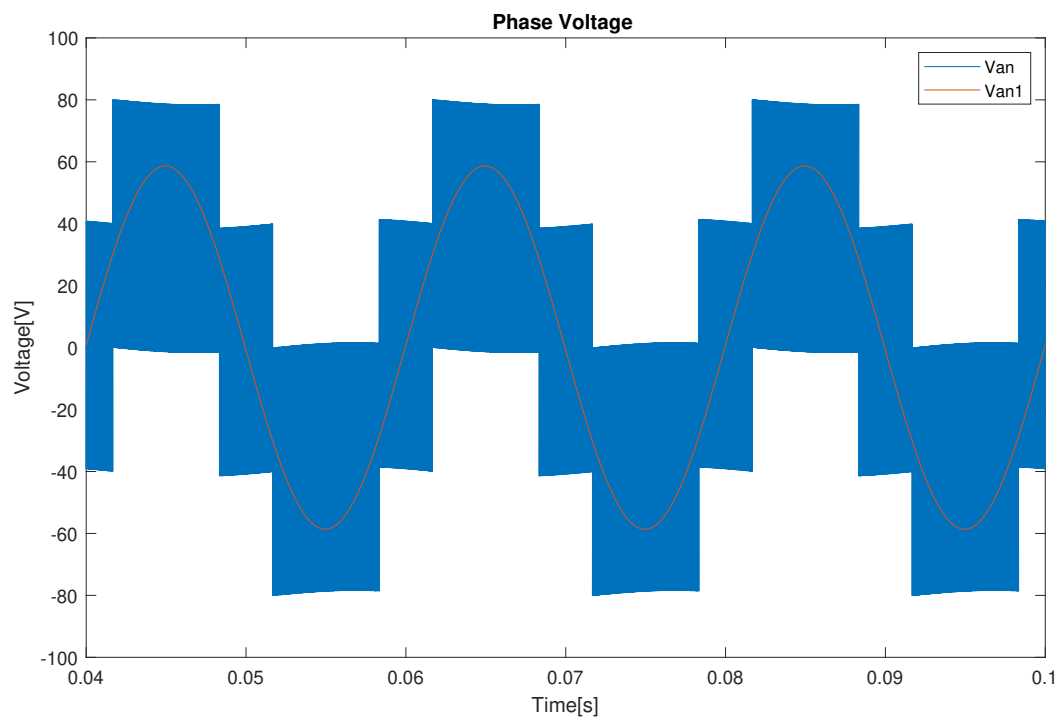
Figure 4.24: Voltage total component and the first harmonics phase voltage
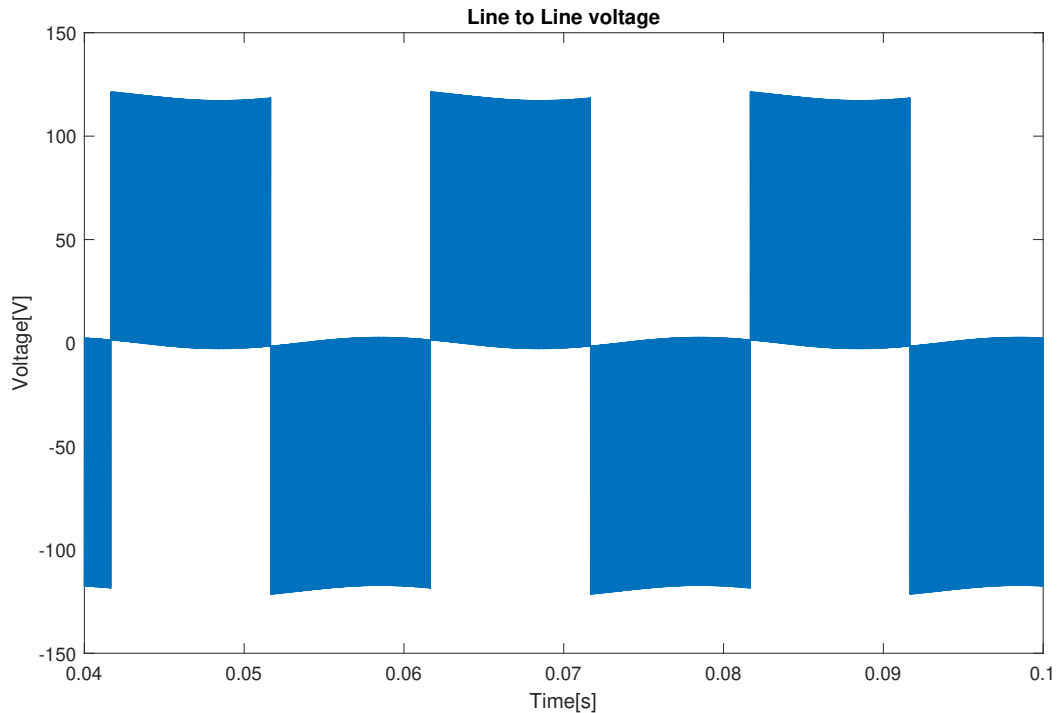
Figure 4.25: Line to line voltage

Various values can be derived for phase voltages and currents with the block that was explained earlier. To evaluate direct current, on the other hand, assumptions must be made; two things must be considered:

- the system has an ideal LC filter in input and output so that there is no stored energy so all power flows from DC to AC

- the switching frequency is infinite

In this way, the current has no high switching component, furthermore, it is possible to express the instantaneous power as a function of the current and phase voltage of the first-order harmonic.

So an energy balance is imposed where the output is equal to the input, without considering energy-storing elements, otherwise, the energy balance must also include the high-frequency components. Which is quite complex to do.

So it is possible to write the energy balance considering the components at 50 Hz:

$$V_d \cdot i_{d*} = v_{An1}(t) \cdot i_A(t) + v_{Bn1}(t) \cdot i_B(t) + v_{Cn1}(t) \cdot i_C(t) \tag{4.7}$$

The current i_d* contains only low-frequency components.

In a balanced three-phase system the phase quantities are out of phase by 120°, therefore the direct component could be expressed as:

$$i_d* = \frac{2V_0 I_0}{V_d} \left[cos\omega_1 t \, cos(\omega_1 t - \phi) + cos(\omega_1 t - 120°) \, cos(\omega_1 t - 120° - \phi) \right.$$

$$\left. + cos(\omega_1 t - 240°) \, cos(\omega_1 t - 240° - \phi) \right] = \frac{3V_0 I_0}{V_d} cos\phi = Id \qquad (4.8)$$

The previous formula demonstrates that i_d* has only direct component.

Where I_d is the direct component, ϕ is the phase shift between voltage and current, V_0 and I_0 are the phase RMS quantities of voltage and current evaluated for the first harmonic order.

In the single-phase inverter, the current contains a wave with a frequency twice as high as the fundamental and a direct component, whereas, in the three-phase case, the i_d current contains the direct component i_d* and harmonics related to the high frequency given by the switching frequency. This high-frequency harmonics are not relevant to the DC bus voltage, due to the presence of the capacitor in the DC side.

The angle between $V_0 I_0$ is calculated with the block in figure 4.20.

The DC current value is, therefore:

$$I_D = \frac{3V_0 I_0}{V_d} cos\phi = \frac{3 \cdot 41.48V \cdot 754A}{120V} cos(31.58°) = 666A \qquad (4.9)$$

After the DC current has been found, it is then possible to calculate the power managed by the converter. To calculate the efficiency it is necessary to consider all losses of the system. In this case, the study focused on the sizing of the power modules, without considering the drive circuit.

Then the conduction and switching losses were considered, with an ideal drive circuit.

The efficiency formula shows the losses for each switch, multiplied by the number of switches that the inverter has.

$$P_{CM} = R_{DS_{ON}} \cdot I^2_{M\,RMS} = 0.015\,\Omega \cdot (49.4\,A)^2 = 36.6\,W \tag{4.10}$$

$$P_{SWM} = E(I_{RMS}) \cdot f_{sw} = 600\,\mu J \cdot 30150\,Hz = 18.0\,W \tag{4.11}$$

$$P_{CD} = R_D \cdot I^2_{D\,RMS} = 0.053\,\Omega \cdot (10.64\,A)^2 = 6.0\,W \tag{4.12}$$

For switch losses, the energy lost during a switching period was considered. The current RMS of the Diode is different from the current RMS of the MOSFET, this difference is given by the modulation ratio, reducing it the Diode RMS would be higher.

$$\eta = \frac{P_{DC} - 60 \cdot (P_{CM} + P_{SWM} + P_{CD})}{P_{DC}}$$

$$= \frac{81030\,W - 60 \cdot (36.6\,W + 6.0\,W + 18.0\,W)}{81030\,W} = 0.955 = 95.5\% \tag{4.13}$$

The calculated efficiency is in line with the efficiency of other SiC inverters from other manufacturers, the efficiency with a maximum load power is generally around 94/96%.

Conclusions

For this project several test were carried out using two different software, Ansys Icepack and Matlab. The former made it possible to define the thermal specifications of the system, the latter made it possible to test a more dynamic and customizable model.

The results obtained from the F.E.M. simulations were the starting point for defining the thermal system, defining the characteristics of the heat sink, while with the aid of Matlab the results were cross-referenced by carrying out complementary tests.

The system proved to be thermally stable in the steady-state test and is able to guarantee a power dissipation per module of 70 W. The exchanger guarantees that the inverter can control an electrical power of 80kW. The first prototype had a lower maximum allowable loss, later improvements were made to allow it to handle higher power.

With the electro-thermal model realized on Matlab it has been seen that it is possible to manage high powers at high speeds. Thanks to the dynamic test we can say that with these specifications we can make a traction inverter and have a fair power margin. The power requirements that the motorcycle has are far below the potential that the inverter has, the power available is almost double that required by the motorcycle.

According to the various tests done, the system has achieved excellent results. A practical future development to improve the design is to increase the speed of the air entering the heat sink by inserting an air conveyor that carries air to the compartment in which it is housed. From what has emerged, excellent results are obtained by increasing the speed of the extraction air. It would be useful to integrate the conveyors while keeping the fans installed to cool the system when the motorcycle is stationary.

Future developments are already a reality, the project has passed to my laboratory partner Matteo, who is working on the driving circuit.

We are satisfied with the results of this thesis, and we are confident that those results will be useful in the future developments and research on the new three-phase inverter with SiC modules.

Bibliography

[1] A. K. Dr. Dušan Graovac, MarcoPürschel. Mosfet power losses calculation using the data-sheet parameters, 2006.

[2] S. Fleeman. Si, sic, and gan for power devices, part one: Electron energy and the semiconductors, 2023. URL `https://www.engineering.com/story/si-sic-and-gan-for-power-devices-part\-one-electron-energy-and-the-semiconductors`.

[3] A. Flockett. Phase change materials: Innovations in thermal management, 2019. URL `https://www.electronicspecifier.com/products/component-management/\phase-change-materials-innovations-in-thermal-management`.

[4] Infineon. Wide bandgap semiconductors (sic/gan), 2023. URL `https://www.infineon.com/cms/en/product/technology/wide-bandgap\-semiconductors-sic-gan`.

[5] R. Mohan, Undeland. *Power Electronics*. John Wiley & Sons, 1995.

[6] Rohm. New 4-pin package sic mosfets, 2019. URL `https://www.rohm.com/news-detail?news-title=4-pin-package-sic-mosfets`.

[7] SAN-ACE. San ace, dc fan 9hva type $60 \times 60 \times 38$mm datasheet, 2022.

[8] S. Sedra. *Microelectronic circuits*. Edises, 2019.

[9] STMicroelectronics. Gan, gallium nitride, 2023. URL `https://www.st.com/content/st_com/en/about/innovation---technology/GaN.html`.

[10] Wolfspeed. C3m0015065d datasheet, 2022.

[11] Wolfspeed. C3m0015065k datasheet, 2022.

A | Mosfet Comparison: TO-247-3L vs TO-247-4L

During the switching transient there is an Energy loss due to the fact that the slope of current and voltage is linear.

This phenomenon could be reduced with the use of a specific Package, on the market in the last few years has been launched a new type of MOSFET that has four pins, while the most conventional has three pins.

This new package reduces the voltage drop between parasitic inductances, thanks to a different driver source, which divides the driver and power source pins. This separation of the two connections increases the switching speed, resulting in a more efficient version of the three-pin MOSFET.

In figure A.1 is reported the turning ON phase of the switch comparison between the 4 and the 3 terminals.
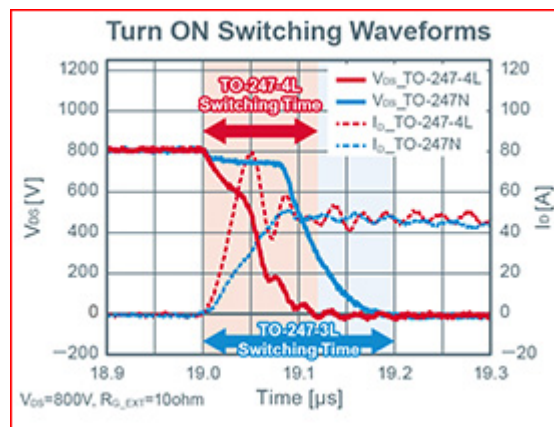
Figure A.1: Turn ON Switching Waveforms comparison [6]

From figure A.1 it is possible to understand how faster is the TO 247-4L respect the 3L. The four pins has a brief overshoot that shortens the rise time of the current of the MOSFET, of course, it is more damped, but has a faster response during the transient

period. From this figure is evident that the switching time of the two different packages is too different.
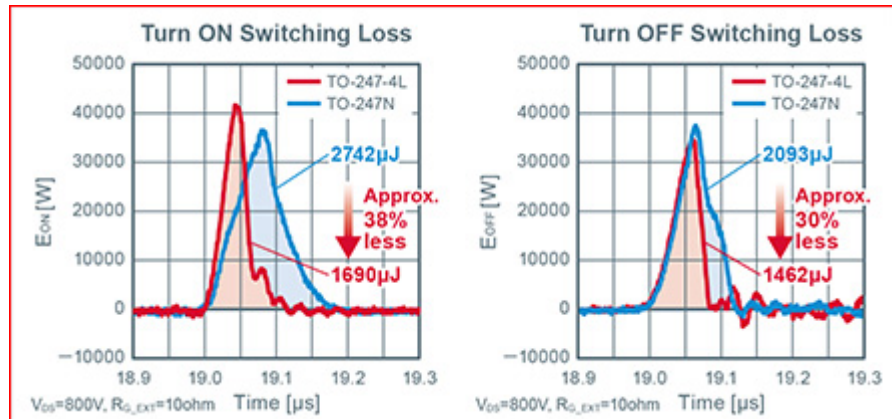
Figure A.2: Mosfet Switching Losses [6]

During the switching-ON period, the time taken from the package TO 247-4L is brief (see fig A.2), instead the convectional one takes more time. During the turning-ON, the four pins model has an energy loss lower of 38%, while during the turning-OFF phase, the energy is about 30% less.

In a context where energy is limited, reducing losses is essential, because it reduces consumption and also because the energy to be dissipated is less.

B | Wolfspeed C3M0015065D

C3M0015065D
Silicon Carbide Power MOSFET
C3M™ MOSFET Technology
N-Channel Enhancement Mode

Features

- 3rd Generation SiC MOSFET technology
- High blocking voltage with low on-resistance
- High speed switching with low capacitances
- Fast intrinsic diode with low reverse recovery (Qrr)
- Halogen free, RoHS compliant

Benefits

- Higher system efficiency
- Reduced cooling requirements
- Increased power density
- Increased system switching frequency
- Easy to parallel and simple to drive
- Enable new hard switching PFC topologies (Totem-Pole)

Applications

- EV charging
- Solar PV Inverters
- UPS
- SMPS
- DC/DC converters
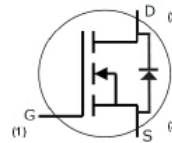
Package

Part Number	Package	Marking
C3M0015065D	TO-247-3	C3M0015065D

Maximum Ratings (T$_C$=25°C, unless otherwise specified)

Symbol	Parameter	Value	Unit	Note
V_{DSmax}	Drain - Source Voltage	650	V	
V_{GSmax}	Gate - Source voltage	-8/+19	V	Note 1
I_D	Continuous Drain Current, V_{GS} = 15 V, T_C = 25°C	120	A	Fig. 19 Note 2
	Continuous Drain Current, V_{GS} = 15 V, T_C = 100°C	96		
$I_{D(pulse)}$	Pulsed Drain Current, Pulse width t_p limited by T_{jmax}	418	A	
P_D	Power Dissipation, T_C=25°C, T_J = 175 °C	416	W	Fig. 20
T_J , T_{stg}	Operating Junction and Storage Temperature	-40 to +175	°C	
T_L	Solder Temperature, 1.6mm (0.063") from case for 10s	260	°C	
M_d	Mounting Torque, (M3 or 6-32 screw)	1 8.8	Nm lbf-in	

Note (1): Recommended turn off / turn on gate voltage V_{GS} - 4V...0V / +15V
Note (2): Package limited to 120 A

Figure B.1: C3M0015065D: wolfspeed datasheet

Electrical Characteristics (T$_c$ = 25°C unless otherwise specified)

Symbol	Parameter	Min.	Typ.	Max.	Unit	Test Conditions	Note
V$_{(BR)DSS}$	Drain-Source Breakdown Voltage	650			V	V$_{GS}$ = 0 V, I$_D$ = 100 μA	
V$_{GS(th)}$	Gate Threshold Voltage	1.8	2.3	3.6	V	V$_{DS}$ = V$_{GS}$, I$_D$ = 15.5 mA	Fig. 11
			1.9		V	V$_{DS}$ = V$_{GS}$, I$_D$ = 15.5 mA, T$_J$ = 175°C	
I$_{DSS}$	Zero Gate Voltage Drain Current		1	50	μA	V$_{DS}$ = 650 V, V$_{GS}$ = 0 V	
I$_{GSS}$	Gate-Source Leakage Current		10	250	nA	V$_{GS}$ = 15 V, V$_{DS}$ = 0 V	
R$_{DS(on)}$	Drain-Source On-State Resistance	10.5	15	21	mΩ	V$_{GS}$ = 15 V, I$_D$ = 55.8A	Fig. 4, 5,6
			20			V$_{GS}$ = 15 V, I$_D$ = 55.8A, T$_J$ = 175°C	
g$_{fs}$	Transconductance		42		S	V$_{DS}$= 20 V, I$_{DS}$= 55.8 A	Fig. 7
			40			V$_{DS}$= 20 V, I$_{DS}$= 55.8 A, T$_J$ = 175°C	
C$_{iss}$	Input Capacitance		5011				Fig. 17, 18
C$_{oss}$	Output Capacitance		289				
C$_{rss}$	Reverse Transfer Capacitance		31		pF	V$_{GS}$ = 0 V, V$_{DS}$ = 400 V	
C$_{o(er)}$	Effective Output Capacitance (Energy Related)		357			f = 100 Khz	Note: 3
C$_{o(tr)}$	Effective Output Capacitance (Time Related)		516			V$_{AC}$ = 25 mV	Note: 3
E$_{oss}$	C$_{oss}$ Stored Energy		29		μJ		Fig. 16
E$_{ON}$	Turn-On Switching Energy (Body Diode)		1500		μJ	V$_{DS}$ = 400 V, V$_{GS}$ = -4 V/15 V, I$_D$ = 55.8 A, R$_{G(ext)}$ = 5 Ω, L= 57.6 μH, T$_J$ = 175°C FWD = Internal Body Diode of MOSFET	Fig. 25
E$_{OFF}$	Turn Off Switching Energy (Body Diode)		700				
E$_{ON}$	Turn-On Switching Energy (External Diode)		1200		μJ	V$_{DS}$ = 400 V, V$_{GS}$ = -4 V/15 V, I$_D$ = 55.8 A, R$_{G(ext)}$ = 5 Ω, L= 57.6 μH, T$_J$ = 175°C FWD = External SiC DIODE	Fig. 25
E$_{OFF}$	Turn Off Switching Energy (External Diode)		1000				
t$_{d(on)}$	Turn-On Delay Time		22		ns	V$_{DD}$ = 400 V, V$_{GS}$ = -4 V/15 V I$_D$ = 55.8 A, R$_{G(ext)}$ = 5 Ω, L= 57.6 μH Timing relative to V$_{DS}$ Inductive load	Fig. 26
t$_r$	Rise Time		125				
t$_{d(off)}$	Turn-Off Delay Time		58				
t$_f$	Fall Time		25				
R$_{G(int)}$	Internal Gate Resistance		1.5		Ω	f = 1 MHz, V$_{AC}$ = 25 mV	
Q$_{gs}$	Gate to Source Charge		54		nC	V$_{DS}$ = 400 V, V$_{GS}$ = -4 V/15 V I$_D$ = 55.8 A Per IEC60747-8-4 pg 21	Fig. 12
Q$_{gd}$	Gate to Drain Charge		62				
Q$_g$	Total Gate Charge		188				

Note (3): C$_{o(er)}$, a lumped capacitance that gives same stored energy as Coss while Vds is rising from 0 to 400V
C$_{o(tr)}$, a lumped capacitance that gives same charging time as Coss while Vds is rising from 0 to 400V

Figure B.2: C3M0015065D: wolfspeed datasheet

Reverse Diode Characteristics (T$_c$ = 25°C unless otherwise specified)

Symbol	Parameter	Typ.	Max.	Unit	Test Conditions	Note
V$_{SD}$	Diode Forward Voltage	4.7		V	V$_{GS}$ = -4 V, I$_{SD}$ = 27.9 A, T$_J$ = 25 °C	Fig. 8, 9, 10
		4.2		V	V$_{GS}$ = -4 V, I$_{SD}$ = 27.9 A, T$_J$ = 175 °C	
I$_S$	Continuous Diode Forward Current		79	A	V$_{GS}$ = -4 V, T$_C$ = 25°C	
I$_{S, pulse}$	Diode pulse Current		418	A	V$_{GS}$ = -4 V, pulse width t$_p$ limited by T$_{jmax}$	
t$_{rr}$	Reverse Recovery time	85		ns	V$_{GS}$ = -4 V, I$_{SD}$ = 55.8 A, V$_R$ = 400 V dif/dt = 1500 A/μs, T$_J$ = 175 °C	
Q$_{rr}$	Reverse Recovery Charge	667		nC		
I$_{rrm}$	Peak Reverse Recovery Current	17		A		
t$_{rr}$	Reverse Recovery time	74		ns	V$_{GS}$ = -4 V, I$_{SD}$ = 55.8 A, V$_R$ = 400 V dif/dt = 1000 A/μs, T$_J$ = 175 °C	
Q$_{rr}$	Reverse Recovery Charge	562		nC		
I$_{rrm}$	Peak Reverse Recovery Current	14		A		

Thermal Characteristics

Symbol	Parameter	Typ.	Unit	Test Conditions	Note
R$_{θJC}$	Thermal Resistance from Junction to Case	0.35	°C/W		Fig. 21
R$_{θJA}$	Thermal Resistance From Junction to Ambient	40			

Figure B.3: C3M0015065D: wolfspeed datasheet

C | Wolfspeed C3M0015065K

C3M0015065K

Silicon Carbide Power MOSFET
C3M™ MOSFET Technology
N-Channel Enhancement Mode

Features

- C3M™ SiC MOSFET technology
- Optimized package with separate driver source pin
- 8mm of creepage distance between drain and source
- High blocking voltage with low on-resistance
- High-speed switching with low capacitances
- Fast intrinsic diode with low reverse recovery (Q_{rr})
- Halogen free, RoHS compliant

Benefits

- Reduce switching losses and minimize gate ringing
- Higher system efficiency
- Reduce cooling requirements
- Increase power density
- Increase system switching frequency

Applications

- EV chargers
- Solar inverters
- UPS
- SMPS
- DC/DC converters
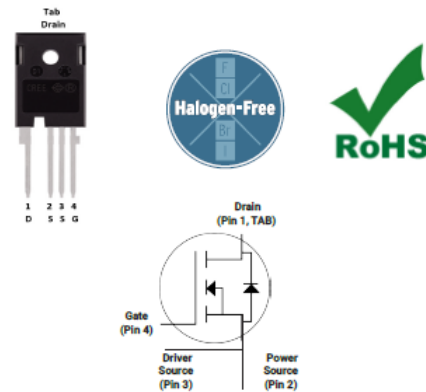
Package

Part Number	Package	Marking
C3M0015065K	TO 247-4	C3M0015065K

Maximum Ratings (T_C=25°C, unless otherwise specified)

Symbol	Parameter	Value	Unit	Note
V_{DSmax}	Drain - Source Voltage	650	V	
V_{GSmax}	Gate - Source voltage	-8/+19	V	Note 1
I_D	Continuous Drain Current, V_{GS} = 15 V, T_C = 25°C	120	A	Fig. 19 Note 2
	Continuous Drain Current, V_{GS} = 15 V, T_C = 100°C	96		
$I_{D(pulse)}$	Pulsed Drain Current, Pulse width t_p limited by T_{jmax}	418	A	
P_D	Power Dissipation, T_C=25°C, T_J = 175 °C	416	W	Fig. 20
T_J , T_{stg}	Operating Junction and Storage Temperature	-40 to +175	°C	
T_L	Solder Temperature, 1.6mm (0.063") from case for 10s	260	°C	
M_d	Mounting Torque, (M3 or 6-32 screw)	1 8.8	Nm lbf-in	

Note (1): Recommended turn off / turn on gate voltage V_{GS} - 4V...0V / +15V
Note (2): Package limited to 120 A

Figure C.1: C3M0015065K: wolfspeed datasheet

Electrical Characteristics (T$_c$ = 25°C unless otherwise specified)

Symbol	Parameter	Min.	Typ.	Max.	Unit	Test Conditions	Note
V$_{(BR)DSS}$	Drain-Source Breakdown Voltage	650			V	V$_{GS}$ = 0 V, I$_D$ = 100 μA	
V$_{GS(th)}$	Gate Threshold Voltage	1.8	2.3	3.6	V	V$_{DS}$ = V$_{GS}$, I$_D$ = 15.5 mA	Fig. 11
			1.9		V	V$_{DS}$ = V$_{GS}$, I$_D$ = 15.5 mA, T$_J$ = 175ºC	
I$_{DSS}$	Zero Gate Voltage Drain Current		1	50	μA	V$_{DS}$ = 650 V, V$_{GS}$ = 0 V	
I$_{GSS}$	Gate-Source Leakage Current		10	250	nA	V$_{GS}$ = 15 V, V$_{DS}$ = 0 V	
R$_{DS(on)}$	Drain-Source On-State Resistance	10.5	15	21	mΩ	V$_{GS}$ = 15 V, I$_D$ = 55.8A	Fig. 4, 5,6
			20			V$_{GS}$ = 15 V, I$_D$ = 55.8A, T$_J$ = 175ºC	
g$_{fs}$	Transconductance		42		S	V$_{DS}$ = 20 V, I$_{DS}$ = 55.8 A	Fig. 7
			40			V$_{DS}$ = 20 V, I$_{DS}$ = 55.8 A, T$_J$ = 175ºC	
C$_{iss}$	Input Capacitance		5011				Fig. 17, 18
C$_{oss}$	Output Capacitance		289			V$_{GS}$ = 0 V, V$_{DS}$ = 400 V	
C$_{rss}$	Reverse Transfer Capacitance		31		pF	f = 100 Khz	
C$_{o(er)}$	Effective Output Capacitance (Energy Related)		357			V$_{AC}$ = 25 mV	Note: 3
C$_{o(tr)}$	Effective Output Capacitance (Time Related)		516				Note: 3
E$_{oss}$	C$_{oss}$ Stored Energy		29		μJ		Fig. 16
E$_{ON}$	Turn-On Switching Energy (Body Diode)		401		μJ	V$_{DS}$ = 400 V, V$_{GS}$ = -4 V/15 V, I$_D$ = 55.8 A, R$_{G(ext)}$ = 5 Ω, L= 57.6 μH, T$_J$ = 175ºC FWD = Internal Body Diode of MOSFET	Fig. 25
E$_{OFF}$	Turn Off Switching Energy (Body Diode)		254				
E$_{ON}$	Turn-On Switching Energy (External Diode)		234		μJ	V$_{DS}$ = 400 V, V$_{GS}$ = -4 V/15 V, I$_D$ = 55.8 A, R$_{G(ext)}$ = 5 Ω, L= 57.6 μH, T$_J$ = 175ºC FWD = External SiC DIODE	Fig. 25
E$_{OFF}$	Turn Off Switching Energy (External Diode)		303				
t$_{d(on)}$	Turn-On Delay Time		23			V$_{DD}$ = 400 V, V$_{GS}$ = -4 V/15 V I$_D$ = 55.8 A, R$_{G(ext)}$ = 5 Ω, L= 57.6 μH Timing relative to V$_{DS}$ Inductive load	Fig. 26
t$_r$	Rise Time		32		ns		
t$_{d(off)}$	Turn-Off Delay Time		57				
t$_f$	Fall Time		15				
R$_{G(int)}$	Internal Gate Resistance		1.5		Ω	f = 1 MHz, V$_{AC}$ = 25 mV	
Q$_{gs}$	Gate to Source Charge		53			V$_{DS}$ = 400 V, V$_{GS}$ = -4 V/15 V I$_D$ = 55.8 A Per IEC60747-8-4 pg 21	Fig. 12
Q$_{gd}$	Gate to Drain Charge		58		nC		
Q$_g$	Total Gate Charge		188				

Note (3): C$_{o(er)}$, a lumped capacitance that gives same stored energy as Coss while Vds is rising from 0 to 400V
C$_{o(tr)}$, a lumped capacitance that gives same charging time as Coss while Vds is rising from 0 to 400V

Figure C.2: C3M0015065K: wolfspeed datasheet

Reverse Diode Characteristics (T$_c$ = 25°C unless otherwise specified)

Symbol	Parameter	Typ.	Max.	Unit	Test Conditions	Note
V$_{SD}$	Diode Forward Voltage	4.7		V	V$_{GS}$ = -4 V, I$_{SD}$ = 27.9 A, T$_J$ = 25 °C	Fig. 8, 9, 10
		4.2		V	V$_{GS}$ = -4 V, I$_{SD}$ = 27.9 A, T$_J$ = 175 °C	
I$_S$	Continuous Diode Forward Current		79	A	V$_{GS}$ = -4 V, T$_C$ = 25°C	
I$_{S, pulse}$	Diode pulse Current		223	A	V$_{GS}$ = -4 V, pulse width t$_p$ limited by T$_{Jmax}$	
t$_{rr}$	Reverse Recover time	22		ns	V$_{GS}$ = -4 V, I$_{SD}$ = 55.8 A, V$_R$ = 400 V dif/dt = 4000 A/μs, T$_J$ = 175 °C	
Q$_{rr}$	Reverse Recovery Charge	510		nC		
I$_{rrm}$	Peak Reverse Recovery Current	39		A		
t$_{rr}$	Reverse Recover time	26		ns	V$_{GS}$ = -4 V, I$_{SD}$ = 55.8 A, V$_R$ = 400 V dif/dt = 2500 A/μs, T$_J$ = 175 °C	
Q$_{rr}$	Reverse Recovery Charge	432		nC		
I$_{rrm}$	Peak Reverse Recovery Current	28		A		

Thermal Characteristics

Symbol	Parameter	Typ.	Unit	Test Conditions	Note
R$_{\theta JC}$	Thermal Resistance from Junction to Case	0.35	°C/W		Fig. 21
R$_{\theta JA}$	Thermal Resistance From Junction to Ambient	40			

Figure C.3: C3M0015065K: wolfspeed datasheet

List of Figures

List of Tables

Acknowledgements